8. Adaptive Optics

8.1 Introduction

Adaptive Optics is absolutely essential for OWL, to concentrate the light for spectroscopy and imaging and to reach the diffraction limit on-axis or over an extended FoV.

In this section we present a progressive implementation plan based on three generation of Adaptive Optics systems and, to the possible extent, the corresponding expected performance.

The 1st generation AO – Single Conjugate, Ground Layer, and distributed Multi-object AO – is essentially based on Natural Guide Stars (NGSs) and makes use of the M6 Adaptive Mirror included in the Telescope optical path.

The 2nd generation AO is also based on NGSs but includes a second deformable mirror (M5) conjugated at 7-8 km – Multi-Conjugate Adaptive Optics – or a post focus mirror conjugated to the telescope pupil with a much higher density of actuators -tweeter- in the case of EPICS.

The 3rd generation AO makes use of single or multiple Laser Guide Stars, preferably Sodium LGSs, and should provide higher sky coverage, better Strehl ratio and correction at shorter wavelengths.

More emphasis in the future will be given to the LGS assisted AO systems after having studied, simulated and demonstrated the feasibility of the proposed concepts.

The performance presented for the AO systems is based on advances from today's technology in areas where we feel confident that such advances will occur (e.g. the sizes of the deformable mirrors). Even better performance could be achieved if other technologies advance at the same rate as in the past (e.g. the density of actuators for deformable mirrors). While the level one requirements are not fully met with the technology assumptions made in this phase A study, assuming no show stoppers and/or favourable technology advances we have confidence that they eventually will.

8.2 First generation Adaptive Optics

The 1st generation Adaptive Optics for OWL relies on the availability of the M6 Adaptive Mirror unit (M6AM) in the telescope optical train, conjugated to the pupil. The M6AM unit, located in the corrector structure (Figure 8-1) provides both the Adaptive Optics and the Field Stabilization functions of OWL. The 1st generation AO is based on Natural Guide Star (NGSs) for wavefront sensing. As an option an additional post-focal corrector will be discussed in the following either to improve the correction on-axis by increasing the number of degrees of freedom of the

Deformable Mirror (DM) or to improve the correction in several specific positions in the 6 arc minute Field of View (FoV).

Three 1st generation AO facilities will be described: Single Conjugate AO (SCAO), Ground Layer AO (GLAO) and Multi-Object AO (MOAO).

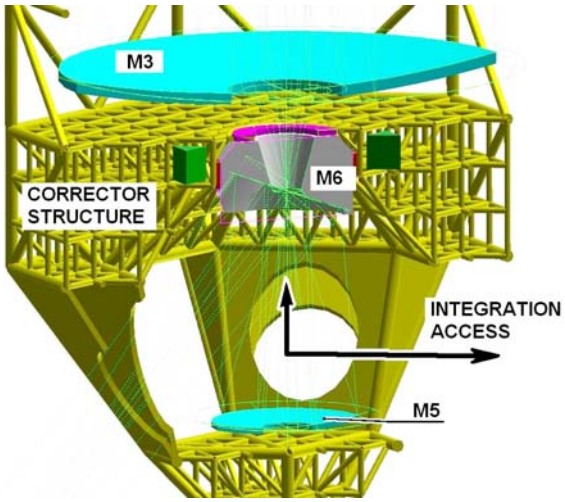

Figure 8-1: M6 Adaptive Mirror located in the corrector structure of the telescope.

8.2.1 Single Conjugate Adaptive Optics

The Single Conjugate Adaptive Optics (SCAO) facility – Figure 8-2 – is essentially an extension of the current AO systems for 8-10 m telescopes to OWL (NAOS, MACAO at the VLT for instance). The performance is usually defined by the Strehl ratio in K-band and ranges from 50 to 60% for bright reference star under average seeing conditions.

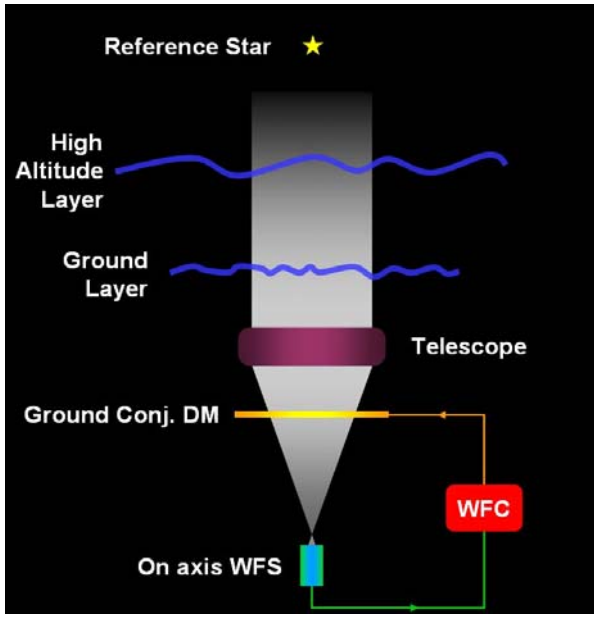

Figure 8-2: Single Conjugate Adaptive Optics concept

SCAO is the AO mode that will be used to commission the telescope at its diffraction limit capability in the Near Infrared.

8.2.1.1 Performance requirements

The SCAO performance requirements are as follows:

- SCAO aims at providing diffraction limited images at the Near Infrared wavelengths (J-K bands) using Natural Guide Stars (NGSs) for wavefront sensing
- SCAO should offer the possibility to observe at longer wavelengths up to 20 microns with a superb correction on-axis using a bright NGS in the visible, Mv<13, or in the IR, MH<12. A specific wavefront sensor close to the instrument is permitted in that case.
- The system should be optimized to obtain >50% Strehl ratio (in K) for bright NGSs and the best possible partial correction for faint NGSs.
- SCAO best correction will be offered on-axis; off-axis performance will essentially be limited by the anisoplanatism (Figure 8-3).
- SCAO should support both a visible and an IR wavefront sensor; the later being required to observe very embedded regions
- SCAO should be able to acquire the wavefront sensing NGS in the central 2' FoV (diameter).
- SCAO shall provide a partially corrected and unvignetted science FoV of 1' diameter.
- SCAO should support telescope nodding at 0.1 Hz by fast opening/closing the AO loop (0.1s)
- SCAO should support small amplitude -0.5"- low temporal frequency -0.1Hz- mosaicking in closed loop by offsetting the Wavefront Sensor (WFS). The accuracy of the WFS offset should be better than 1/2 of the spatial pixel size at the considered wavelength (~1mas in J-band)
- SCAO does not support chopping (chopping for TOWL will be performed in the instrument itself).
- SCAO should provide in closed loop Field Stabilization to the telescope with the maximum amplitude characteristics provided in Table 8-1. For wavefront sensor dynamic reasons, the telescope guider will support SCAO for closing the AO plus Field stabilization loop before the control of the field stabilization corrector is taken over by the SCAO in closed loop.
- SCAO should permit to observe without AO (but with Field Stabilization) without any transmission loss with respect to the telescope. In that case, the field stabilization corrector is not controlled by the AO system.
- SCAO should have the capability to correct for some of the telescope aberrations left by the active optics with an amplitude lower than 20% of the atmospheric wavefront at all spatial and temporal frequencies. Errors beyond these values are handled by the active optics.
- The transmission of SCAO should be maximized for the observing wavelength of the instrument for the visible WFS: T>95%. For the infrared wavefront sensor, the transmission toward the instrument depends on the best trade-off between object observed and the observing wavelength. This trade-off may require several beam splitter/dichroic elements.
- For the performance evaluation of SCAO seeing assumptions should be: 0.53" and 1" at 0.5 μm at zenith; with τ_0=3 and 2ms. For the performance evaluation the outer scale of turbulence should be L_0=25 m. For the determination of the AO design parameters the following atmospheric parameters should be assumed: turbulence outer scale L_0=100m, seeing=1.5", τ_0=2ms (Figure 8-4).
- SCAO shall be able to correct for differential atmospheric dispersion between the NGS and the Science object during an observation by applying offsets to the wavefront sensor. The calculation of the offset shall be done by the software based on the science beam effective wavelength provided by the instrument, the spectral type of the NGS provided by the

observer, the science and guide star coordinates provided by the observer, the relevant atmospheric data (Temperature, Pressure, and Humidity) provided by the observatory.

- SCAO will not correct for the atmospheric dispersion within the scientific band pass of the instrument.
- SCAO Strehl ratio versus magnitude, observing wavelengths and seeing characteristics are provided in Table 8-2 and Table 8-3. These are given at the telescope focus, without taking into account static aberrations created by the instrument.

Maximum tip-tilt signal amplitude (mirror tilt)	Frequency
± 75”	<0.1Hz
± 10”	0.1-1Hz
± 1”	1-10Hz
± 0.1”	>10Hz

Table 8-1: Spectral Envelope of maximum Tip-tilt signal (mirror tilt) to be corrected by M6AM. On-sky tip-tilt is ~ mirror tilt/20.

	Wave band	K-band		H-band		J-band	
	Guide star magnitude	V=12	V=16	V=12	V=16	V=12	V=16
seeing, τ_0, L_0 @ 0.5µm	0.53”, 3ms, 25m	55	30	34	12	16	2
	1”, 2ms, 25m	25	10	8	1	1	0.08

Table 8-2: SCAO Strehl ratio (%) with the visible wavefront sensor

	Wave band	K-band		H-band		J-band	
	Guide star magnitude	K=9	K=12	K=9	K=12	K=9	K=12
seeing, τ_0, L_0 @ 0.5µm	0.53”, 3ms, 25m	57	33	37	14	17	3
	1”, 2ms, 25m	27	14	10	3	1	0.2

Table 8-3: SCAO Strehl ratio (%) with the infrared wavefront sensor

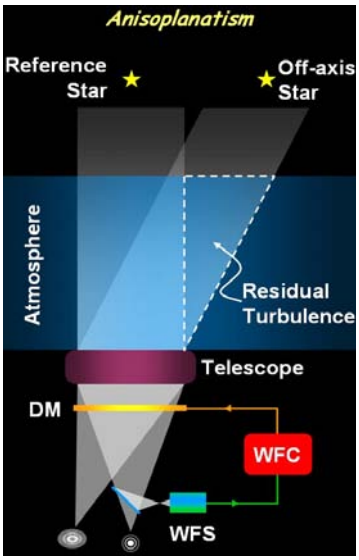

Figure 8-3: Limited corrected FoV due to anisoplanatism in the SCAO concept

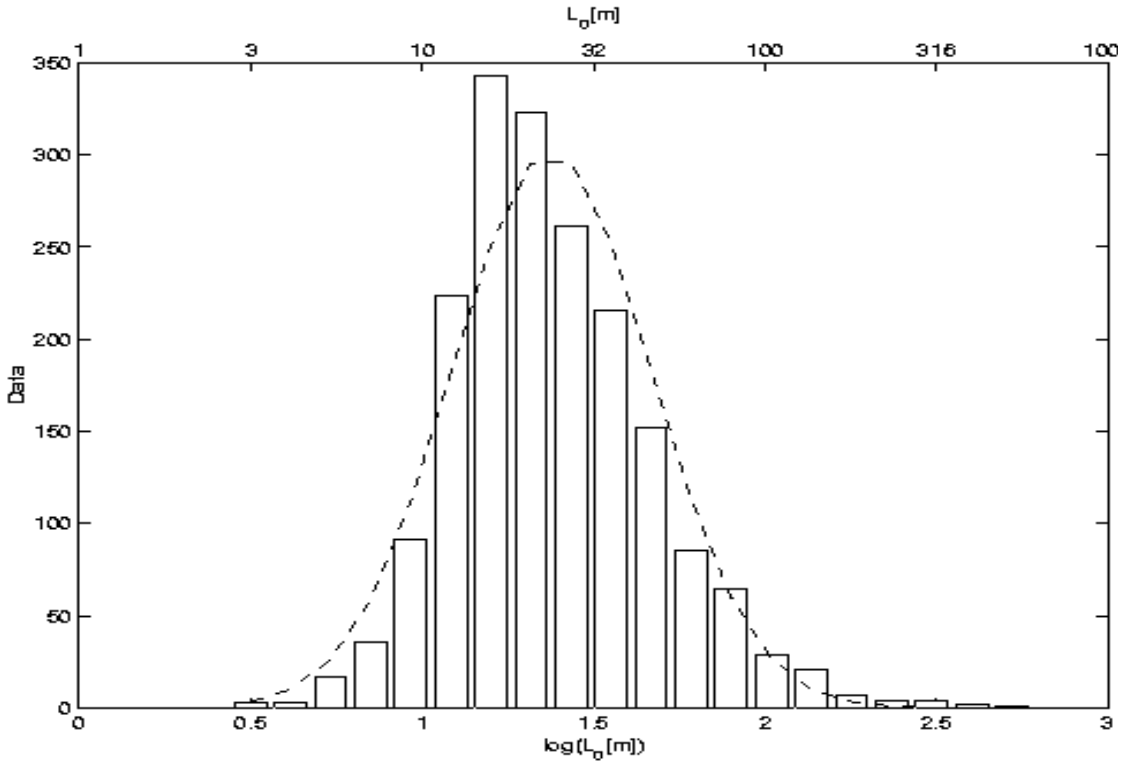

Figure 8-4: Statistical distribution of the outer scale

8.2.1.2 Implementation Concept

The SCAO concept is based on four key elements:

- The M6AM unit
- The Shack-Hartmann visible wavefront sensor
- The Pyramid Infrared wavefront sensor (option)
- The Real Time Computer

8.2.1.2.1 M6 Adaptive Mirror unit

The M6AM unit forms part of the telescope optical train and is tilted with respect to the ground. It is therefore conjugated conjugated to A= + 48.8 m (center), B= + 552 m, C= - 475 m, with A, B, C as shown in Figure 8-5, with positive values “above” the primary mirror, negative ones “below”.

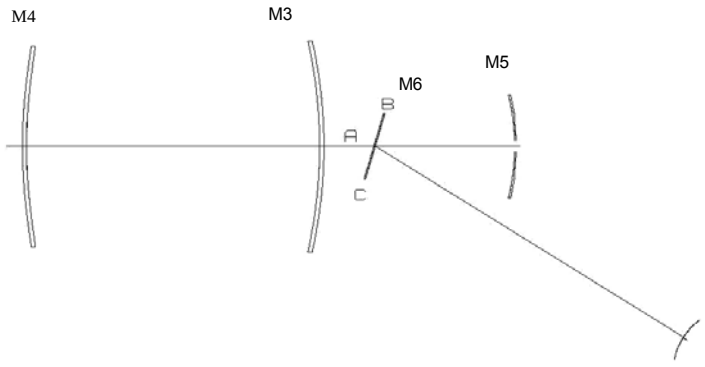

Figure 8-5: Conjugation altitudes of the M6AM unit

In addition to the Adaptive Optics correction, the M6AM unit will be capable of a tip-tilt motion about the mirror M6 vertex, in order to provide field stabilization with respect to the interface with instrumentation.

The mirror design and technology will preferably be based on a single, monolithic shell. A segmented geometry of the adaptive mirror, with six petals at 60^{o} and a maximum inter-petal gap of 15 mm may be considered as an alternative with a metrology for real-time phasing of the petals.

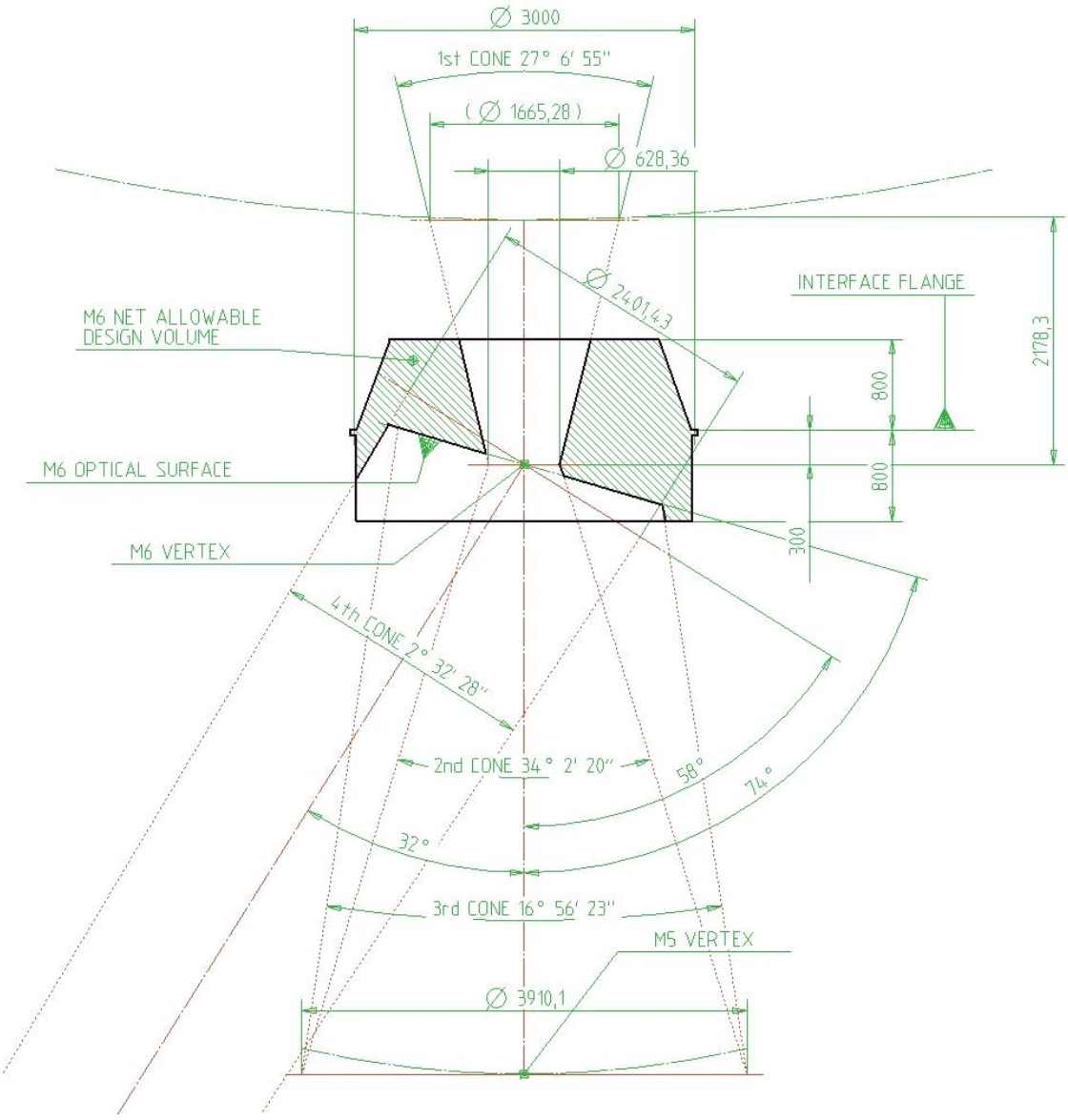

Figure 8-6: Geometrical characteristics of the M6 Adaptive Mirror

The detailed specifications of the M6AM unit are provided in RD23. The M6AM unit has a flat deformable mirror with an annular elliptical diameter of 2.6 x 2.4 m (tilted by 17º) and a linear central obscuration of 35%. The M6 actuator pitch is ~25 mm corresponding to ~1 m sub-aperture projected on the primary mirror of OWL leading to 6670 active actuators in the pupil - 98 actuators across the pupil-. This choice is a trade-off between the performance -from the experience acquired at ESO with NAOS and MACAO, the number of degrees of freedom and the technological steps to be achieved in the field of Large Deformable mirror (see section 8.2.1.4.3).

An important parameter of a deformable mirror is the total and inter-actuator mechanical stroke. For OWL this strongly depends on the outer scale of turbulence L_0 which reduces dramatically the amplitude of the disturbances and low spatial frequencies and therefore reduces significantly the mechanical stroke. For the specification of the mechanical stroke a pessimistic seeing of 1.5" (median value ~ 0.75" TBC) and L_0=100m (median value 25m) has been assumed at this stage: this is justified by the variability of these parameters during the nights and the rapid decrease of performance when the actuators are out of range. Nevertheless, these assumptions may be relaxed if it appears the M6AM requirements are too challenging. Assuming the von Karmann model is valid and adding 20% of stroke for the correction of the telescope residual aberrations, the total and inter-actuator mechanical stroke are respectively 90 µm and 6 µm excluding Field Stabilization.

The modal response time of the M6AM unit -for a stroke of ± 3µm- is specified to 1-2 ms at 90% respectively 95% of the command with a maximum overshoot of 10% of the command.

Figure 8-7 provides an overview of the control scheme of the M6AM unit and its interface to the external world in particular its interaction with the active optics. Actually, the Adaptive Optics will correct for all wavefront errors measured by the wavefront sensor. To avoid saturation of the AO WFS, it is necessary to off-load the large amplitude low temporal frequency to the active optics as shown Figure 8-7.

The M6AM unit will also be operated when AO is not required. In this mode the M6AM unit will provide either field stabilization or simply an optimum optical surface to the telescope. The flat vector of the M6AM is calibrated and can be applied to the unit in active mode. A local metrology loop makes sure the shape of the M6AM is maintained during operation.

Thanks to the outer scale effect the atmospheric tip and tilt is essentially inexistent and most of the Field stabilization specification comes from the telescope motion. The large amplitude requirements at low temporal frequency (<1Hz) is expected to be corrected with a tip-tilt stage while the high temporal frequencies might be corrected by the glass shell leading to a P-V stroke at the edge of 300µm. The dynamic aspect of the unit is currently under study.

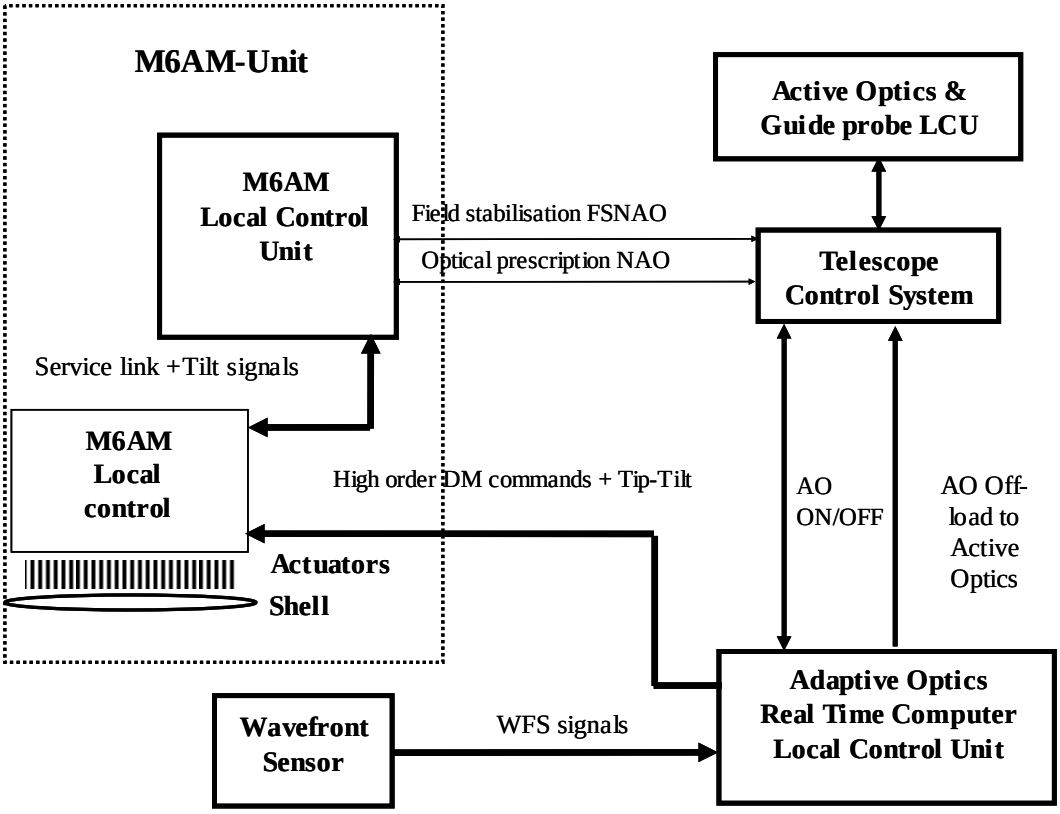

Figure 8-7: Control scheme of the M6AM unit and interface with the active optics.

8.2.1.2.2 Visible wavefront sensor unit

As a baseline, the wavefront sensor is a Shack-Hartmann with 97 x 97 sub-apertures and will be installed in the OWL adapter. A pick-up arm will allow acquiring the Natural Guide Star (NGS) within the central 2' FoV. The input optical beam is F/6.03 (2.920 mm/arcsec) and the pick-up arm will be located at 50-150 mm before the telescope focal plane. The pick-up arm will be equipped with a dichroic mirror reflecting the visible light toward the wavefront sensor and transmitting the infrared light for the instrument with a high efficiency (see Figure 8-8). The dichroic will be shaped in order to reduce the induced astigmatism when the convergent beam pass through it. The focus shift of the dichroic can be taken over by the science instrument or compensated by the WFS by changing the reference slopes. In general the non common path aberrations produced by the dichroic can be eliminated by applying static offset to M6AM measured with an independent method (for example phase diversity). This process has to be implemented for each science wavelength.

This pick-up arm will allow us to correct the differential atmospheric refraction between the observing wavelength and the effective wavelength of the wavefront sensor NGS. The tracking accuracy of the pick-up arm should be better than a fraction of the diffraction limit in J band: 2mas/5 = 0.4 mas corresponding to 1.2 µm.

Since the output focus of OWL is not telecentric, the pick-up arm displacement should have a concave trajectory such as the re-imaging of the M6 mirror always matches the lenslet array for all field positions. The amplitude of the angle along the trajectory (0-3 arcmin) is 0-2.1 degrees; the accuracy required on this trajectory is ±3" (corresponding to a pupil mismatch 1/50th of an actuator spacing).

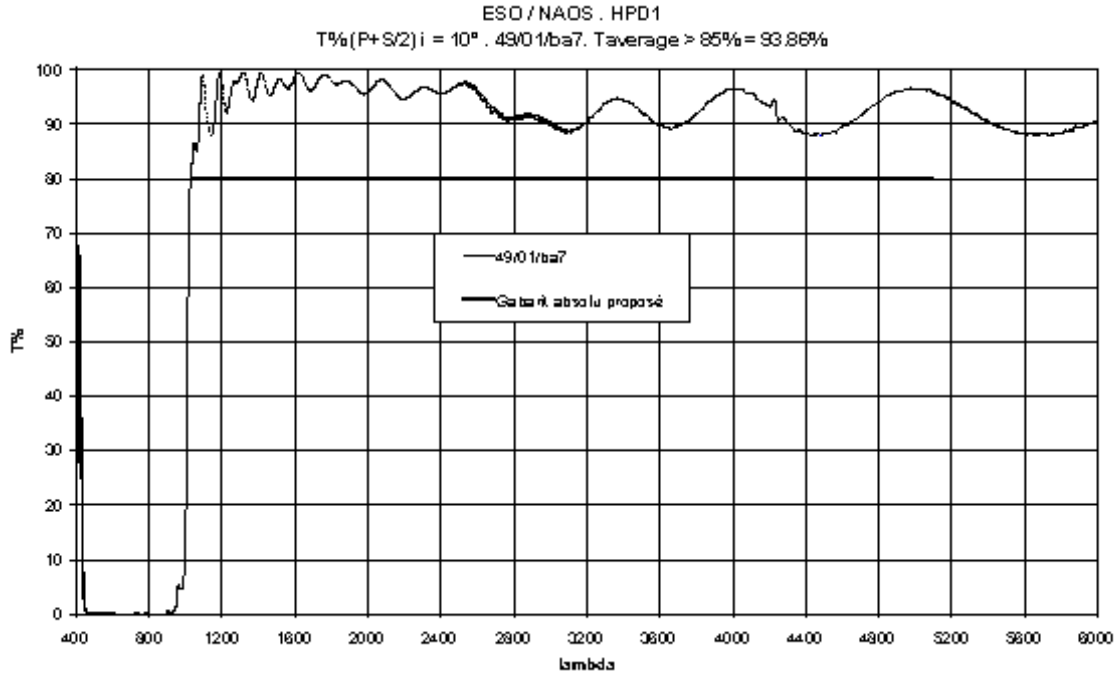

Figure 8-8: Transmission of the wavefront sensor pick-up dichroic

To correct for the convex field curvature of the OWL focal plane the wavefront sensor should be equipped with a focusing stage with a range provided in Figure 8-9.

To compensate for pupil rotation -M6 rotating with respect to the lenslet array- the wavefront sensor design will include an optical derotator. This optical derotator should have a rotation accuracy of ±0.02 degree (corresponding to a pupil mismatch of 1/50th of the actuator pitch). Wobble and run out of the optical derotator should be limited to another 1/50th of the actuator pitch. Pupil derotation by software is not envisaged at this stage because of the additional computing power required and complexity.

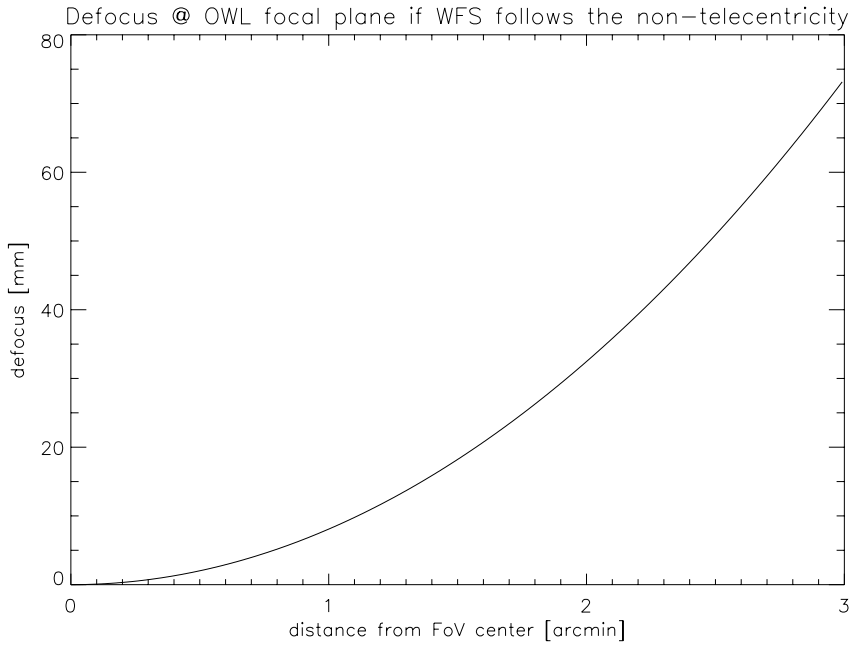

Figure 8-9: Defocus of the wavefront sensor versus field position

We expect that the mechanical flexures between the M6 Adaptive Mirror unit and the wavefront sensor pupil plane will contribute to another 2/50th of an actuator pitch maximum. The overall pupil mismatch will then be 1/10th of the actuator pitch leading to a Strehl reduction of 2% in K band.

The atmospheric dispersion within the band pass of the wavefront sensor - [450-900nm] - should be corrected with an Atmospheric Dispersion Compensator (ADC) for three reasons:

- spot elongation reduces the centroid accuracy in one direction
- spot elongation reduces the wavefront sensor linearity range
- tilt measurement will depend on star spectral type and will vary with zenith distance

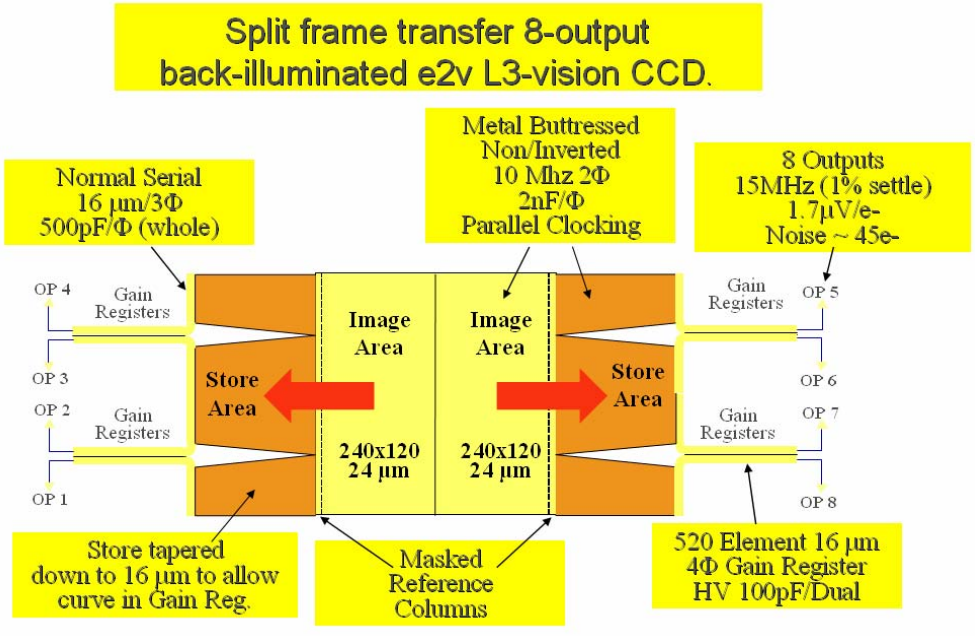

Figure 8-10: Technology concept of the WFS L3CCD detector

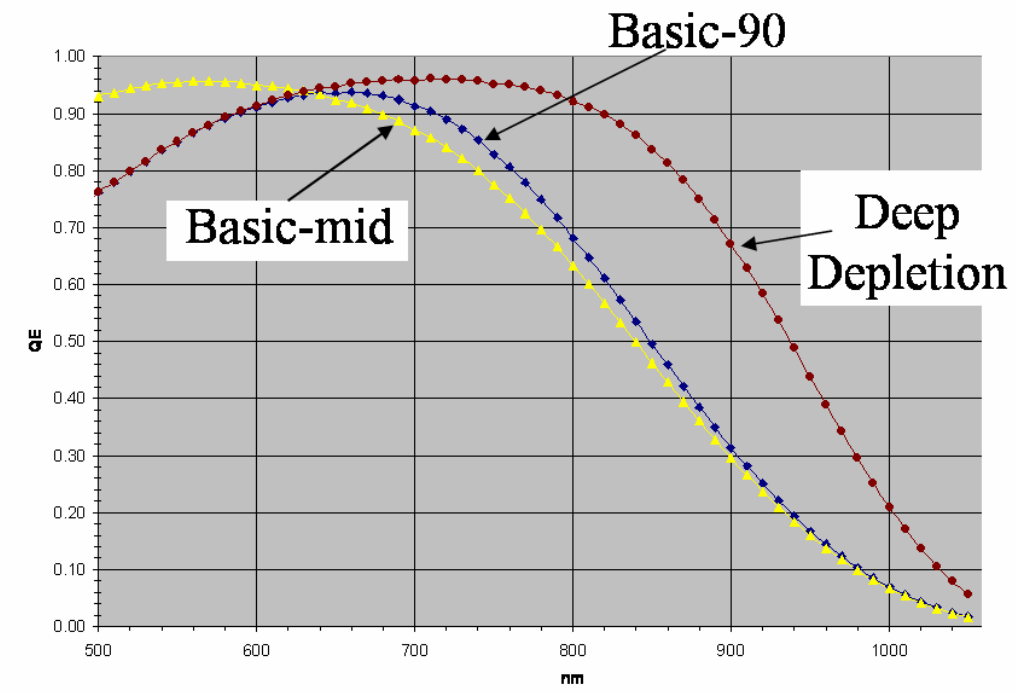

Figure 8-11: Quantum Efficiency with deep depletion enhancement in the red

To avoid pupil chromatism (and actuator-lenslet array mismatch), the ADC should be located very close to the pupil plane. For short integration time –few minutes- it may be acceptable to set the ADC to the zenith position at the start of the observation and not rotate the ADC during the observation.

For the wavefront sensor detector, one option is to make use of the CCD detector from E2V currently developed in the frame of the second generation Adaptive Optics system for the VLT - Figure 8-10. This detector (RD25) has 240 x 240 pixels and can be read up to 1.5 kframes/s using 8 outputs.

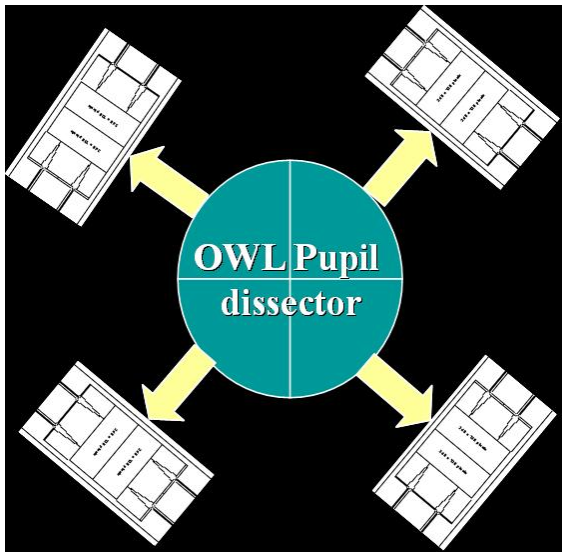

Figure 8-12: OWL pupil dissector for the Shack Hartmann wavefront sensor

It is based on the L3CCD technology using register amplification reducing the apparent Read-out Noise below $1e^-$. This detector technology has however amplification noise which is equivalent to a reduction in efficiency up to 2. A best effort contract is in place to complement

the excellent Read Out Noise (RON) performance with a deep depletion technology – see Figure 8-11- which will enhance the red response of such detector. Most of the Natural Guide Stars are very red and significant gain in limiting magnitude can be achieved with redder response.

However, the 240x240 pixels fast low noise CCD will not be large enough for the SCAO system of OWL. One way around is to implement on optical beam splitter which will send one quarter of the OWL pupil to each CCD detector equipped with its own lenslet array - Figure 8-12.

Alternatively, an extension of the present technology to 582x582 pixels - 6x6 pixels per sub aperture- possibly with a large pixel - 50µm - will need to be developed. For stability and compactness reasons, this option seems achievable and preferable at this stage.

The Shack-Hartmann will have 6x6 pixels per sub apertures with a pixel scale of about 0.4"/pixel (TBC) equivalent to a wavefront sensor FoV of 2.4" and to a magnification factor γ=0.03425. In this case the pupil size will be 29.1mm, sub aperture size 300 µm, the pupil re-imaging lens will have a focal length of 175 mm and the lenslet array focal length will be about $f_{\mu l}$=6mm (F/ratio=20).

Figure 8-13 shows an overview of the wavefront sensor design for SCAO.

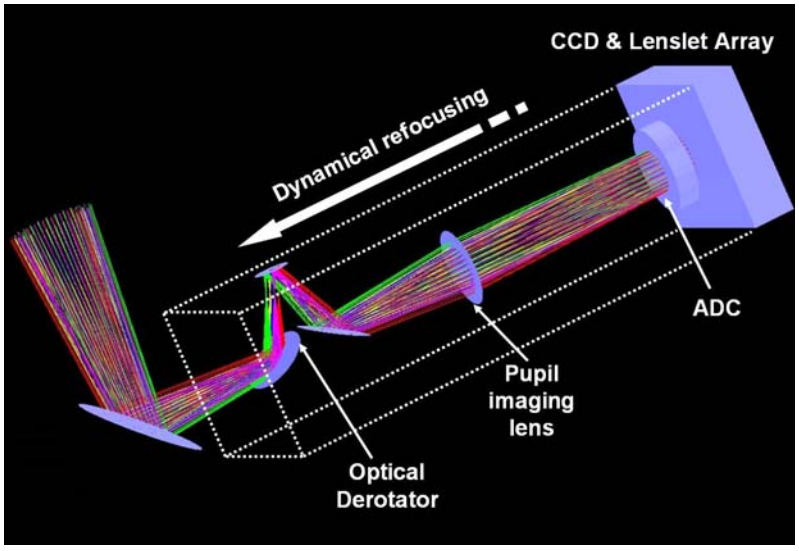

Figure 8-13: Shack Hartmann wavefront sensor concept

8.2.1.2.3 Infrared Pyramid WFS

The IR pyramid wavefront sensor is based on the concept of re-imaging the telescope pupil "filtered" by a refractive pyramid located at the OWL focal plane. In the near IR, the pyramid WFS benefits from the AO correction, and an (almost) diffraction limited spot is sent to the vertex of the pyramid, which makes the WFS process much more linear. This is not true in the visible, where non-linearities of the pyramid are much more severe (see RD26 for a more thorough analysis). As shown in 8.2.1.3, the performance if an (infrared) pyramid WFS is theoretically significantly better than that of a Shack-Hartmann, in terms of propagated aliasing. The depth of the aliasing "basin" is much larger, which is beneficial to some science cases (like high contrast imaging).A curvature sensing scheme was not considered because of the very high noise propagation coefficient for low order modes (f^{-4} on curvature, f^{-2} for SH).

The pyramid located at the focal plane acts as a 2-dimensional knife-edge spatial filter which produces four pupil images containing the information on the wavefront phase. The pupil sampling is 97 x 97 sub-apertures.

As in the Shack Hartmann wavefront sensor the infrared pyramid wavefront sensor is either installed on the OWL adapter or close to the instrument using reflection off the entrance window for instance. In case the infrared Pyramid wavefront sensor is installed in the adapter, a pick-up arm will acquire the NGS within the central 2 arcmin FoV. The input optical beam is F/6.03

(2.920 mm/arcsec) and the pick-up arm will be located at 50-150 mm before the telescope focal plane. The pick-up arm will be equipped with a dichroic mirror splitting the IR light (e.g. from 1.0 to 2.5 μm) between the wavefront sensor and the infrared instrument. The dichroic will be shaped in order to reduce the induced astigmatism when the convergent beam pass through it. The focus shift of the dichroic can be taken over by the science instrument or compensated by the WFS by changing the reference slopes. In general the non common path aberrations produced by the dichroic can be eliminated by applying static offset to M6AM measured with an independent method (for example phase diversity). This process has to be implemented for each science wavelength.

This pick-up arm will allow us to correct for the NGS field rotation and for the differential atmospheric refraction between the observing wavelength and the effective wavelength of the wavefront sensor NGS. The tracking accuracy of the pick-up arm should be better than a fraction of the diffraction limit in J band: 2mas/5 = 0.4 mas corresponding to 1.2 μm.

Since the output focus of OWL is not telecentric, the pick-up arm displacement should have a concave trajectory such as the re-imaging of the M6 mirror always matches the sub apertures or pixel of the pyramid wavefront sensor for all field positions. The amplitude of the angle along the trajectory (0-3arcmin) is 0-2.1 degrees; the accuracy required on this trajectory is ±3" (corresponding to a pupil mismatch $1/50^{th}$ of an actuator spacing).

To correct for the convex field curvature of the OWL focal plane the wavefront sensor should be equipped with a focusing stage with a range provided in Figure 8-9.

To compensate for pupil rotation -M6 rotating with respect to the IR detector- the wavefront sensor design will include an optical derotator. This optical derotator should have a rotation accuracy of ±0.003 degree (corresponding to a pupil mismatch of $1/50^{th}$ of the actuator pitch). Wobble and run out of the optical derotator should be limited to another $1/50^{th}$ of the actuator pitch. Pupil derotation by software is not envisaged at this stage because of the additional computing power required and complexity.

We expect that the mechanical flexures between the M6 Adaptive Mirror unit and the wavefront sensor pupil plane will contribute to another $2/50^{th}$ of an actuator pitch maximum. The overall pupil mismatch will then be $1/10^{th}$ of the actuator pitch leading to a Strehl reduction of 2% in K band.

As in the case of the Shack-Hartmann, and ADC is implemented to correct for atmospheric dispersion and be in a diffraction regime in closed loop in the Near Infrared (NIR) where the expected gain of the pyramid is expected.

As a baseline no pyramid modulation (i.e. fast shifting of the pyramid perpendicularly to the optical axis) is foreseen. Further theoretical and experimental studies are required to confirm this choice.

In order to keep low the thermal background given by refractive elements in the optical path of the WFS, the pyramid and the pupil re-imaging lens will be included in a cryostat with the IR detector.

The IR detector characteristics assumed for the performance estimate are those defined for the Calico-MUX development funded by Caltech and ESO (see Table 8-4). We expect that significant progresses can be achieved on this kind of component if resources can be invested in this development. With the current specifications four infrared detectors would be needed and a pupil dissection system should be implemented as in the case of the Shack Hartmann wavefront sensor - Figure 8-12. Alternatively a 240 x 240 format needs to be developed in order to locate all four pupil images on the same infrared detector.

The infrared pyramid wavefront sensor FoV is 2 arcsecs (5.8 mm) and a pupil re-imaging lens of 23.9 mm focal length is required for generating four pupils of 3.88 mm on the infrared detector – detector pixel assumed here is 40μm corresponding to one sub aperture-. The angle between the faces of the pyramid is 37 degrees in order to allow the four pupil images to be separated by ~40 pixels. The equivalent focal length of the pupil re-imaging lens is ~F/2, within the range of feasibility of normal lenses.

Figure 8-14 shown the implementation concept for the IR Pyramid WFS.

Parameter	Specification	Goal/Comment
Format	128 × 128	Design iterations to 512 × 512
Operating temperature	~ 80 °K	Goal cooling without liquid N2
Spectral range	0.80-2.3 μm	Actual spectral range of delivered FPAs will depend upon available assets but it will have NIR/SWIR cutoff wavelength
Pixel pitch	40 μm	-
Frame rate	800 Hz @ 128 × 128 1.5 kHz @ 2 × 2 window	8 outputs @ 3 MHz easily achieved
Read noise	< 1 e^- @ 250 fps < 5 e^- @ 500 fps < 7 e^- @ 800 fps	Prototype goals is < 5 e^- rms @ 800 fps
Well depth	TBD	Goal >> 10^4 e^-
Dynamic range	TBD	Goal > 5000
Quantum efficiency λ = 1.25 μm (J band) λ = 1.65 μm (H band) λ = 2.2 μm (K band)	 > 50% > 60% > 65%	Conservative numbers specified: with AR coating the quantum efficiency will be 10% higher than in non-AR coated devices
Uniformity	± 10%	-
Dark current	< 1 e^-/sec	< 0.1 e^-/sec
Operability	> 98%	> 99% goal
Cluster outages	-	Goal no cluster
Nonlinearity	-	Best effort goal: calibratable nonlinearity < 1%
Self emission dark count	Not to degrade the specified read noise by more than 10%	Expected to be <<1000 e^-/read
Power dissipation	< 100 mW	Goal < 40 mW

Table 8-4: Requirements for the Calico- Mux development funded by Caltech and ESO

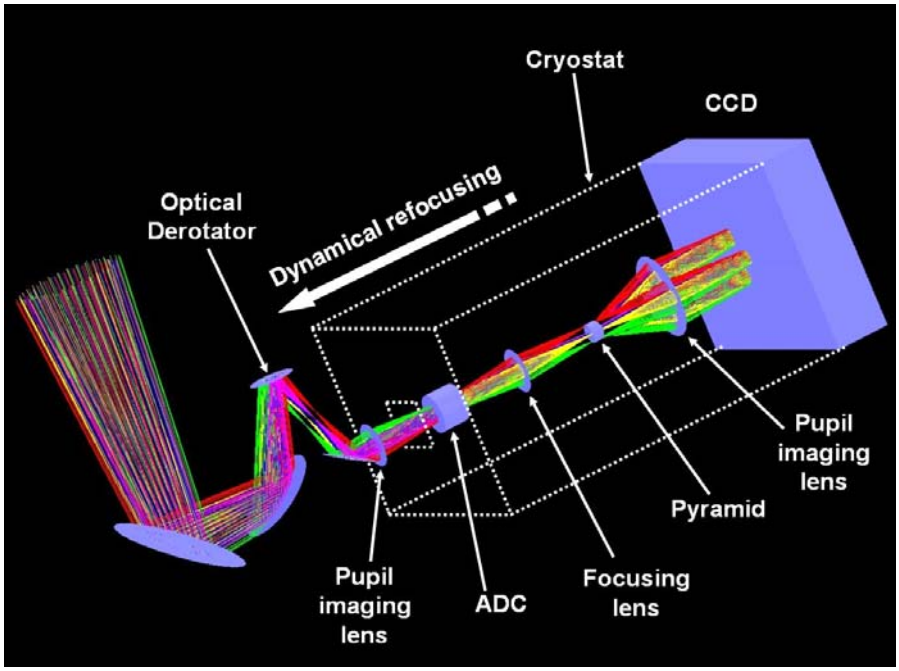

Figure 8-14: Pyramid wavefront sensor concept

8.2.1.2.4 Real Time Computer (RTC)

The proposed design for the Real Time Computer (RTC) is based on the SPARTA concept which is presented later in section 8.2.1.4.6. SPARTA is the platform that provides the RTC for all the AO instruments for OWL. In this paragraph we only present the relevant information for the SCAO system. More information can be found in [RD25].

SCAO is a single-sensor / single-mirror system with two architectural options: a Shack-Hartmann system and a Pyramid-based system. In both cases the deformable mirror will be the M6AM, which features a grid of 98x98 actuators. The detector technology is also common and it will be based on a 588x588 CCD, readable at 1.5 KHz. In both cases the loop frequency considered will be 500Hz and the maximum tolerable Real Time Computer delay will be of 10% of the loop frequency.

The architecture we will use is based on a hybrid structure where a chain of ***F**ield-**P**rogrammable **G**ate **A**rray* (FPGA) chips will create the hard real-time backbone that will compute the matrix-vector product, while on-board CPUs (Central Processing Unit) will monitor the system. The computational unit is based on a dual FPGA plus dual CPU system. The technology is available today: a board like this is already on the market, but it is not using the latest powerful chipset. We will assume that a new version of the same board uses the latest and most powerful chipset, commercially available but not yet integrated in off-the-shelf boards. Each CPU will feature a 10Gb/s optical input to receive the input stream. One FPGA in the board will be used to process the input stream, the second to process the matrix-vector computation, for one quarter of the input stream.

A fast internal bus (10Gb/s or more in the future) will let the FPGA chips exchange information. The last board will have an additional optical output to send the final results to the DM. The FPGA on this board will collect the results from all the other, compute the control signals and send the results to the DM.

The Real Time Computer delay of this architecture will be almost zero, i.e.: the computation can be completed before the next frame starts to be read-out. In this estimate we consider that FPGA-to-FPGA communication time is very fast: the amount of data that the chips need to exchange is rather low, consisting of partial controls.

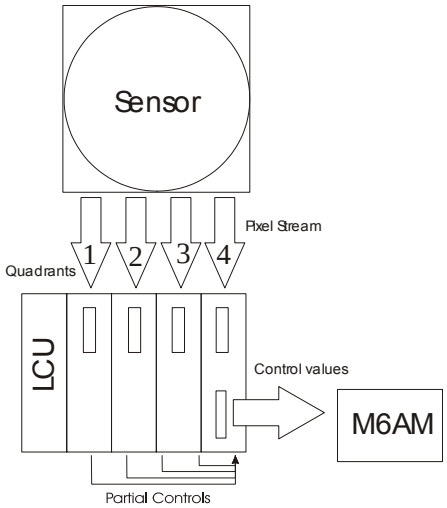

Figure 8-15: SCAO Shack Hartmann or Pyramid Real-time architecture

In the pyramid wave-front sensor case, the number of pixels to read out is smaller by a factor 4 to 9. Exploiting the faster read-out and using the same hardware, one can improve the RTC performance, i.e.: the computation can finish earlier by the amount of time saved in the read out. However, if one dimensions the Real Time Computer to complete in the same time as for the previous case (same performance) a significant saving can be achieved in the real time core, from 30% to 50% of the hardware cost, depending on the detector read-out architecture. While it is more difficult to assess what would be the effect on to the remaining functions a reasonable estimate is that hardware cost savings of a pyramid-based system will be around 15% to 20%.

Architecture of the Real-Time Control Computer is provided Figure 8-15.

8.2.1.3 Predicted performance

A detailed analysis of the SCAO performance based on end-to end simulations as well as the assumptions and AO parameters are provided in RD25. Note that the SCAO performances provided here do not include yet all error sources -calibration errors, optical quality of the telescope, wavefront sensor and instrument optical paths, mis-registration error, atmospheric chromatism etc…- but only the pure AO performance part. In the SCAO mode, the impact of all error sources on the final SCAO performance can become significant. It is planned to perform a full error budget of the SCAO system during phase B.

8.2.1.3.1 Visible Shack Hartmann wavefront sensor

In the following we provide the performance of the SCAO using a visible Shack Hartmann wavefront sensor for both the “good” and “bad” seeing conditions” respectively r_0~20cm and r_0~10cm -0.53” and 1” seeing at 0.5 µm.

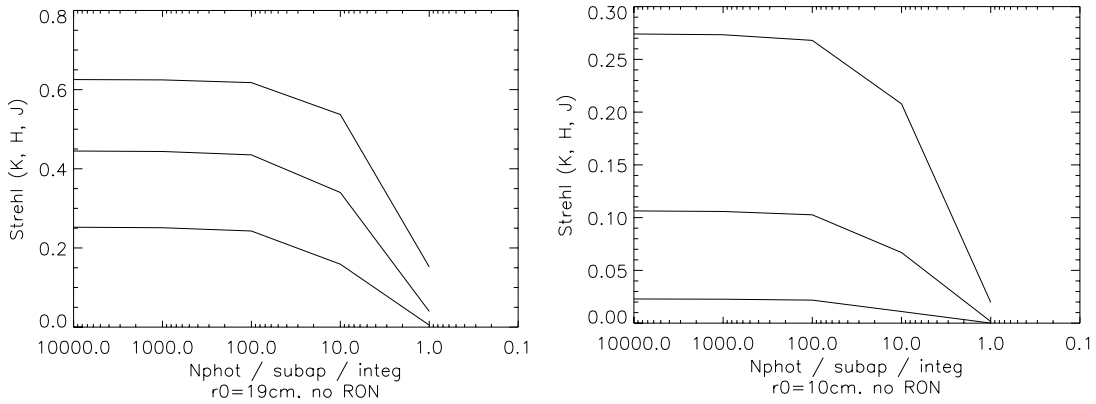

Figure 8-16: Strehl vs. Magnitude for the SH-WFS (without RON), in K, H, J bands (top to bottom), for the good seeing model (left) and bad seeing model (right). Results are on-axis

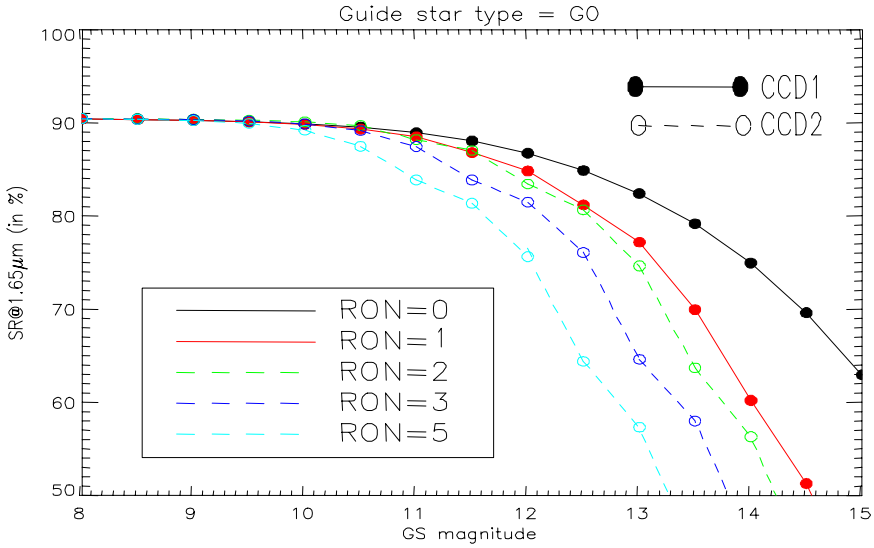

Figure 8-17: VLT Planet Finder performance for different Readout Noise

Figure 8-16 provides the Strehl versus the number of photons per sub aperture and integration time –frame rate is 500Hz- for different NIR wavelengths. 1 Photon/sub aperture/frame

corresponds Mv=17.5 for a G0 star. This limiting magnitude and the Sr(K)=15% are quite consistent with the performance obtained with the MACAO and NAOS systems under good seeing conditions. MACAO using Avalanche Photo Diode (APD) detectors without Readout Noise should in principle behave like SCAO with the L3CCD for low magnitude stars – note that the Quantum Efficiency band pass, especially the red response, and the peak response is higher for the L3CCD than for the APD but as mentioned earlier the excess noise due to the amplification gain limits this advantage. Extensive simulations performed in the frame of the VLT Planet Finder study show that no Readout Noise is always better than excess noise and not fully optimized red response.

Figure 8-18 provides the Ensquared Energy versus the pixel size for near infrared wavelengths in case a spectroscopic mode is intended to be used behind SCAO. From these curves, we see that 50% of the energy can be concentrated into a pixel of 10 mas under good seeing conditions.

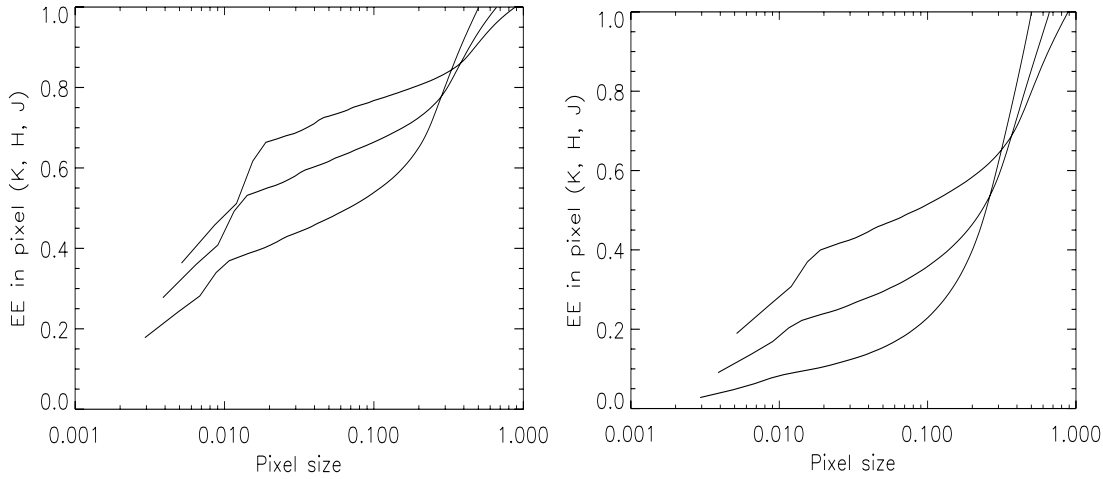

Figure 8-18: Ensquared Energy versus pixel size (K-H-J; top to bottom), for good seeing (left) and bad seeing models (right). Bright stars are considered.

The anisoplanatism effect for our two considered atmospheric models can be seen in the curves below. We can see that in good seeing, 50% of the Strehl is lost in the K band at a distance of ~30'' (radius). In bad seeing, this number drops to less than 20'' (radius).

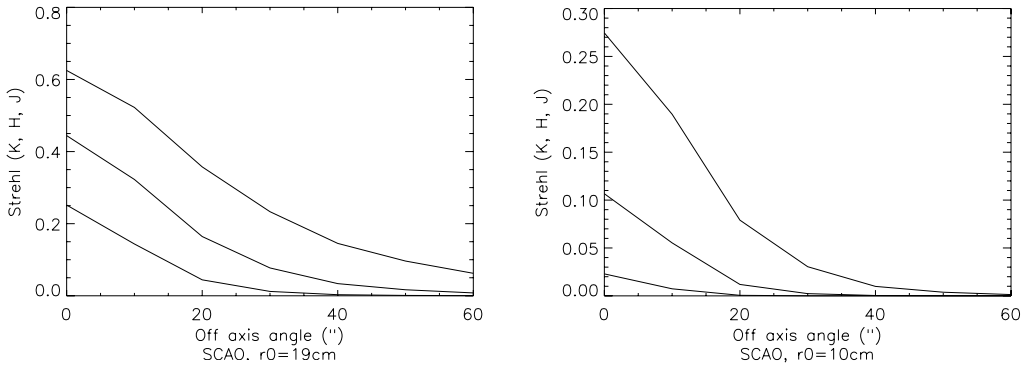

Figure 8-19: Affect of anisoplanatism on the performance of the SCAO system, in K, H and J bands (top to bottom), in good seeing model (left), and bad seeing (right).

8.2.1.3.2 Infrared Pyramid Wavefront sensor

In the following we provide the performance of the SCAO using an Infrared Pyramid wavefront sensor for both the "good" and "bad" seeing conditions" respectively r_0~20cm and r_0~10cm - 0.53" and 1" seeing at 0.5 µm: Figure 8-20. Two cases have been studied: infrared detector

without readout noise and with a more realistic 5e$^-$ readout noise. The performance curves show a dramatic drop of the Strehl for faint magnitude star due to the Readout noise. Note that the sky background in H band –mH~14.5- will be the limiting factor in the case of a noiseless near infrared detector. Some improvements is expected for faint stars in the case of the RON=5 if a larger pixel scale is used – this was used for NAOS to increase the limiting magnitude with the two set of lenslet array-. The Strehl ratio performance using the pyramid wavefront sensor is slightly higher than in the case of the Shack Hartmann wavefront sensor. Figure 8-21 shows the corrected Point Spread Function (PSF) image with the reduction of the aliasing in the area corresponding to the 1/actuator pitch. Figure 8-22 provides the Ensquared Energy after correction quite similar to the Shack Hartmann case.

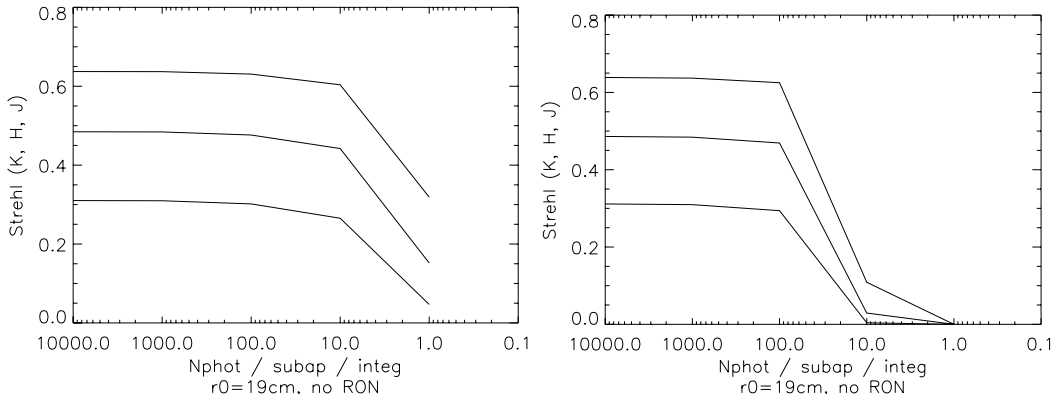

Figure 8-20: Strehl vs. Magnitude for the IR PYR (without RON on the left, 5e- ron rms on the right), in K, H, J bands (top to bottom), for the good seeing model. Results are on-axis.

Figure 8-23 shows the simulated deformable mirror shape during closed loop operation. The artifacts near the centre are probably due to diffraction effects in the area close to the telescope central obstruction. The exact explanation for this problem is not yet fully understood at this stage. We intend to continue the detailed simulations activities in the frame of the ELT design study as well as some complementary work on our High Order Test bench developed in the frame of OPTICON-JRA1.

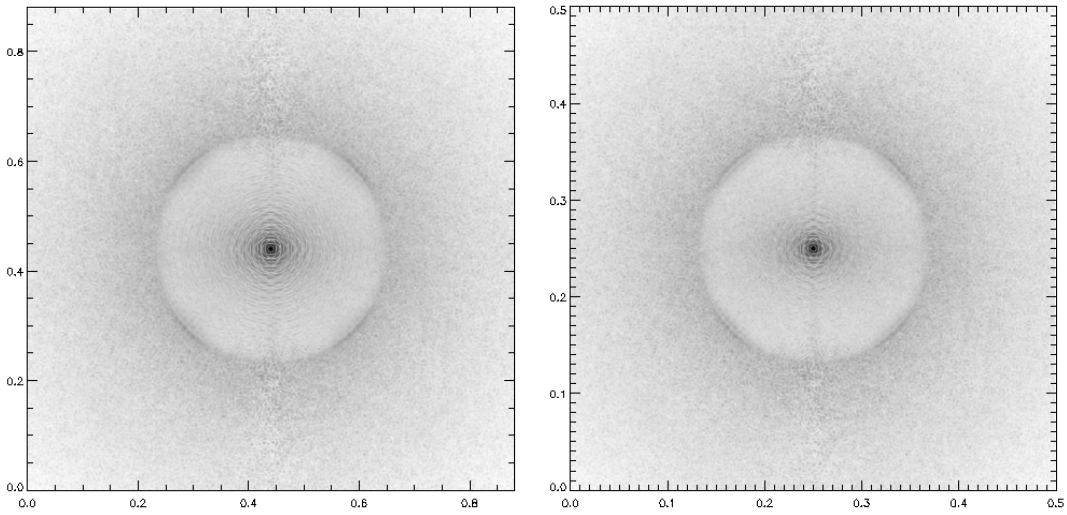

Figure 8-21: Long Exposure PSF with 10000 ph/subap/integ (bright NGS), for the K band (left) and J-band (right). Both pictures are on-axis. Stretch is logarithmic.

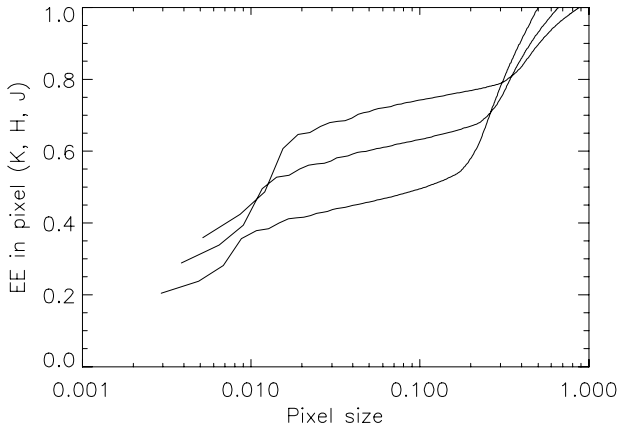

Figure 8-22: EE vs. pixel size, in the K, H and J bands, good seeing, and bright guide star.

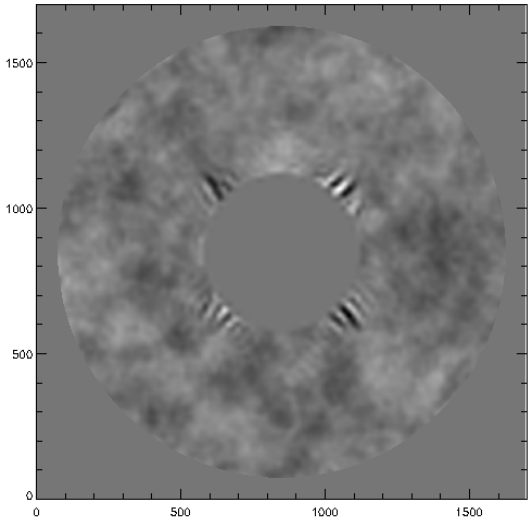

Figure 8-23: Shape for the DM during closed loop. The "spikes" near the telescope central obstruction, created by diffraction effects on the PYR WFS.

8.2.1.3.3 Performance at 10 microns and beyond

In the frame of the Mid-Infrared imager instrument (TOWL) presented in section 12.2.3.6, the performance of SCAO has been simulated.

Figure 8-24 provides the Strehl versus observing wavelength for good seeing conditions and a bright reference star. We see the Strehl ratio is essentially above 90 % longward of 5 micron. Figure 8-25 shows the Point Spread Function (PSF) at 2.2, 5 and 10 microns. Important point to note is the significant gain of contrast in the so-called “circle of correction” close to the PSF peak when the Strehl ratio is at 95%.

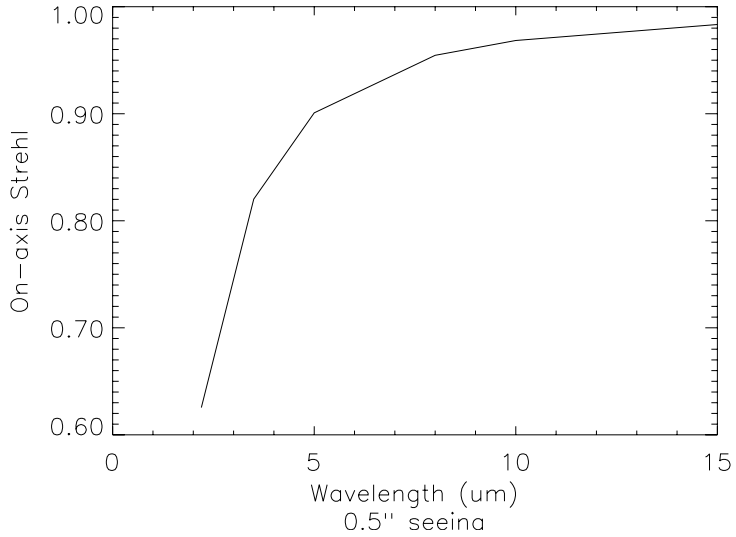

Figure 8-24: On-axis strehl versus wavelength for a bright reference star

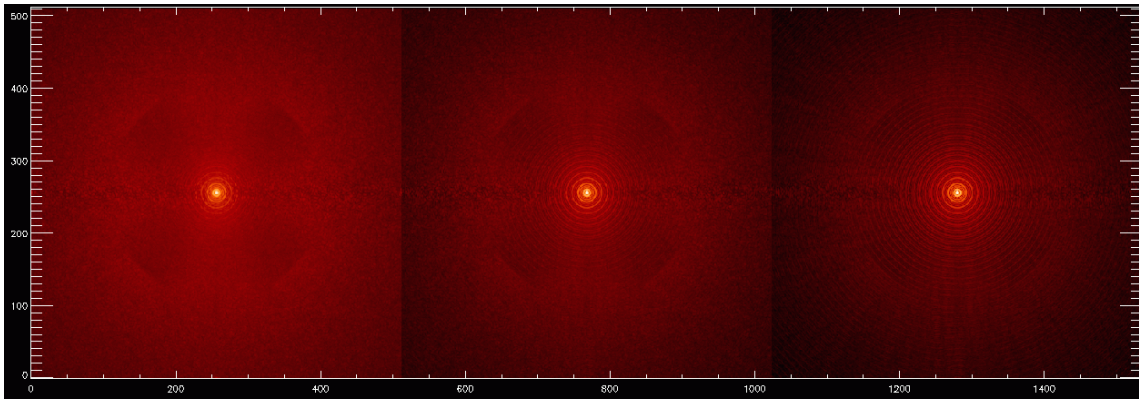

Figure 8-25: Point Spread Functions obtained with SCAO. From left to right 2.2, 5 and 10 µm. Good seeing conditions, bright on-axis star.

8.2.1.3.4 Effect of the outer scale of turbulence on performance

Apart from the seeing and atmospheric correlation time τ_0, the outer scale of the turbulence is an important parameter to be considered for the simulation and AO design parameters in the case of an ELT.

Assuming a von Karmann model the outer scale of the turbulence essentially reduces the amount of turbulence to be corrected at low spatial frequencies. The direct effect is to dramatically reduce the deformable mirror stroke requirements at high spatial scale as shown in Figure 8-26 in the case of very bad seeing conditions.

Figure 8-27 shows the SCAO performance depending on the Outer scale in the case of the SH WFS system.

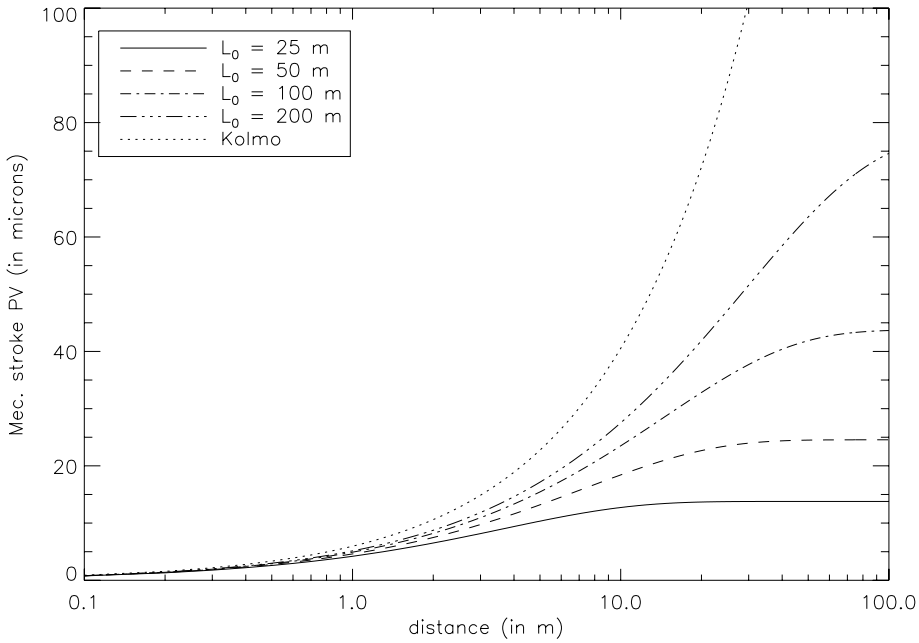

Figure 8-26: P-V DM mechanical stroke requirements versus spatial frequency for a seeing of 1.5" and different outer scales (Courtesy, T. Fusco-ONERA)

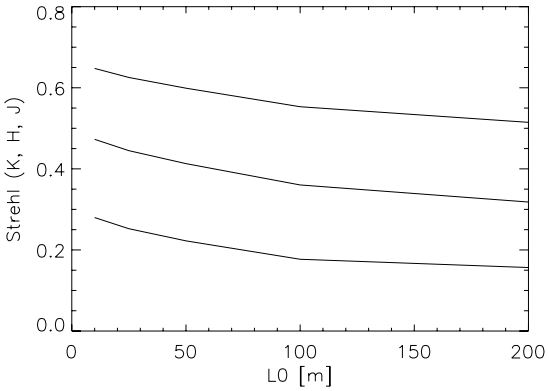

Figure 8-27: Strehl (on-axis) vs. L0, for the SH based SCAO system (good seeing), in K, H and J bands

8.2.1.4 Near-Term development plan

8.2.1.4.1 Modelling and Simulation

First order simulations have been performed to estimate the SCAO performances in near Infrared with a 98x98 actuator systems. Extensive parametric simulations remain to be done to tune the design parameters in particular:

- Optimization of the Shack Hartmann wavefront sensor geometry fitting the M6AM geometry (Circular, hexagonal, squared)
- Optimization of the Shack Hartmann wavefront sensor pixel scale and FoV
- Effect of wavefront sensor frame delays (depending on the wavefront sensor detector readout scheme) on performance for both wavefront sensors depending on the median τ0
- Study of the effect of the Deformable mirror- wavefront sensor lateral pupil matching for both the pyramid and Shack-Hartmann wavefront sensor
- Study of the diffraction effect on the Pyramid wavefront sensor

- Study of the pupil segmentation and cophasing error effects on the AO loop on performance
- Study of the variable M6AM conjugation altitude effect on the performance
- Optimization of the infrared wavefront sensor depending on the detector Readout noise and sky background
- Full error budget of the SCAO system
- Analysis of the differential atmospheric dispersion correction accuracy
- Analysis of the residual image motion after field stabilization in SCAO loop
- Effect of the atmospheric dispersion within the band pass of the wavefront sensor equipped with an ADC.

8.2.1.4.2 AO Concept and design

The detailed implementation of the SCAO wavefront sensors (visible Shack-Hartmann and Near Infrared Pyramid) into the OWL Adapter-rotator remains to be developed during phase B. Requirements and constraints for active and adaptive optics and for instruments need to be studied carefully and trade-offs analyzed in the context of the planned optical design iteration at the start of Phase B.

Accuracy of the wavefront sensor “Field Selector” functionality needs to be carefully analyzed. This is crucial in SCAO for the differential atmospheric dispersion compensation, for the Field stabilization and for the mosaicking capabilities.

The optimum wavelengths for the SCAO IR wavefront sensor s and the instruments will need to be reassessed in view of the selected instruments using SCAO: Commissioning instrument in Near Infrared, TOWL, first correction stage of EPICS, etc. This may require more than two SCAO wavefront sensors dichroic configurations in the adapter rotator. In some cases, like for the IR instrument TOWL, there might be some advantages to implement the wavefront sensors very close to or in the instrument itself to minimize the number of warm optical surfaces (for instance the dichroic as entrance window). The effect of the differential atmospheric refraction between the wavefront sensor NGS effective wavelength and the instrument observing wavelength may drive also these choices.

Compromises between the length of the wavefront sensor / instrument non-common optical path and the stability of the pupil matching should be studied. To correct for flexures, an internal metrology system may be required between the wavefront sensor and the instrument.

A feasibility and conceptual design for the M6AM is being developed based on the specifications provided in RD23 and will be available in the coming year. An extensive discussion of the currently available large deformable mirror technology is given in 8.2.1.4.3 based on the feasibility and conceptual design study performed for the VLT Adaptive secondary. The development of the VLT Adaptive secondary is an important element of our road-map securing and promoting this key technology in view of OWL.

The volume constraints due to the tilt of the M6AM unit may need special attention in particular for the positioning of the edge actuators. The large stroke and inter-actuator stroke requirements combined with the higher density of actuators will be carefully analyzed both in the frame of the feasibility study and the ELT design study. A trade-off between the glass shell thickness and material, the actuator force required and the power dissipated by the actuators will also be done. The field stabilization amplitude requirements – ±75” at f<0.1Hz – should be analyzed. Whether this should be produced by the shell itself or by a second stage tilt-tilt unit needs further investigation.

In case the required density of actuator appears not to be achievable in the time and budget allocated, a fall-back solution is envisaged, based on M6AM acting as a woofer plus a second stage post-focal deformable mirror (based e.g. on piezo technology with actuator spacing of ~ 4mm, extension of the VLT Planet Finder Deformable Mirror).

As in the case of the VLT Adaptive Secondary, a test facility will be designed for the extensive testing of the M6AM in the laboratory, first as a single unit then together with the rest of the

SCAO in closed loop. This test facility should also allow the testing of the other first generation AO modes like the GLAO and the MOAO modes (see section 8.2.2 and 8.2.3).

Simulations on both Shack Hartmann and pyramid wavefront sensors will need to be cross-checked experimentally on a dedicated test bench. The diffraction effect at the edge of the telescope central obstruction of OWL with the pyramid wavefront sensor will need to be studied experimentally. The segmentation and cophasing error effects on the final AO performance will also benefit from some experimental validation. The High Order Test bench developed in the frame of the VLT Planet Finder and OPTICON-JRA1 will be a good basis for these studies.

Accurate calibration of an Adaptive Optics system is crucial especially when using large deformable mirrors. In particular the measurement of the interaction matrix will require more investigations. Several solutions are being envisaged at this stage also in the frame of the VLT Adaptive secondary:

- Insert a calibration source at the focal plane close to M6 at the location of the central obstruction
- Perform synthetic interaction matrix using measured influence functions of the M6AM in the laboratory and calibration of the WFS optical path
- Perform on-sky interaction matrix measurements

Even if the synthetic interaction matrix is the most attractive solution (noiseless, simplicity, no calibration time required), it still has to be demonstrated that the accuracy of the models (DM and WFS) can be high enough to ensure the expected performance. In particular, the amplitude of the off axis static aberrations might be a problem.

Regarding the experimental estimation of the interaction matrix, novel techniques have to be investigated in order to deal with the new issues that we have to face:

- There is turbulent noise either because the calibration is performed on sky or because of the telescope internal turbulence. Indeed, the use of the calibration source at the focal plane may be limited by the internal turbulence of the telescope over long distances (M6AM unit-wavefront sensors) as already observed with MACAO at the VLT in which the calibration source is about 10 m from the wavefront sensor. Telescope flexures and optics drifts (temperature, gravity…) might also bias the measurement. Regarding the calibration of M5, it will have to be performed on sky since no artificial source will be available upstream.
- The calibration time may be long because of the large number of degrees of freedom.

Several methods are being investigated through simulations and laboratory tests as well as on sky tests when possible. The different schemes aim at minimizing the noise and bias on the measurement in order to optimize the quality of the reconstructor. Several modal bases (expansions) are under study to maximize the signal to noise ratio:

- Zonal: classical actuation of each Deformable Mirror electrode one after the other
- Hadamard: modal actuation of all electrodes at a given control voltage in order to maximize the signal in the Deformable Mirror space. This method is optimal for infinitely linear wavefront sensor. Another strong advantage is that the calibration time is independent of the system dimension for a given sub aperture size.
- System modes / mirror modes able to maximize the Signal to Noise within the dynamic range of the deformable mirror and of the wavefront sensor.
- Atmospheric modes: Zernikes, Karhunen Loeve
- Zonal-sparse basis using the sparseness of the influence function of the high order DM.

Using those modal bases, several techniques are foreseen and being compared:

- Open loop fast DM actuation, which allows freezing the disturbances between modal push and pull and thus avoid the turbulent noise as well as any low frequency effect as drifts, DM creep, etc…

- Open loop DM modulation and demodulation by homodyne or Fast Fourier Transform detection. The stimulus power is concentrated on a single frequency beyond the modal atmospheric bandwidth. Low frequency effects are canceled out and it allows for multiplexing. This way, several modes can be measured at the same time and time can be saved.
- Closed loop calibration. Dynamic bias is applied as offset on the wavefront sensor signal. The DM command is measured as a response to this bias and therefore the reconstruction matrix (or control matrix) is measured directly. This technique presents the strong advantage to calibrate the system around its operating point. Nevertheless, the turbulent noise instead of affecting the wavefront sensor measurements is translated to the DM closed loop command. To overcome this, we can couple the closed loop measurement to the modulation technique, the modulation being applied to the WFS offset. This calibration scheme is iterative and it has to be demonstrated that it converges well under nominal conditions of noise. To avoid an iterative process and keep the advantages of the closed loop scheme (wavefront sensor working in its linear regime), the bias could be applied at the DM level at a frequency well above the AO system bandwidth. The loop could also be closed on the Tip and Tilt modes only.

Furthermore, there is a key issue related to calibration. The pupil mis-centering may have a strong impact on the system performance and must be addressed properly. Indeed, for high order AO systems such as OWL, the tolerance in diameter ratio is very tight.

One must distinguish two different cases:

- A mismatch between the DM and the wavefront sensor, that is to say that the image of the DM in the lenslet array plane is shifted or rotated with respect to the lenslet geometrical pattern. This can affect the system performance if the misalignment was not calibrated in the Interaction Matrix (IM). A typical unacceptable shift is 10% of a sub aperture size.
- A misalignment between the telescope pupil and the whole adaptive optics system. This yields vignetting and therefore a non uniform illumination of the lenslet array inducing an error in the slope computation of the poorly illuminated sub apertures.

The impact of a pupil misalignment can be minimized in two different ways:

- Take it into account into the control matrix of the system by simulating it or by measuring its effect on the IM.
- Correct for it either statically (if it does not evolve with time during the observation) or dynamically by moving physically the pupil. Some solutions have already been investigated on the MACAO projects and the VLT Planet Finder design study.

8.2.1.4.3 AO key elements status and development

Introduction to the large deformable mirror technology

The concept of thin shell and force actuators is one of the most promising in the field of large deformable mirrors; the largest deformable mirror have been built/designed with this technology. A 642mm diameter convex secondary mirror with 336 actuators has been developed and is being used by the MMT (Multi-Mirrror Telescope, Mt Hopkins, Arizona), while the two 911mm diameter and 672 actuators concave secondary mirrors of the LBT (Large Binocular Telescope, Mt Graham, Arizona) are being integrated (at the time of this writing). A similar design is being studied for feasibility for one of the VLT Unit Telescope; the deformable secondary design is 1120mm in diameter and offers 1170 actuators for adaptive correction Figure 8-28, Figure 8-29 and Figure 8-30.

Figure 8-28: Conceptual design for the 1120mm diameter, 1170 actuators VLT deformable secondary mirror.

MMT-LBT-VLT large Deformable mirror concepts

These mirrors are composed of 3 basic elements: a back-plate, holding the voice-coil force actuators, a reference body and the thin shell. Each voice coil applies a force to a corresponding magnet glued onto the back face of the thin shell. A ring of conductive material (chrome, aluminium, gold…) is deposited around each magnet and is mirrored on the reference body. These two opposite coatings constitute a capacitance used as space sensor. The reference body being a calibrated optical surface, an equal spacing for all capacitive sensors insures a high optical quality on the shell.

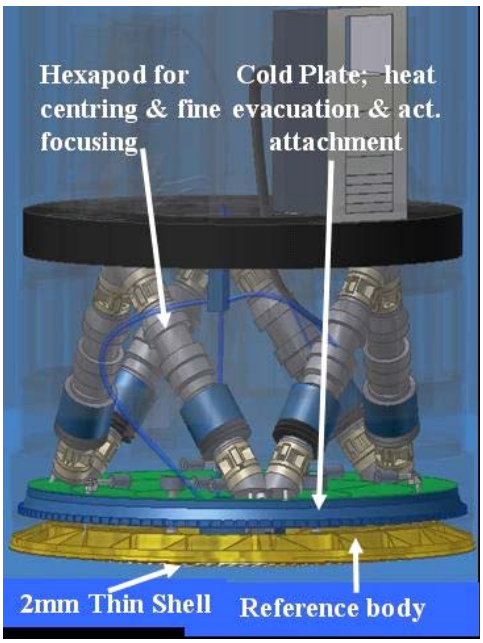

Figure 8-29: Force/thin shell mirror (VLT design) based on Cold plate, Reference body & thin shell. A Hexapod, attached to the cold plate, provides fine focusing & centering (Courtesy, Microgate/ADS, Italy)

A typical gap of ~50 μm is proposed for the VLT and provide air damping between the shell and the reference body. Increase of this gap to 200 μm is being studied in the frame of the ELT design study to meet the higher stroke requirements. An internal control loop at 80 kHz insures that the force applied maintains the capacitive sensor to a constant gap

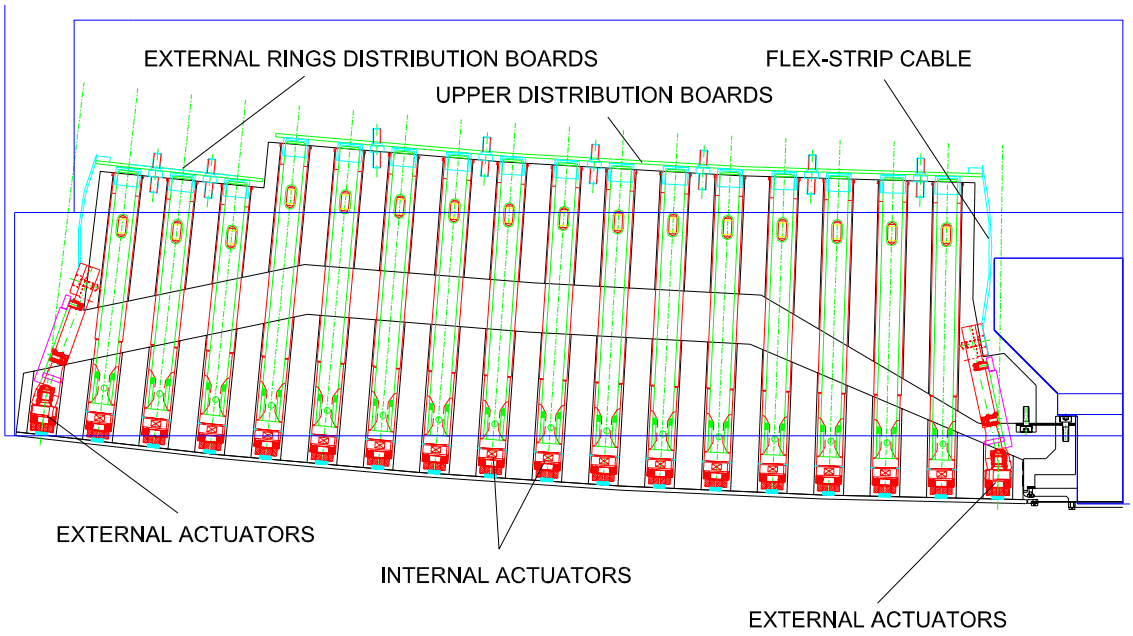

Figure 8-30: Closer view of the actuator distribution on one half of the DSM (Courtesy Microgate/ADS)

The back plate has two functions: holding the voice coil actuators and evacuating heat dissipated by the coils with the help of an integrated cooling fluid circuit. Therefore, the material used must combine rigidity and high thermal conductivity. It is made of aluminium for good heat conductivity and to reduce weight (compared to copper). Alternative materials like SiC are being studied in the frame of the ELT design study. The cooling circuit is divided in several sections in parallel providing cooling to an equivalent number of actuators; this insures more homogenous cooling & temperature across the cold plates & voice coil actuators. The back plate is usually cooled in series after the electronics crates (first components to be cooled) and before the Hexapod actuators (if present).

The reference body can be a conventional, thick, ULE or Zerodur optical component, with the exception of the numerous cylindrical openings allowing passage for the actuators. These are aligned toward the centre of curvature of the mirror (if it has optical power). More recent designs (VLT Deformable Secondary Mirror) explored with industrial partner a light-weighting scheme (50-60% light-weighted Zerodur or SiC) to reduce the weight of the complete assembly (realistic without being a huge cost driver). SiC offer the added advantage of being extremely rigid compared to ULE or Zerodur. Open-loop stability of the optical surface of the shell is directly linked to the reference body intrinsic rigidity, and a good optical quality of the reference body front surface insures an easy integration of the deformable mirror; constant gap on all capacitive sensors define a shell front surface perfectly matching the reference body figure. The light weighted option for the reference body is of prime interest for the M6AM unit in case the Field Stabilisation is performed with a second stage tip-tilt unit.

Note that the front surface of the reference body can be “rough”; the requirement is not strictly speaking the one of an optical surface. Image quality can be specified from the largest linear scale down to a fraction of the inter-actuator spacing. An increased surface roughness even improves the deposition of conductive coatings for the capacitive sensor.

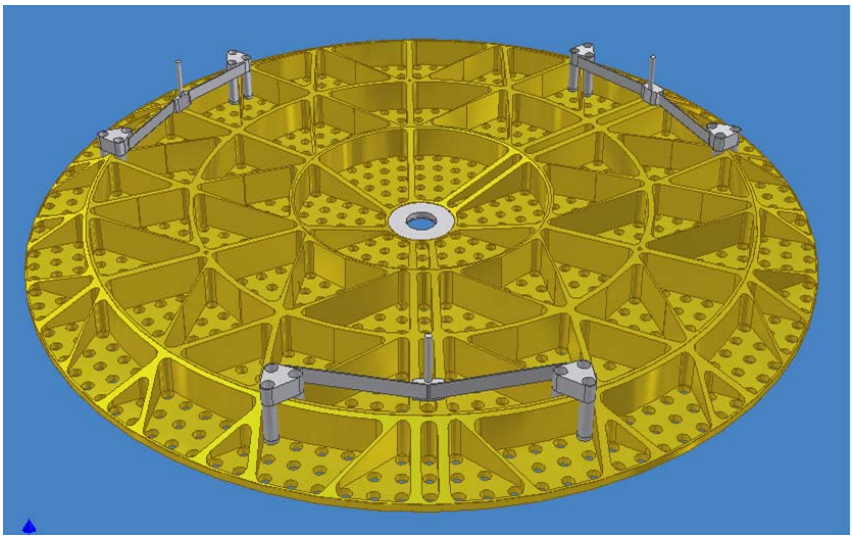

Figure 8-31: Light weighting scheme of the VLT design Reference Body; estimated weight (Zerodur) is 27kg while a monolithic design would lead to 130 kg (Courtesy Microgate/ADS, Italy)

Other materials can also be considered, e.g. SiC (Boostec, ECM CeSiC) providing high stiffness and proper optical quality polishing possibility. Price inquiries have been launched; trade-off areas for cost are the following:

- High surface roughness €↓
- No nickel plating for low roughness optical surface €↓
- Ease/low-risk of light weighting scheme compared to Zerodur €↓
- Lower large scale optical quality €↓
- Long polishing (hardness) €↑
- Costly fabrication €↑

To specify a lower optical quality on large scale would reduce price but at the expense of a more complicated integration; a proper test setup must be provided to insure an optical characterization of the mirror at the first integration and testing stage.

Thin glass shells for large DMs

This is a high-technology, costly, high risk venture. Up to now only the Steward Observatory Mirror Lab has been producing thin shells:

- MMT: Convex aspheric Rc=1795mm, k=-1.409, diameter=642 mm, 2mm thick, Zerodur 336 actuators
- LBT (2 units): Concave aspheric, k=-0.7328, diameter=911 mm, 1.6mm thick, Zerodur 672 actuators

A Call for Tender for the manufacturing of the Zerodur thin shell for the VLT DSM has been launched recently and results are expected in the coming months:

- VLT: Convex aspheric, Rc=4553mm, k=-1.66926, diameter=1120 mm, 1-1.8mm thick, Zerodur 1170 actuators

The production of an aspheric convex (VLT- Defromable Secondary Mirror) or concave (M5AM for OWL) thin shell adds substantial complexity to the manufacturing process. In that respect the flat M6AM unit for OWL is definitely “simpler”.

First estimate of the required glass thin shell thickness for the OWL M6AM is in the order of 1 mm. Several options are investigated in the framework of the ELT design study.

Other industrial partners have been involved in the fabrication of flat thin shell. There is a high synergy in the industry due to the high demand for thin glass plate for flat screen computer displays and digital TV's.

All the products listed below look promising but none has undergone detailed characterisation and it is unclear whether they fulfil the image quality criteria required. Most likely further optical polishing or ion beam polishing would be required. Furthermore, they do not have the advantage of low thermal expansion like Zerodur or ULE. This is not a show stopper for a deformable optics, but represents an added risk.

Corning EAGLE ^{2000} Display Grade substrates offer the following characteristics:

- 1100x1250 mm max. size
- 0.5-0.7 mm thickness
- <20□m thickness deviations

This line of product is available commercially. However, 0.7mm is thin for our applications and requiring a custom thickness would cancel the advantage of using this commercial line of production (at low cost).

SCHOTT also provide the following AF37 material also for LCD display applications:

- Alkaline-earth alumino silicate glass with high content of Al2O3
- 2160x2400 mm max. size
- 0.7mm thickness
- <50 □m thickness variations

This line of product is available commercially. Same comment as above on 0.7mm thickness.

SCHOTT BOROFLOAT® 33 is another line of products where thin shells are available:

- Material: B2O3 (13%), Na2O/K2O (4%), Al2O3 (2%), SiO (81%)
- 3000x2300mm max. size
- thicknesses in the range of 0.7mm to 25.4 mm
- ±70 µm thickness variations (for 0.7mm thick)

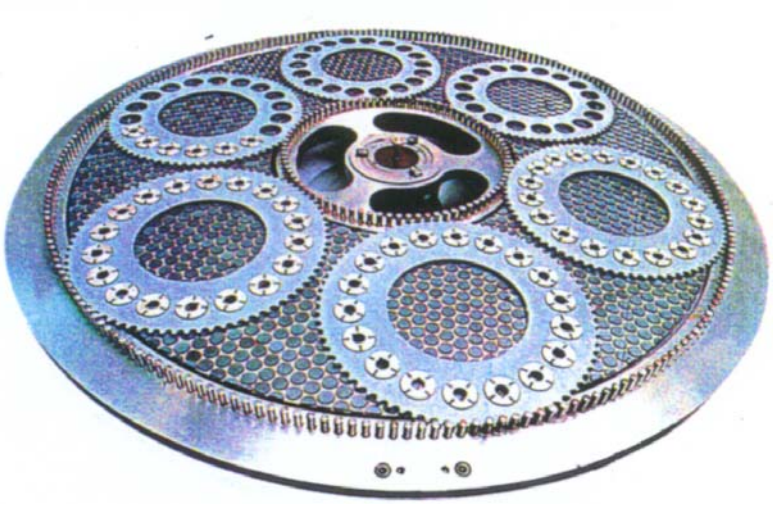

Figure 8-32: Double side polishing device for flat shell. Six shells, maximum diameter of 68mm each can be polished at once (Courtesy SESO, France)

SESO (Aix en Provence, France) have produced 680mm flat shell 3mm thick using a double side polishing apparatus (Figure 8-32). In the framework of the ELT design study they will investigated the possibility to manufacture a 1mm thick Zerodur thin shell of the same size.

- Different materials : glass, Zerodur, silica, ceramics, silicon, germanium
- Polishing of pieces with flatness of less than 3 μm up to 680 mm diameter
- Roughness as low as 1 Å RMS
- Parallelism of the 2 surfaces < 2" RMS

SAGEM is another company that is known to have contributed in the field of thin shell production. Especially space applications where lightweight mirrors are required (assembly of thin phase-sheet with reinforcing ribs).

Among the promising techniques to produce a thin shell with power (M5AM for OWL) are polishing under stress and slumping. The first technique is being investigated in the frame of OPTICON JRA1 and the second in the frame of the ELT design study.

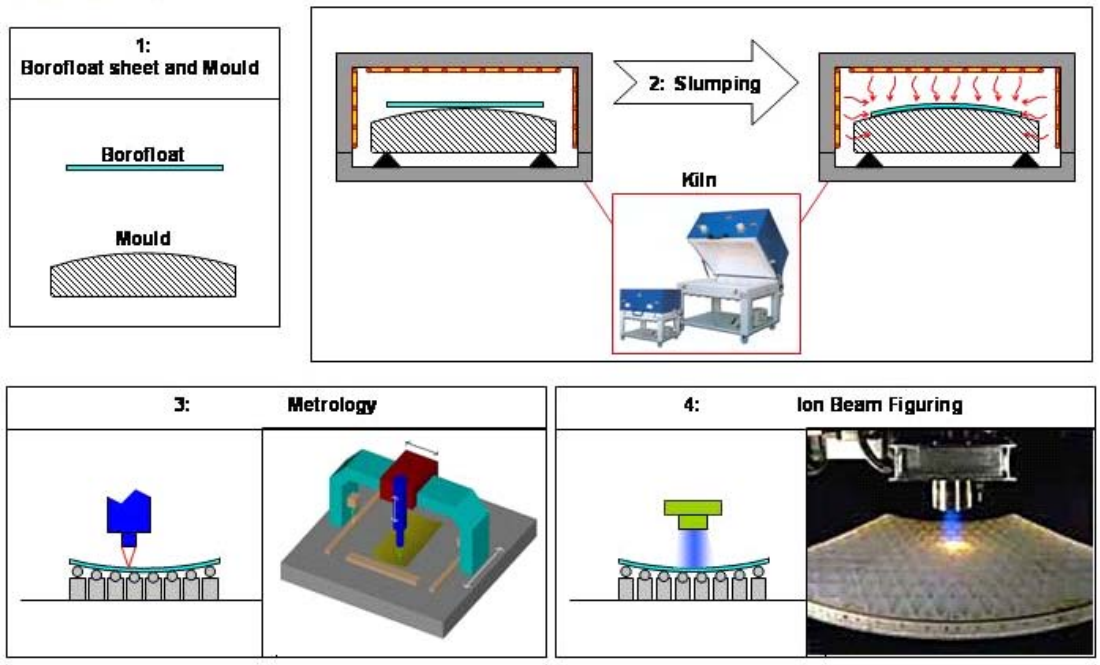

Figure 8-33: The successive steps of thin shell slumping (Courtesy INAF)

Stress polishing proceeds by grinding a thin meniscus being maintained in contact with a mandrel by air depression. The latest thinning steps are done by smoothing with finer tools. The process is completed after the proper optical quality is reached. If an aspherical shell needs to be produced the mandrel is aspheric and the polishing is spherical. Relaxation of the shell leaves it with the shape of the mandrel thus aspheric. This technique is still in development and has not produced a thin shell yet.

Slumping uses Borofloat glass and a high temperature oven to melt a flat thin shell onto a mould of the appropriate shape. Figure 8-33 shows the basic steps of this technique. The main disadvantage is the necessary use of non-Zerodur shell; due to thermal warming of the shell by the actuator local deformation at scale smaller than the inter-actuator spacing could be produced and could not be corrected for.

All the above possibilities are being investigated in the framework of OPTICON, ELT design study (Task 9300) and within the framework of the VLT Deformable Secondary Mirror (DSM) Feasibility study.

Control of large deformable mirrors

Contrary to piezo-stack DM's, this type of mirror implements a servo-loop between the capacitive sensor and the force actuator; this internal loop is sampled at a 80 kHz frequency for the VLT design and provides the capability to maintain the gap for each capacitive sensor at a predetermined value. A command vector sent to the DM defines a new position for each

capacitive sensor and the internal local loop sets the force corresponding to this new position for each sensor. Commands sent to perform a deformation are sent using a so-called “feed-forward” matrix which is a typical command matrix linking position to force (Figure 8-34)

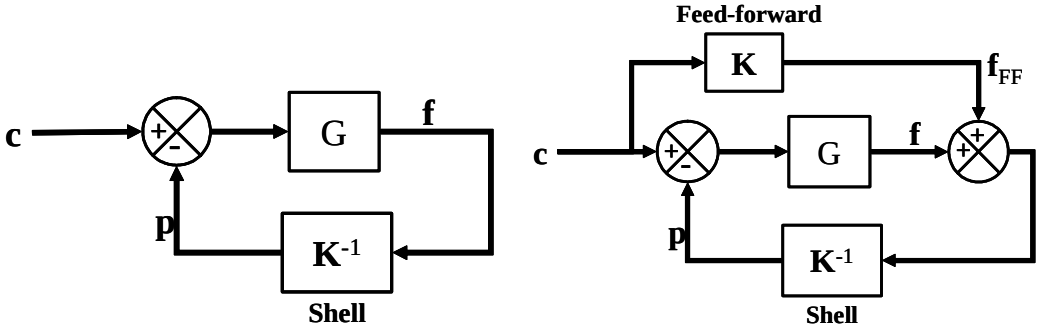

Figure 8-34: Scheme of internal control loop of actuator positions (left hand side). Feed-forward force added to the control schematic on the right hand side.

The derivative of the capacitive sensor positions provides a measure of the velocity of the shell displacement which in turn is used by the system to define an electronic damping matched to mode stiffness. This feature allows reaching high bandwidth for the system even if some control modes have low resonance frequency.

The electronics is organized in pair of racks that contain the DSP local processors; each individual rack contains up to 15 boards. In each rack two positions must be reserved for a communication board and a reference signal generation board. Each control board is populated with 2 DSP processors; one processor controls 8 channels (actuators) thus 16 channels per board. All boards are coupled with aluminium plates in contact with liquid cooled pipes for efficient vibration-less cooling.

The electronics receives commands from an external Real Time computer. Commands are transmitted via a 2.125 Gbit/sec bidirectional daisy chain connection. A service link (Gigabit Ethernet) insures diagnostic control of the DSM electronics.

Increased number of actuator does not preclude performance since a constant number of actuators are controlled per DSP.

Table 8-5 and Table 8-6 provide the overview of the typical control parameters.

Digital control loop frequency	80 kHz
Time latency between position update and command	41 µsec (transfer 10 µsec)
Local loop delay	4 µsec
Real time communication	100 Mbit/s (each crate)
Computational power	90 GMAC/s, float (6 crates)

Table 8-5: Local Loop Characteristics

Capa. Sensor bandwidth	-3dB @ 42kHz
Capa. Sensor noise	1.8 nm rms @ 50 µm gap
Capa. Sensor stability	1.5 nm/ºC
Capa. Sensor resolution	1.5 nm
Current driver bandwidth	-3dB @ 35 kHz
Actuator force resolution	140 µN
Maximum actuator force	±1.2 N

Table 8-6: Analog performance (Capacitive Sensor)

Large deformable mirror systems aspects

Mode stiffness

As for other AO system a base of modes can be defined for these mirrors. This base has the characteristic that low order modes are generally very "soft" while higher order modes are very "stiff". This can be understood easily; tilt or astigmatism have very low constraint and can be produced with weak forces. Conversely, high order modes imply very steep slope, and large local deformation of the glass; there forces required are important. Figure 8-35 illustrates this behaviour. One can see a substantial step at mode # 3; this corresponds to focus which is relatively stiff despite being a low order mode. This is due to the powered shell since it corresponds to trying to compress the shell in the radial direction.

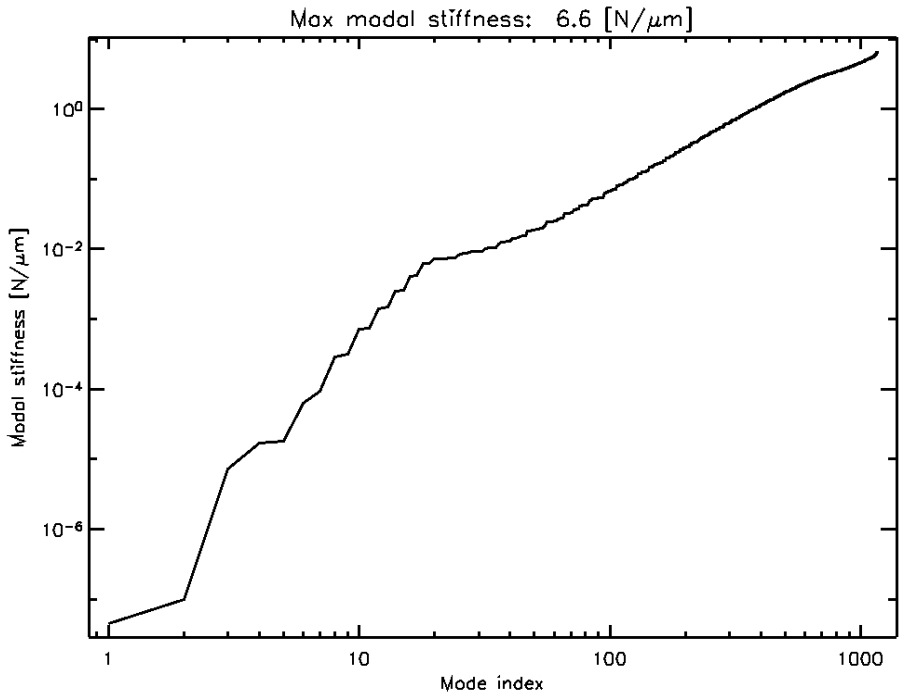

Figure 8-35: Mode stiffness versus mode number for the VLT DSM.

The implications of this is that the power required to control "n" high order modes is much larger (by order of magnitude) than the one to control "n" low order modes. The vertical axis spans 8 orders of magnitudes! Maximum force that can be applied by the actuator is ~1 N.

A consequence is that power consumption can greatly be reduced if one limits the number of modes corrected (by eliminating the stiffest modes).

Power dissipation is related to the force applied through the efficiency of the voice coil actuators. Present technology allows 0.52 N/√W. Knowing the mode stroke required (simulated wavefront time sequence) one can deduce the linear stroke requirement, link it to force through mode stiffness and obtain power requirement from the above efficiency. The total power consumption for the VLT Deformable Secondary Mirror is as follow:

- Median seeing conditions (ro=12.1cm @ 30deg), 1170 modes corrected, 62.5 nm rms WF fitting error, 1.48 kW dissipation
- Bad seeing conditions (ro=5.2cm), 738 modes corrected, 149 nm rms wavefront fitting error, 1.47 kW dissipation
- The following preliminary simulations have been run for a M6AM type mirror and lead to:
- 1.0mm shell (Zerodur); seeing 0.85" at 30º zenithal angle; Force 0.13 N rms, 0.6 N max.; 6.4 kW total power; 250 nm residual WF

- 1.0mm shell (Zerodur); seeing 1.5" ; Force 0.20 N rms, 0.9N max.; 6.8 kW total power; 400 nm residual WF
- 1.2mm shell (Zerodur); seeing 0.85" at 30º zenithal angle; Force 0.22 N rms, 1.0N max.; 6.9 kW total power; 250 nm residual WF
- 1.2mm shell (Zerodur); seeing 1.5"; Force 0.35 N rms, 1.5N max.; 7.9 kW total power; 400 nm residual WF

Note that in the last case the maximum force exceeds the 1 N maximum that can be produced by the currently available actuator; therefore the number of modes to be corrected should be limited and residual wavefront error correspondingly increased.

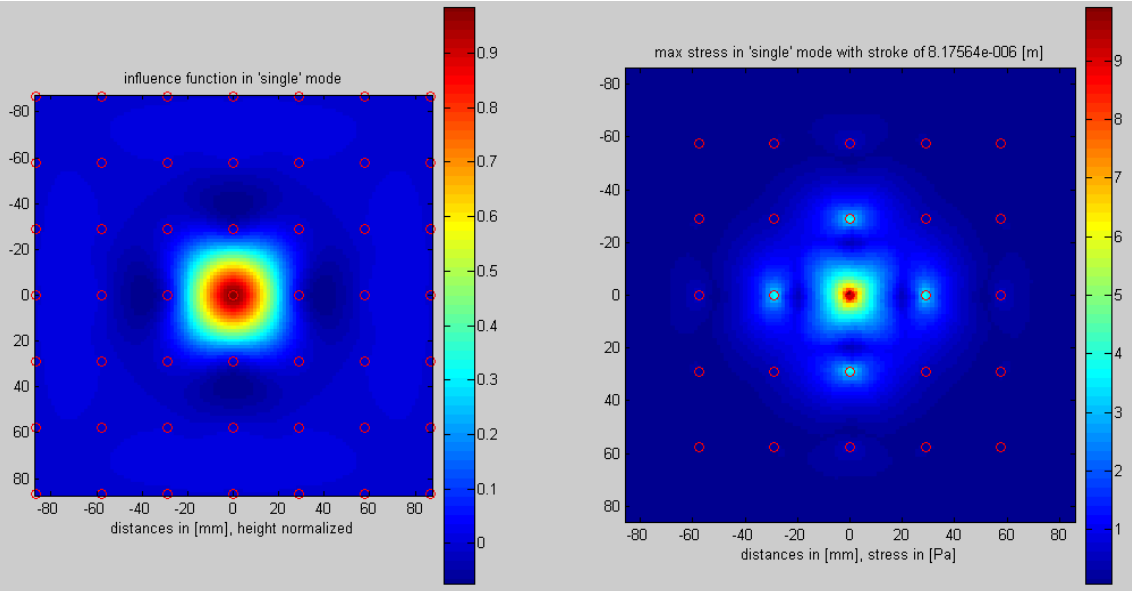

Figure 8-36: Theoretical Influence Function of a thin shell DM. Left: the IF (scale in mm), right: the associated stress in the glass (square grid of actuator at 29mm spacing, 2mm thick)

Influence functions

The typical influence function shape of this kind of DM is a damped sinc (*sin(x) / x)* function. Coupling as defined for other types of DM (piezo-stack) is irrelevant. When a displacement is commanded to a single actuator, neighbouring actuators get a command from the internal control loop to maintain their corresponding positions as defined by the capacitive position sensors. This explains the undershoot (below average surface) 1.5 actuator spacing from the deformation peak (see Figure 8-36).

The Figure 8-36 shows that the influence function of these mirrors is very close to a Sinus cardinal. The deformation is maximum at the position of the commanded actuator, crosses zero at the first next neighbours, goes through a minimum and again crosses zero at the 2nd next closer actuator and so on. The difference with a sinc function is that this function is slightly damped (the amplitude of the wave patterns decreases faster than a real sinc). This is a positive feature since a sinc function contains all spatial frequencies up to the Nyquist criteria for a given actuator spacing and its power is null for spatial frequencies above the inter-actuator spacing. Thus, such function appears ideal for wavefront correction since it provides full coverage of all useful spatial frequencies without introducing uncorrectable higher spatial frequencies. The damped sinus cardinal comes closest to this ideal influence function.

Note that with the increased performance of DSP based controllers, electronic damping is also used (proportional to the velocity of the shell at an actuator point; derivative of the capacitive sensor position is used). This damping allows limiting resonance of low order modes and increasing system bandwidth.

Large deformable mirror scaling laws and Trade-offs

Actuators and magnets

The magnets are made of a complex assembly of “pie shape” pieces providing an optimal force / magnet surface. A Zerodur “puck” is glued between the magnet and the shell back surface with no local deformation of the shell optical surface (Figure 8-37 and Figure 8-38).

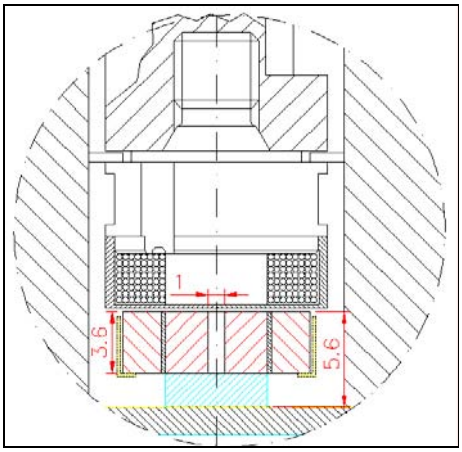

Figure 8-37. Permanent magnet mounted on the shell.

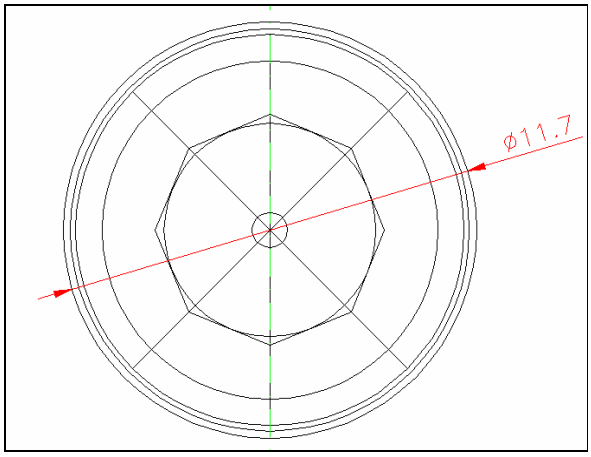

Figure 8-38. Permanent magnet sizing.

Actual technology imposes magnet sizes of the order of 12mm in diameter and this is what drives the minimum inter-actuator spacing. Reducing this size further brings also complications at the level of the voice coil, but would also reduce the actuator stroke (force).

Thin Shell

Let’s define the following parameters:

- t : shell thickness
- Y: shell material Young’s modulus
- ρ: shell material density
- a: actuator spacing
- r_o: force radius distribution (radius of the area on which the actuator force is applied)

Material	**Young’s Modulus N/m^2**	**Density Kg/m^3**	**Poisson Ratio (0.33=>adhoc)**
Zerodur	90.3 10^9	2.53 10^3	0.243
SiC	450 10^9	3.12 10^3	0.21
CVCSiC	466 10^9	3.20 10^3	0.33
Steel (17-4 PH)	200 10^9	7.80 10^3	0.29
Ester Graphite	101 10^9	1.8 10^3	0.33
Nickel	214 10^9	8.9 10^3	0.33
Borosilicate	63 10^9	2.23 10^3	0.22
ULE	67.6 10^9	2.205 10^3	0.25

Table 8-7: Characteristics of potential materials for thin shells.

The desired characteristics are a combination of trade offs. The list below summarizes the important characteristics:

- Weight: low density helps to reduce the total weight of the shell; less actuator power is used for compensating gravity. Compensation force is proportional to ρ.

- Quilting: this describes the sage of the shell between the actuators. High density makes it worse; high Young modulus helps prevent it. It is proportional to $a^2 / (Y\ t^2)$.
- Stroke: Low Young modulus helps, but mainly shell thickness. Proportional to $a^2\ \rho^2/(Y\ t3)$

Table 8-7 provides the characteristics of the investigated materials for the thin shell manufacturing.

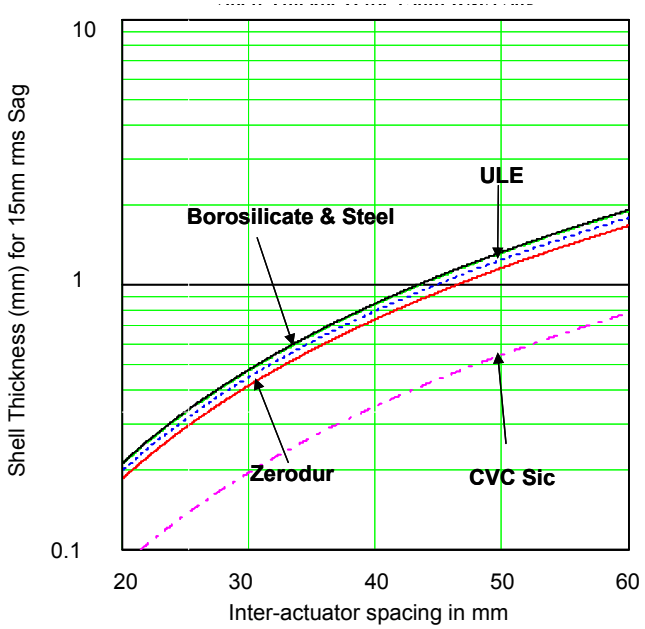

Figure 8-39: Shell thickness producing 15 nm rms gravitational sag (30nm rms wavefront error) vs. actuator pitch

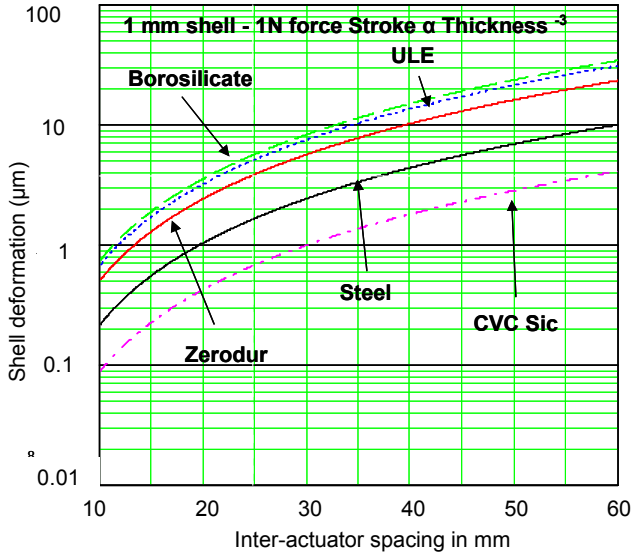

Figure 8-40: Shell gravitational sag (nm) vs. act. pitch for Zerodur, ULE, Borosilicate, Steel & CVCSiC.

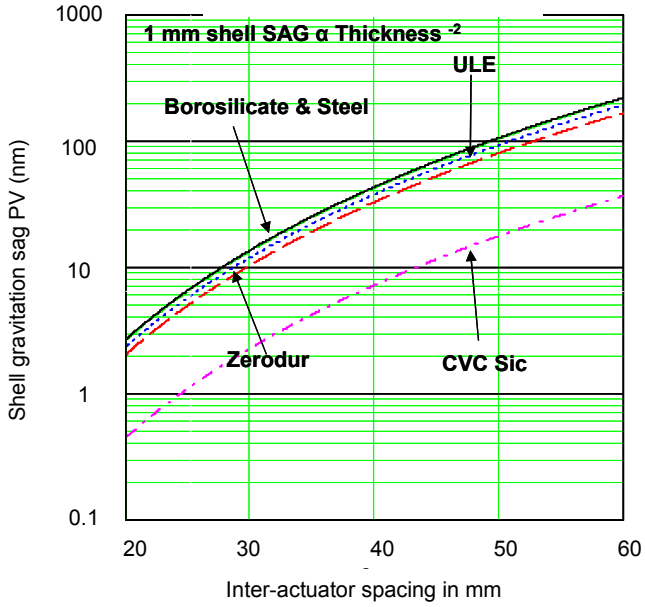

Figure 8-41: Shell deformation or stroke. Absolute analytical model accuracy: 50%; valid for relative material comparison

One may be tempted to study materials like steel since breakage is less likely than for glass. However, with Steel and ULE the ratio ρ/Y remains high which makes these materials worse from the point of view of quilting (see Figure 8-39). Note also that high conductivity material may trigger unwanted effects; besides sensitivity of the optical surface to ambient temperature variation, the actuators themselves dissipate and may induce local deformations. On the other hand the very low equivalent ratio for Silicon Carbide (SiC) does not represent a huge advantage because in order to benefit from it one would need to envision unrealistic and unpractical shell thicknesses (~200 μm).

As for stroke a CVCSiC shell would need to be nearly half the thickness of a Zerodur one in order to allow a similar stroke. Figure 8-41 shows a comparison of stroke between different materials considered. Note that this analytical model overestimate the stroke by ~50% with respect to Finite Element Analysis performed on the VLT Deformable Secondary Mirror shell.

From Figure 8-41 we see that a stroke of 4 μm can be achieved with a Zerodur thin shell of 1mm thick, an actuator spacing of 25 mm and a force of 1 N. The inter-actuator stroke requirement at the spatial scale of 1 m on OWL pupil is about 5 μm for a seeing of 1.5" and for an atmospheric outer scale of L_0=100m -Figure 8-26- which is the worse case.

We see that present technology is nearly able to meet the requirements for SCAO. Refining of the numbers should be done in the phase B. The production and the handling of 1mm glass thin shell of 2.4 m diameter remains challenging. However, the fact that M6 is flat relaxes significantly the difficulty of manufacturing this shell. Handling is a matter which has been partially addressed by industry for other applications (flat screen display). Fall back option would be to segment the M6AM unit in six flat petals following the OWL spider geometry

The conclusion of these considerations is that Zerodur although a conservative choice represents a safer approach to thin shell fabrication and can fulfil adequately the requirements.

Other exotic materials like Ester Graphite do not seem to present significant advantages. Note also that they are known to present sensitivity to humidity. Furthermore, homogeneity of the material depends on the number of anisotropic layer deposited and an adequate isotropy might require an excessive number of individual layers to represent a thin shell (few 100 μm per layer).

Power dissipation and control electronic

The actual VLT Deformable Secondary Mirror is expected to dissipate 1.47 kW. This power is distributed as such:

- 311 W in Coils, 1123 W in racks and 43 W in cables with a 2mm thick shell

For OWL M6 with a Zerodur shell of 1mm the estimated power dissipation is:

- Seeing 0.85":
  - Power at coil level: 0.25W/act (1.6kW total)
  - Power at crate level: 6.4kW total (non linear current drivers)
- Seeing 1.5":
  - Power at coil level: 0.39W/act (2.5kW total)
  - Power at crate level: 6.8kW total (non linear current drivers)

Other important properties are the size of the electronic racks. The VLT Deformable Secondary Mirror design is based on the following distribution of control per channels:

- 13 control boards per rack, 2 DSP per boards, 8 channels per DSP = 208 channels per racks (6 racks are required)

The actual design could implement a 16 channels control per DSP which would results in a gain by a factor of 2 leading to about 400 channels per rack. Table 8-8 provides the main characteristics of the OWL large deformable mirrors.

Mirror	Size (m)	# actuators	Act. pitch (mm)	Scale on sky (m)	# racks
M5	3.85	17241-6727	25-40	0.78-1.250	43-17
M6	2.44 x 2.66	6720	25	1.02	17

Table 8-8: Main characteristics of the OWL large DMs

Further improvement would require substantial new development. Electronic racks would be reduced drastically and most electronic miniaturized and deported in the actuator electronic. The actuator itself would contain its Deformable Secondary Mirror controller and switching power driver. Although the control requirements are reduced by a factor of 8-16 (1 CPU per channel) the driver would imply a substantial new development.

Hexapods are often used to produce fine motions on the back-plate; they are particularly well suited for this application allowing fine accurate repeatable motions and high rigidity. They can provide high accuracy movements and are extremely sturdy devices against gravitational flexures. Any motion applied to the back-plate is transmitted on the optical surface of the thin shell. It can be typically used for small focusing motion and centering correction. Table 8-9 lists a few basic characteristics of the VLT design.

Mass Budget		**Hexapod Actuators Req.**		**Achieved Performance**	
Mirror+magnets	9 kg	Stroke	16mm	Step response (10mm, 4000 N load; 23Hz sampling)	~2sec
Reference body	27 kg	Resolution	1 μm	Fixed position	10nm rms
Cold plate	89 kg	Op. Axial load	≤2000 N	Power Dissipation (3000N load)	Min: 6 W Max: 12 W
Actuators	54 kg	Survival axial load	≤14000 N		
Support levers	5 kg	Speed	≥0.5mm/sec		
Total weight	**184 kg**				

Table 8-9: Essential characteristics of the VLT adaptive secondary mirror.

8.2.1.4.4 Testing a large DM in closed loop

The testing of deformable mirrors of the size envisioned for OWL Telescope, or for 8m telescope class secondary mirrors for that matter, represents a new challenge for the integration phase of such systems. It is not only a question of size but also of shape; concave, convex or flat. A versatile and complete test facility to characterize and understand well these systems is necessary. An exhaustive integration and test phase with adequate equipment in Europe will insure a successful and shorter integration phase at the telescope.

It is with similar considerations in mind that the integration phase of the VLT Deformable Secondary Mirror was envisioned. Not only this facility shall allow testing of the Deformable Secondary Mirror itself, but it will provide also a turbulence generator and VLT standard opto-mechanical interfaces to the AO pre-stages SCAO and GLAO (GRAAL and GALACSI for the instruments HAWK-I and MUSE respectively).

The optical design shown in Figure 8-42 is composed of 2 mirrors plus the VLT Deformable Secondary Mirror. The latter is mounted on a vertical structure holding the M2 unit thus providing a support identical to the one of the VLT. Gravity vector is along the M2 optical axis. Two other optical components are required: a main 1.65 m diameter aspheric mirror and a smaller 140mm diameter aspheric mirror. The asphericity of the former can be handled by conventional polishing techniques while the fabrication of the second would require diamond turning. This setup would offer a 2 arcmin field of view and no pupil distortion. The image plane is located at the centre of curvature of the 3 mirrors system: 1.65 m concave aspheric, 1.1 m convex DSM, and strongly aspheric 140mm third mirror. 45º flat mirror and beam splitters are used to transport the source and image planes at convenient locations.

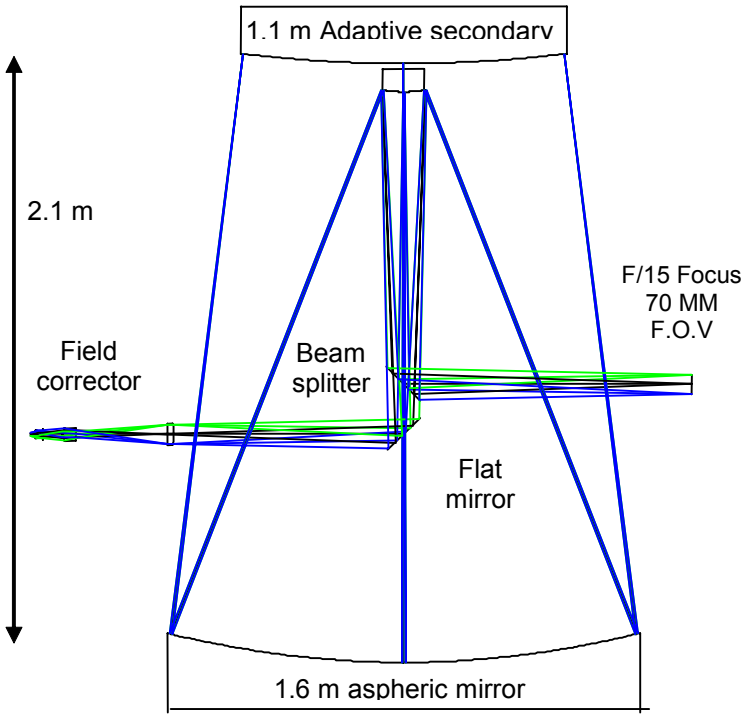

Figure 8-42: Optical diagram of the VLT Deformable Secondary Mirror test setup

Figure 8-43 illustrates the opto-mechanical implementation. The table on the right-hand side would support the turbulence generator and a 45º beam splitter re-directs the beam onto the 140mm mirror. After reflection onto the primary and DSM a 45º mirror will direct the beam toward the Nasmyth focus mechanical interface. There an f/15 beam is provided the SCAO and GLAO systems.

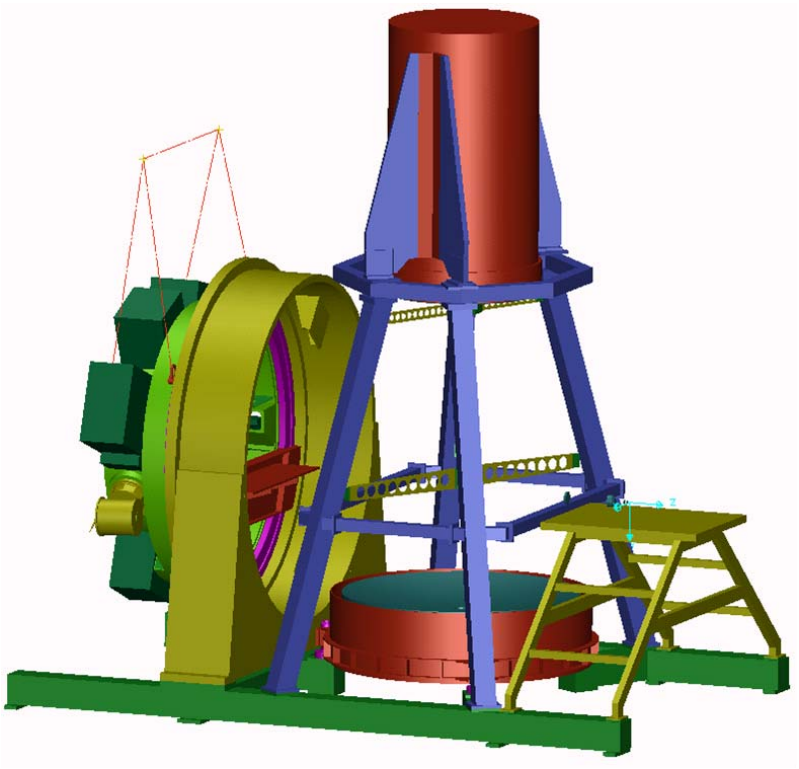

Figure 8-43: Mechanical setup of the VLT deformable secondary mirror Test facility.

As we have shown here, it is clear that a lot of experience will be gained on the VLT large deformable mirror to prepare for the next generation of even larger deformable mirror for OWL.

A similar strategy could be imagined for OWL M6 as shown in Figure 8-44. The optical set-up could consist either of a parabolic mirror or a spherical mirror with small focal ratio and a corrector. The orientation could be vertical to simulate conditions closer to the real ones.

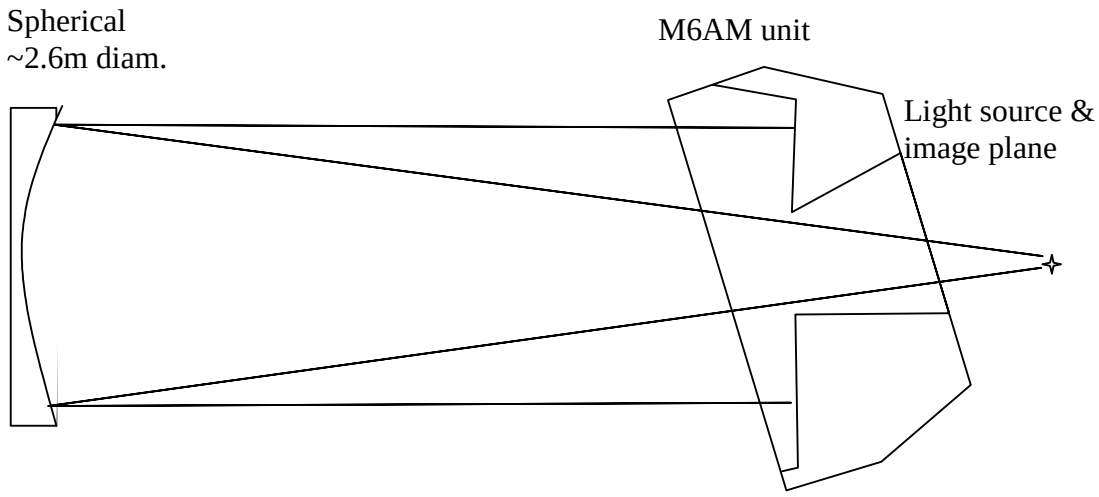

Figure 8-44: Possible test setup for the OWL M6. In the case of spherical mirror a corrector is needed for aberration compensation (not shown here)

The following items provide a non-exhaustive list of all tests and characterization that would be performed before any use at the telescope:

- optical characterization of the large DM

- optical measurement of the influence functions
- definition of the flat vector
- optical measurement of stroke, non-linearities, cross coupling
- Interaction matrices measurements (artificial source, with turbulence opened-loop and closed-loop)

- Closed loop operation with wavefront sensors of the instruments
- Characterisation of correction capability, image quality improvement
- Characterisation of different algorithm of correction (on-axis single source, GLAO multi-source, LGS correction etc.)

Finally it is undeniable that the experience gained while testing and operating the deformable mirror in Europe would be invaluable during integration and test at the telescope.

8.2.1.4.5 Detectors for wavefront sensors

An extension of the current Electron Multiplication CCD detector technology or equivalent for wavefront sensing will be launched early in Phase B in order to reach the required 600x600 pixels at a kilo frame per second. High depletion devices are very promising and should be pursued further. Larger pixel – up to 50 µm – combined with a low dark current at Peltier temperatures should also be investigated.

Alternative technology, like the Pn CCD detector developed by the semiconductor laboratory of the Max Planck Institut for Extraterrestrische Physik might become very attractive if the present RON – 2.4 e^- - can be further reduced. This type of detector has several advantages:

- Predicted high Quantum Efficiency down to the red - Figure 8-45-
- High parallelization for the output readout channels - up to 512 outputs for the existing 256x256 pixels detector
- On chip multiplexer to reduce the number of outputs -Figure 8-46-
- Large pixel –up to 50 µm-

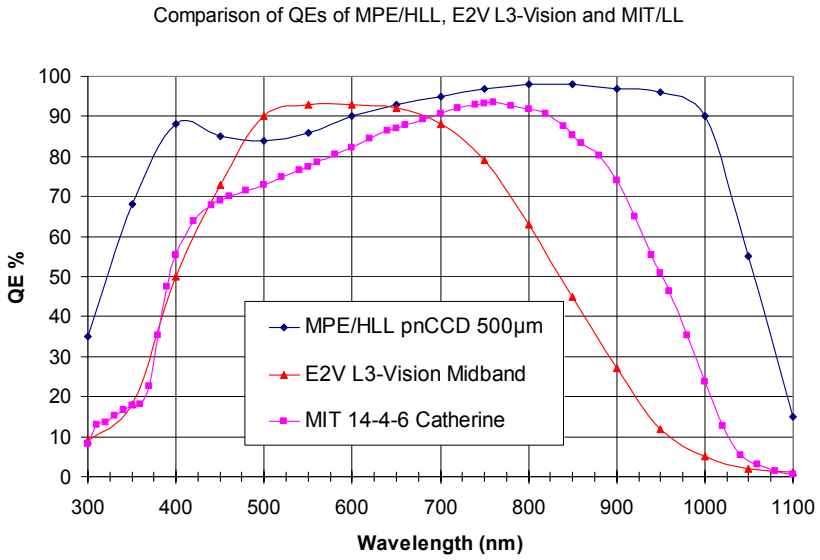

Figure 8-45: Quantum Efficiency curves of the L3 CCD and the PN-sensor

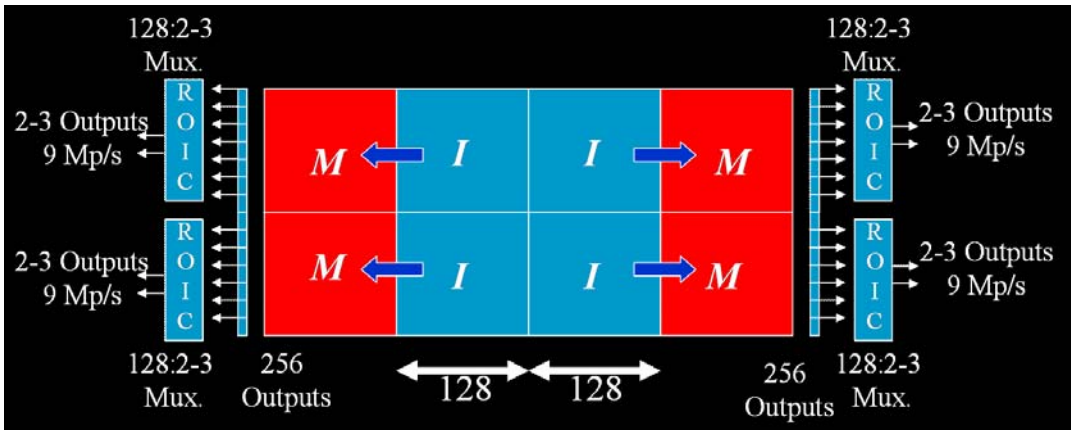

Figure 8-46: Pn-Sensor readout principle for the 256x256 detector.

The effort initiated by Caltech and ESO on low Readout noise high frame rate infrared detectors for wavefront sensing – for instance the Calico Mux from Rockwell – need to be further expanded to reach the level of few e^- Readout noise at 500-1000 frames/s. WFS volume constraints will benefit from cooling without Nitrogen and compact cooling system should be studied.

We plan also to investigate alternative approaches for IR detectors like the components developed by INTEVACS (US).

8.2.1.4.6 Real Time Computer

Real-Time Computers of past ESO-AO Projects

ESO has developed several AO systems:

- NAOS, a 14x14 Shack-Hartmann system with one 185-actuators mirror, driven at 480Hz. The RTC is a custom development made of an array of C40 chips tied together by custom designed boards
- MACAO for VLTI/SINFONI and CRIRES: a modular system installed in 6 different instances. It is a curvature system with 60 sub-apertures and a deformable mirror with 60 actuators, capable of running at 700Hz. The Real Time Computer is a dual-CPU system based on standard Power PC boards.

All these systems are routinely used at Paranal. The experience gained from the development, the commissioning and the operations of such instruments is being exploited for the new projects for the 2nd generation instrumentation.

Current Activities

The second generation instrumentation for the VLT includes several AO-assisted instruments – see Table 8-10. This new generation of AO systems require new development in several areas, including the Real Time Computer.

Currently no single-board computer is capable of processing the amount of real-time data required to run these AO systems. Extreme AO (XAO), Multi-conjugate AO (MCAO) or Multi-Target Ground Layer Correctors will require about one thousand actuators at a Kilohertz rate or more for the VLT and up to almost a million actuators and more than 2 Kilohertz frequency for OWL.

The new Adaptive Optics Real Time Computers will have to be based on multi-CPU multi-board computers in order to achieve the required computational power. The complexity of each of these systems and their number raise concerns about the complexity of their development, their reliability and their maintenance. Individual efforts aimed at developing different custom systems are not a solution, not only because of the duplication of the design and development effort to build similar products for different systems, but also for the amount of resources required to test, maintain and upgrade systems which are different in spite of being similar.

		MACAO	NAOS	MAD	Planet Finder	MUSE	HAWK-I	
Acquisition	Nb of detectors	1 Curvature	1+1 SH	3SH, 2Pyr	1 SH	4 SH	4 SH	1 SH
	Detector size (used size)	-	112x112	80x80 (64x64)	256x256 (240x240)	256x256 (192x192)	256x256	256x256 (240x240)
	Nb of subapertures	60	14x14	8x8	40x40	32x32	32x32	40x40
	Pixels per subaperture	-	8	8x8	6x6	6x6	8x8	6x6
	Tip/tilt sensor	-	-	-	-	quad-cell	yes	-
	Max. frame rate	420Hz	480Hz	400Hz	1.0/1.5kHz	1kHz	500Hz	1kHz
	Integration time	2381µs	2083 µs	2500 µs	1000/667 µs	1000 µs	2000µs	1000 µs
	Input bandwidth [per det/total]	0.1MB/s	11.48MB/s	9.38MB/s	110/165MB/s	70.31/281.25MB/s	62.5/250MB/s	110MB/s
	ACQ blocks	1		4				
DM	DM type	Bimorph	Piezo	2 Bimorph	Piezo	DSM	DSM	
	Nb of actuators	60	185	2x60	1370	1170	1170	
	Size of control vector	0.12kB	0.36kB	0.23kB	2.68kB	2.29kB	2.29kB	
	Output bandwidth	0.05MB/s	0.17MB/s	0.09MB/s	2.61/3.92MB/s	2.23MB/s	1.12MB/s	2.23MB/s
	Tip/tilt Mirror	TT mount	separate	TT mount	separate	no	no	
Control	Supported modes	SCAO	SCAO	SCAO, MCAO	SCAO	Wide/Narrow	SCAO,GLAO	SCAO
	Nb of used slopes	60	144	156	1096	800/3200	796	1096
	Control matrix size [elements]	60x60	288x185	312x120	2192x1370	1600x1170/ 6400x1170	1592x1170	2192x1170
	Control matrix size [Mbytes]	0.01MB	0.20MB	0.14MB	11.46MB	7.14MB/ 28.56MB	7.11MB	9.78MB
	Memory bandwidth for matrix access	4.2MB/s	96MB/s	56MB/s	11.46GB/s, 17.19GB/s	7.14GB/s, 28.56GB/s	3.56GB/s	9.78GB/s
	Controller type	integrator	integrator	integrator	integrator + Kalman(tip/tilt)	integrator	integrator	integrator

Table 8-10: AO systems commissioned or under development. SPARTA support starts with MAD

We believe that the solution is a common standard platform that can achieve all the goals of the AO systems. SPARTA is a standard platform that provides both a hardware and software common infrastructure in which all the previously mentioned applications can run.

The main goal of SPARTA is to provide a product for the 2nd generation AO facilities for the VLT and a concept for OWL. It is clear that the final RTC for OWL could be rather different from the one proposed from the SPARTA concept, since another goal of SPARTA is to be able to track the technology as it evolves.

The goal of the conceptual design of an RTC for OWL is to prove that it is feasible or to identify what has to be improved and to show that the “improvement factors” are within reach. To this end we will show that the SPARTA concept can be a possible solution.

The standard hardware platform will be scalable to accommodate different needs of the different projects. It will be easily maintainable, designed with deployment scenarios in mind and strongly based on Commercial Off-The-Shelf components. It will also be upgradable to follow the technological evolution, and will be reliable because it is based on a common software platform and it shares similar benefits as the VLT Common Software[64].

The main problem to face while designing such big AO controllers is not the total computational power, which can be easily reached by piling up a considerable number of CPUs, but, instead, the critical factor is the latency. It is in fact relatively simple to process gigabyte of data per

[64] Developed once, tested and run multiple times.

second, given a pipeline of CPUs which is long enough. What is difficult is ensure that the computation completes in the shortest possible time when the total available time is measured in hundreds of microseconds.

A standard CPU suffers from the instruction-fetch, load/store bottlenecks of the traditional von Neumann microprocessor architectures, shared also by most DSP chips. This prevents reaching the latency performance required in large parallel systems, where large means more than 4 chips. Instead FPGA-based systems achieve true parallel processing, executing DSP algorithms based on the inherent parallelism of the hardware. In addition, FPGAs are far more scalable into the higher throughput realms because they can dedicate specific logic for I/O functions. However FPGAs are harder to program and thus less flexible to use from a software point of view.

The choice for SPARTA falls into a hybrid architecture where the central computing element is a board with at least two last generation FPGA chips and two last generation multi-core CPUs. We can then create a double pipeline, one based on the FPGA talking to each other by using a very low latency bus, and another pipeline where the CPUs can talk using a standard fast fabric.

In fact SPARTA uses CPUs, DSPs and FPGAs in a equal ratio. Every FPGA is coupled with a last generation CPU that contains a DSP (AltiVec) so we are using all three worlds at the same time, with the goal of using each of them for the application it is best suited. In fact FPGAs will be used only for the very hard-time part, where every single microsecond counts and the intelligence is concentrated on the CPU that can use the companion DSP for mathematical computations.

SPARTA for the VLT has already reached some important milestones: a Conceptual Design is available together with the definition of the external interfaces, the CCD/IR controller and the deformable mirror controller. Important work on both the CPU pipeline and the FPGA pipeline has already been performed and several parts of the software architecture are under test on the ESO MCAO Demonstrator (MAD) project, which uses a scaled-down version of SPARTA.

Future Activities for SCAO

The AO system for SCAO is challenging but also will be operational in several years from now so that we can benefit from the technological advances that will take place during these years. It is therefore important to keep on the radar the most interesting technological developments that are surfacing now since they will take some time to become products we can actually buy. If the time interval is about 5 years, then only technology that is being talked about now could be usable in 5 years. A longer period could bring new developments that are not under consideration at the moment, so it is more difficult to predict what we could have.

There are two kinds of problems we will need to face in designing the RTC for OWL:

- The total computing power

While the control frequency remains more or less unchanged, the number of degrees of freedom needed to achieve a certain Strehl ratio increases with the square of the telescope diameter, so the number of DM actuators or sensor sub-apertures will be 100 fold if compared with the VLT. Since standard control algorithms use a matrix-vector multiply (MVM) as the core function in the control algorithm, then the required computing power is 10.000 bigger than an equivalent VLT system (the matrix dimensions are number of sub-apertures and number of actuators). This alone is not a big problem: as said above, one can create a massive CPU pipeline that is able to cope with the required throughput. This is a problem similar to the car industry where one can get one new car produced every hour, by lining up several workers in a production pipeline.

- The total latency

If throughput is about delivering one car per hour, latency is about the total time each car spends in the pipeline. It is relatively easy to build a computer able to implement a 100x100 Shack-Hartmann system at 1 KHz with a latency of one second. That means that this system can acquire sensor data at 1 KHz, but each frame takes one second to be fully processed by the system before any action based on those data is taken. In fact the system is processing 1000 frames at the same time, each frame in a different stage. This is of course would not work:

a closed-loop control system has not only to have the required throughput but also the latency in order to keep the complete computation associated with a certain frame short, ideally before the next frame arrives.

We considered several architectures and technologies to solve both the throughput and the latency problems. Those can be grouped into three main areas:

- General Purpose CPUs. These are the standard processors equipping PCs. They are characterised by a bus-based architecture: data normally reside in memory. Input devices store data through the bus into memory, where the CPU can fetch them, again through the bus to bring them into one of the caches for fast processing. Results are deposited into memory where output devices can take them for transmission. As it is clear from the description, the bottleneck is the bus since everything has to travel through it. However, CPUs feature very advanced technology, they have very fast cores and many includes a DSP unit inside.
- DSPs (Digital Signal Processors). These are specialised processors with special instruction to deal with standard signal-related operations. For the rest, they are similar to CPUs and share many advantages and drawbacks. We will not consider this option since modern CPUs come with integrated DSP units.
- FPGA (Field Programmable Gate Array). Those are specialised chips that include a large number of logical elements that can be logically wired together to create a circuit in which the flow of the current will “execute” the hardware program, in a similar way the core of a CPU is designed. In fact, to program these chips one needs to use a dedicated language which is the same used to design integrated circuits. All the gates of the FPGA chip can be active at the same time thus implementing a low-level massive parallelism. The chip can feature multiple busses to talk to memory and devices so that multiple areas of the chip can be active and process data at the same time with the advantage to be on the same chip.

General purpose CPUs are easier to program and better tools are available. DSP are slightly harder and FPGA are the most difficult ones, since one needs to deal directly with the hardware.

In terms of commercially available products, one can buy boards featuring any of the previous technologies and even a combination. DSPs are not very appealing for what said before if compared to CPUs. However custom designs that gather together a large array of DSPs (hundreds) can be made competitive with a standard board based on FPGAs. The first guideline for SPARTA is to maximise the usage of commercially available components, so here is another reason not to consider DSPs.

Technological evolution is an important factor in designing the RTC for OWL, since the deployment of the OWL-RTC will happen not before 5 years from now, so that we can benefit from the technological evolution. However different technologies will have a different rate of evolution. In RD25 we recall the so-called Moore’s Law “governing” the technological evolution of integrated circuits, but one can immediately observe the following:

- Current CPU architectures are approaching the limit. The major CPU manufacturers have focused in the past years on increasing the clock speed of the CPU as the best way to increase its computational power. In fact since the introduction of the Intel 80486, companies have been increasing the clock frequency of the CPU while leaving the bus speed unchanged or slowly increasing it. This is another factor why the peak computing performance of a general purpose CPU can never be achieved in AO because AO is not just computationally intensive, but it also needs to transfer a large amount of data to and from the CPU.

Moore’s Law predict the evolution of the transistor density, but computing power is more complex to predict since clock speed, bus speed, peripheral performance come into play. The 100 times increase that a plain application of the Moore’s Law would predict might not be applicable to CPUs.

- Instead, an FPGA is a huge array of logical elements. Making a more powerful FPGA is like adding more elements to the chip, which is much easier. Of course, real performance gain can be obtained by re-implementing the application to exploit the additional

parallelism. And of course clock speed increases for FPGAs too. So one can expect a bigger increase in performance for FPGAs than for CPUs.

The SPARTA architecture, which is based on a combination of CPUs and FPGA chips on the same computational unit, is then well positioned to benefit from the next generation of hardware and we are confident that it can deliver the performance required to implement the SCAO system for OWL and even more.

There are other developments that are required to run the RTC at the maximum speed, but that do not directly belong to the RTC and the SPARTA project.

The detector controller must provide multiple output interfaces, in order to split the pixel stream in multiple streams that can be computed in parallel by different sections of the SPARTA-RTC. To achieve this goal the detector controller (IR or CCD) must also offer switching capabilities, in order to route a certain pixel to a certain output interface, with a fixed routing map. This requirement is indepented from the number of detector amplifiers. The switching capability is of particular importance for the pyramid wavefront sensor where the equivalent concept of sub-aperture is distributed over the four pupils so to start the computation of the gradients one must first acquire a large portion of the detector if care has not been taken upfront by designing appropriate routing maps.

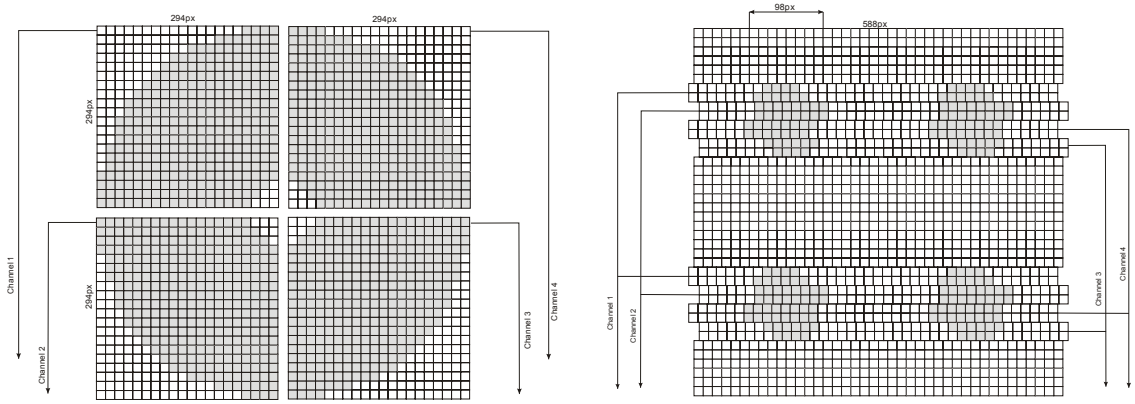

Figure 8-47: Left: Shack-Hartmann read-out; right: Pyramid read-out

Another required development is fast mirror drive electronics. At a very high loop frequency, a significant part of the processing time will be spent to send the control voltages to the deformable mirror electronics and have it distribute the commands to the actuators. A multi-channel parallel architecture would then be mandatory.

A critical issue that is common to all the RTC designs is to verify as soon as possible the degree of parallelism that can be achieved with this architecture. The estimate of the computing power of the FPGA chip here considered is quite reliable and rather easy to check since the Virtex4 is going to be integrated very soon into commercial products. What is more difficult and definitely more critical is to test a set of 2 or more boards based on this technology and verify that all communications (intra-board, board-to-board, I/O) are as expected.

Reference Architecture

The reference architecture is derived from the latest developments in the SPARTA Conceptual Design - Figure 8-48- and it is based on a hybrid architecture made of FPGAs running the hard real-time part and the CPUs running the remaining of the system. FPGAs do not show very good performance while dealing with floating point numbers thus one direction of research is the usage of integer arithmetic.

The advantage of using FPGA is the high degree of parallelism that can be achieved through a relatively slow device. Instead a CPU is much faster but requires serialisation while accessing resources as memory or input/output ports.

Several optimisations can be made by sharing the hard real-time part between the FPGA and the CPU and lower the final cost. But a very significant improvement can be made if FPGAs run

only in finite-precision (fixed point) arithmetic while the CPU can run the infinite-precision (floating point) arithmetic. By reducing as much as possible the infinite-precision arithmetic part, one could fully exploit the potential of this architecture and improve performance increasing the speed or reducing the cost.

This is, however, a long study which is inder way in the framework of the FP6 ELT Design Studies and results are expected by 2007.

A CPU-only based system can hardly be used because of the very high over-head required to transfer data to and from the CPU. This at the moment makes impossible to use even the most performing CPUs. Some optimism can be derived from the fact that technology is moving fast on bus technology and multi-core CPUs and in the near future it seems likely that proper exploitation of the floating point capability of the next generation CPUs will become possible.

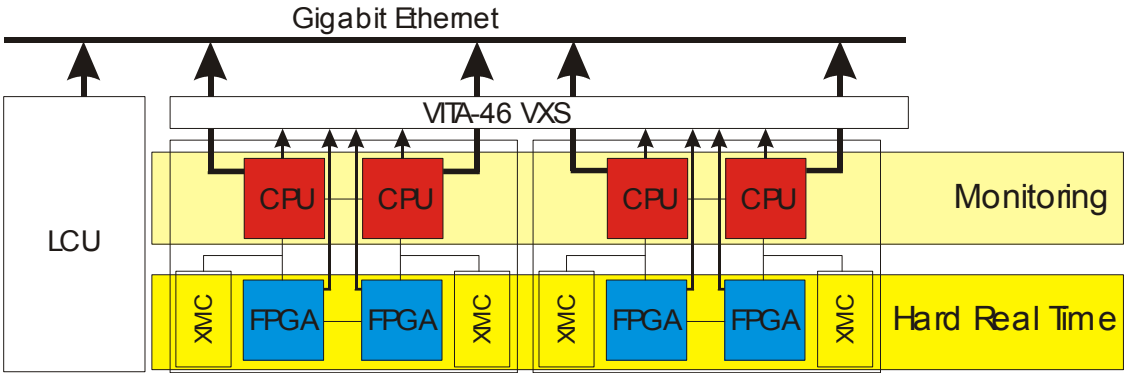

Figure 8-48: SPARTA Architecture

Required Developments

The hardware to build SPARTA for OWL does not need to be bought today and moreover a certain degree of hardware development still needs to be done. The dual-CPU plus dual-FPGA architecture implemented in a board with several banks of fast memory is sufficient to implement 4 of the 5 AO RTCs. A board similar to this one exists already on the market so the first steps in the design phase will be to acquire two of these boards and their interconnecting hardware and to measure their performance.

These two boards cannot be used for OWL RTC, but can be used as test bed and development system and could also be used for SPARTA for the VLT.

- It is also necessary to initiate a co-operation with the industry in order to ensure that the next generation of the same product based on the next generation FPGA chip (the Virtex4) is able to achieve the performance we require.

Given the SPARTA philosophy of maximising the usage of off the shelf products, we would not start a special development to meet the specifications, but instead we would like to work with the industry to see if there is a market opportunity for boards of such computing power in order for the industry to independently develop such boards and make them a real product.

Even if not critical for this first application, efforts shall be made to study new and efficient algorithms. More will be discussed about the more challenging systems, but efficient algorithms can help also at this level to reduce the hard real-time requirements of the RTC. In particular the impact of fixed point arithmetics or reduced precision computation shall be studied since significant improvements can be obtained with an FPGA-based hard real-time pipeline.

8.2.2 Ground Layer Adaptive Optics

Preliminary measurements of the turbulence profile (Cn2) made at Paranal with the SLODAR monitor have shown that 60% of the turbulence is located within the first two kilometers and that 40% of the turbulence is concentrated at 200m. We no have reasons to believe this type of turbulence profiles is specific to Paranal and at least similar properties can be assumed for the

site eventually selected for OWL. Even more favorable profiles have been observed in Antarctica: whether this is a reason sufficient to install OWL in Antarctica is of course debatable.

Based on this turbulence profile and assuming we intend to correct only for the ground layer, a simple geometrical approach shows that the well-known anisoplanatism angle limitation becomes very large and therefore permits to perform wavefront sensor tomography of the turbulence over a large FOV. The net result is an increase of the number of NGSs available for wavefront sensing and finally an increase of the sky coverage in which GLAO correction can be offered.

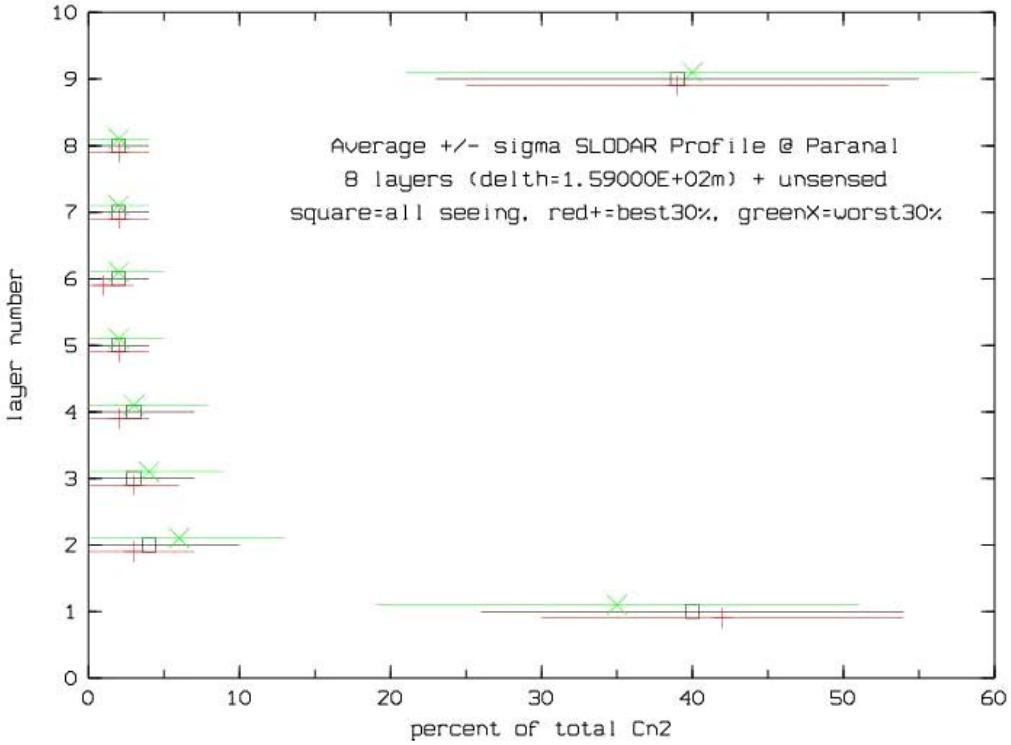

Figure 8-49: Preliminary statistics of the turbulence profile at Paranal

Correcting only the ground layer will in principle not be enough to achieve the diffraction limit of the telescope. However GLAO is a “seeing reducer” system which will provide a better sensitivity for a given integration time, a better ensquared energy and a reduction of confusion for very crowded fields. GLAO can also be considered as a “seeing stabilizer” providing at least median seeing values all the time and is therefore equivalent to install OWL on a better site.

Several scientific programs, especially those concerned with faint extended objects, do not require diffraction limited images because of the low surface when sampling the diffraction at Nyquist. For these programs, GLAO is probably an interesting option which in addition will be available over a much larger sky than SCAO.

The concept of Ground Layer Adaptive Optics is shown Figure 8-51.

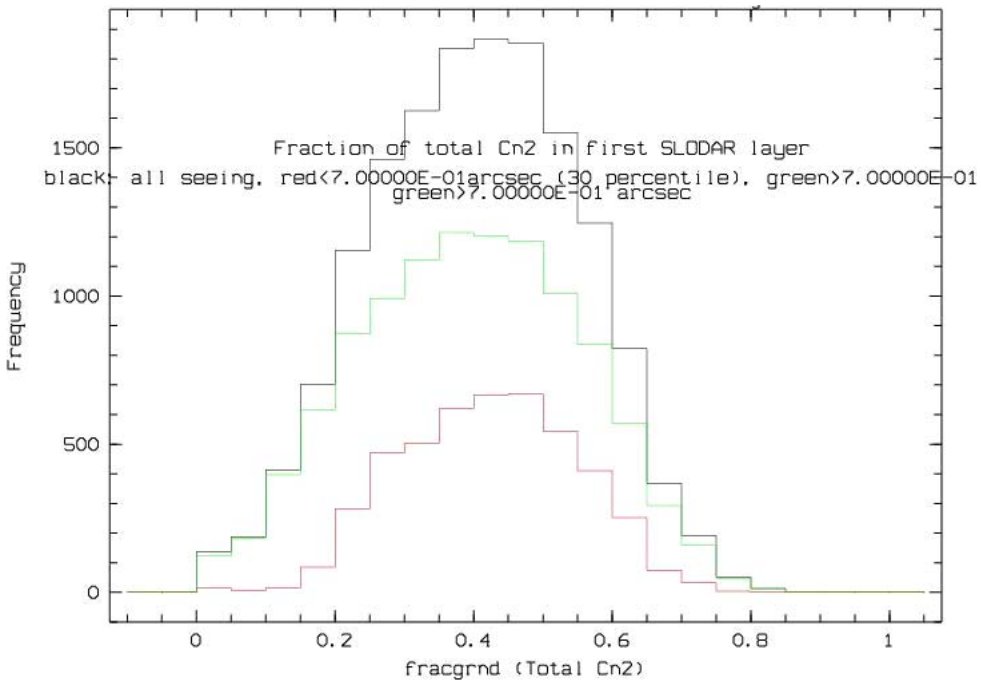

Figure 8-50: Fraction of turbulence located at 200 m as measured by the SLODAR at Paranal

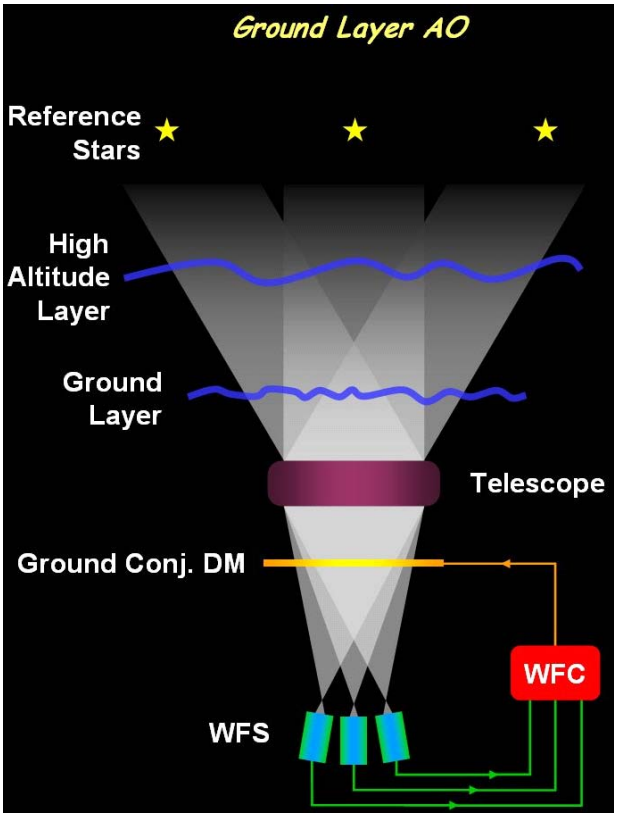

Figure 8-51: Ground Layer Adaptive Optics concept

8.2.2.1 Performance requirements

The GLAO performance requirements are as follows (FoVs specified herein are in diameter):

- GLAO aims at providing reduced seeing images at NIR wavelengths (J-K bands) using Natural Guide Stars (NGSs) for wavefront sensing.

- GLAO aims at providing improved Ensquared Energy (EE) within 50 mas pixel at NIR wavelengths (J-K) according to Table 8-11 and Table 8-12
- GLAO should provide the above correction over 3 goal 6' FOV.
- The maximum un-vignetted technical FOV usable by the GLAO system is 6'.
- GLAO should provide corrected PSF uniformity according to Table 8-13.
- GLAO should maximize the sky coverage over which the GLAO correction can be provided: 70-80 % at the North Galactic Pole and 100% at l=0° and b=50°
- GLAO should offer the possibility to optimize further the Ensquared Energy (EE) in a so-called "narrow field mode" (1-2') using the available NGSs over the technical 6'FoV. The expected gain is at least a factor 2 compared to the correction optimized over 6' FoV.
- GLAO should offer the possibility to optimize the correction on-axis ("very small narrow field mode") using the NGSs available over the 6' FoV. This can be seen as an extension of the SCAO at relatively low Strehl ratio but with a much larger Sky coverage.
- In this mode, GLAO should provide on-axis Ensquared Energy in 50mas pixel in K-Band of 20% and 6% under 0.53" and 1" seeing using a cluster of NGSs of 16th magnitude.
- GLAO should support telescope nodding at 0.1 Hz by fast opening/closing GLAO loop (0.1s).
- GLAO should support small amplitude -1"- mosaicking in closed loop by offsetting the WFSs synchronously. The accuracy of the offset should be better than 1/5 of the spatial pixel size -50mas-
- GLAO does not support chopping
- GLAO should provide in closed loop Field Stabilization to the telescope with the maximum amplitude characteristics provided in Table 8-1. For wavefront sensor dynamic reasons, the telescope guider will support GLAO for closing the AO plus Field stabilization loop before the control of the field stabilization corrector is taken over by the GLAO in closed loop.
- GLAO should permit to observe without AO (but with Field Stabilization) without any transmission loss with respect to the telescope. In that case, the field stabilization corrector is not controlled by the AO system.
- GLAO should have the capability to correct for some of the telescope aberrations left by the active optics with an amplitude lower than 20% of the atmospheric wavefront at all spatial and temporal frequencies. Errors beyond these values are handled by the active optics.
- The transmission of GLAO should be maximized for the instrument observing wavelength T>95%;
- Vignetting of the scientific FOV by the GLAO wavefront sensors should be minimized (TBC)
- For the performance evaluation of GLAO seeing assumptions should be: 0.53 and 1" at 0.5 μm at zenith; with τ_0=3 and 2ms. For the performance evaluation the outer scale of turbulence should be L0=25 m. For the determination of the AO design parameters the following atmospheric parameters should be assumed: turbulence outer scale L0=100m, seeing=1.5", τ_0=2ms – Figure 8-4.
- GLAO shall be able to correct for differential atmospheric dispersion between the NGS and the Science object during an observation by applying offsets to the wavefront sensors. The calculation of the offset shall be done by the software based on the science beam effective wavelength provided by the instrument, the spectral type of the NGS provided by the observer, the science and guide star coordinates provided by the observer, the relevant atmospheric data (Temperature, Pressure, and Humidity) provided by the observatory – with the required accuracy. GLAO will not correct for the atmospheric dispersion within the scientific band pass of the instrument.

	Wave band	K-band		H-band		J-band	
	Guide stars magnitude (per star)	V=15	V=17	V=15	V=17	V=15	V=17
seeing, τ_0, L_0 @ 0.5µm	0.53", 3ms, 25m	12	11	7	6	4	3.5
	1", 2ms, 25m	2.2	2	1.3	1.2	1	0.9

Table 8-11: GLAO Ensquared Energy (%) in 50mas pixel over 6' FOV

	Wave band	K-band		H-band		J-band	
	Guide stars magnitude (per star)	V=15	V=17	V=15	V=17	V=15	V=17
seeing, τ_0, L_0 @ 0.5µm	0.53", 3ms, 25m	4	3	2.8	2.3	2	1.7
	1", 2ms, 25m	2.9	2.6	1.9	1.7	1.5	1.4

Table 8-12: GLAO – Gain in Ensquared Energy in 50mas pixel over 6' FOV, corrected PSF vs. seeing.

	Wave band	K-band		H-band		J-band	
	Guide stars magnitude (per star)	V=15	V=17	V=15	V=17	V=15	V=17
seeing, τ_0, L_0 @ 0.5µm	0.53", 3ms, 25m	**±10%**	**±10%**	**±9%**	**±9%**	**±8%**	**±8%**
	1", 2ms, 25m	**±10%**	**±10%**	**±9%**	**±9%**	**±8%**	**±8%**

Table 8-13: GLAO Ensquared Energy variation in 50 mas pixel over FOV (PSF uniformity)

8.2.2.2 Implementation Concept

8.2.2.2.1 Corrector and wavefront sensors

The GLAO concept is conceived as an extension of the SCAO system equipped with 6 wavefront sensors. The corrective element is the M6AM unit described in section 8.2.1.2.1 and the wavefront sensor is essentially six units of the wavefront sensor described in section 8.2.1.2.2, which permits a high standardization in WFS design and allow the correction of high order modes, which is required by GLAO to pump energy from the PSF wings towards the core. The specific linearity requirement of the GLAO mode may require 6x6 pixels for the Shack Hartmann wavefront sensor already assumed for SCAO. The maximum closed loop update frequency is 500 Hz. Slower frames rates may be used, if the site shows a slow ground layer turbulence.

8.2.2.2.2 Control and Real Time Computer

The maximum closed loop update frequency is 500 Hz.

The slope computation is performed in the following way (2 options):

- The signal of each sub-aperture is obtained by co-adding numerically the signals of the same sub-aperture from all the wavefront sensors and then the related slope is computed;
- The slopes are computed for each wavefront sensor and averaged per sub-aperture.

Two types of reconstructions can be implemented in GLAO depending on the degree of uniformity across a specified FoV and the concentration of light required.

Control of Wide-field mode

The wide-field mode is designed to provide a uniform correction in the whole scientific FoV. A good estimate of the ground-layer phase perturbation is given by the average of the phases estimated from several wavefront sensors coupled to the NGSs located in the FoV.

The closed loop reconstructor is the average of the reconstructors computed individually for each wavefront sensor at a specified FoV location in order to take into account the field-dependent non common path aberrations and the possible difference in linearity of each WFS. The vector of reference slopes for each wavefront sensor is obtained by a look-up table previously calibrated.

Control of Narrow-field mode

The narrow-field mode is designed to boost the performance in a given direction (or smaller portion) of the scientific FoV. The improvement in correction at this specified direction is achieved at the expense of the uniformity of the correction in the whole FoV.

The wavefront reconstructor for the narrow-field GLAO mode is based on the minimum-variance (MV) reconstructor, R_{MV}, which can be expressed as the product of two matrices:

$$R_{MV} = P \times E \qquad \textit{Eq. 8-1}$$

The matrix E represents a full tomographic reconstruction of the turbulence volume (possible only when the vertical distribution of the atmospheric turbulence, obtained in real time from a vertical profilometer, is known), and the matrix P stands for an optimal projection from the reconstructed turbulent layers onto the deformable mirror taking into account the direction(s) where optimization is desired.

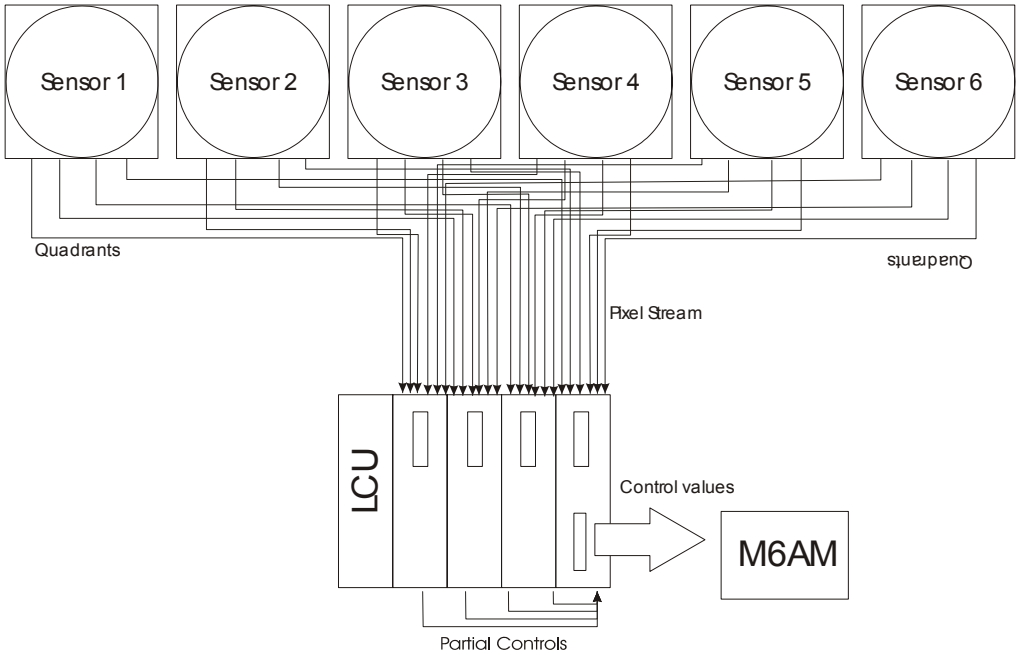

Figure 8-52: GLAO real-time hardware architecture

Real Time Computer

This mode is a multiple-sensors / single-mirror system. Only the option based on a Shack-Hartmann sensor will be considered here. Both the deformable mirror and the detector technology will be the same as for SCAO, although in this case we will have 6 sensors. Gradients computed on each sensor will be averaged before running the reconstructor. This operation approximates the ideal solution (reconstructing each sensor measurement individually and only later averaging them). In this way we average the gradients coming from each sensor and we multiply them with an average reconstructor: this is correct as long as the difference

between the various reconstructors is small. Therefore the complexity of such a system will be similar to the one previously analysed, where the additional complexity lies only in the acquisition. Control strategy, loop frequency and tolerable delay are also the same.

By using the same concept as in the previous case, we obtain that the only difference is the input architecture (Figure 8-52) where multiple streams coming from the 6 detectors have to be merged together. We assume the same architecture of the SCAO case, where the pixel data stream of each detector had been split in four channels, one for each quadrant. The corresponding quadrant of each detector will be routed to the same input processor for averaging. The rest of the system will be identical to the SCAO case.

8.2.2.3 Predicted performance

A detailed analysis of the GLAO performance based on end-to end simulations, as well as the assumptions and AO parameters, are provided in RD25. Note that the GLAO performances provided here does not include yet all error sources -calibration errors, optical quality of the telescope, wavefront sensor and instrument optical paths, mis-registration error, atmospheric chromatism etc…- but only the pure AO performance part. In the GLAO mode, we believe that the impact of the error budget on the final performance should have a little impact due to the partial correction provided by the GLAO system.

The evaluation of the GLAO performance should cover two main aspects:

- The Ensquared Energy within a given pixel size here assumed to be 50mas.
- The Sky Coverage over which the correction is available.

8.2.2.3.1 Sky coverage

The proposed GLAO system is based on Natural Guide Stars. In the following, we will present the sky coverage achievable with a GLAO system. More details about this are provided in RD27.

The Sky Coverage (SC) has been computed using the coordinates and the magnitudes of the star fields at different galactic latitudes. The star fields have been extracted from the USNO B1.0 catalogue.

In the following, we have limited the number of NGSs for wavefront sensing to 6, which is a reasonable trade-off between the complexity of the tomography and the sky coverage achieved. The determination of the optimum number of NGSs is a complex trade-off which involves a large number of parameters and simulations to be conducted during phase B:

- Layer Oriented (LO) vs. Star Oriented (SO) -see [124].-
- Optical or numerical co-addition of NGS flux over the whole FOV
- RON of the WFS detector versus feasibility of the optical co-addition
- Vignetting of the scientific FOV by the WFSs
- GLAO performance uniformity due to NGSs random distribution vs. number of GSs
- Faintest acceptable guide star for wavefront sensing
- Optimisation of NGSs magnitude difference for the LO

Figure 8-53 and Figure 8-54 provide the sky coverage achievable versus the NGS magnitude at the North Galactic Pole and at b=50. If the faintest guide star usable for wavefront sensing is around m_R =17 - RON=0e$^-$ (which is typically the limiting magnitude of the ESO SINFONI-MACAO-NAOS systems -

Figure 8-55[65]- still providing a correction comparable with a “seeing reducer”) we see that the SC achievable is in 10% at the Galactic Pole and close to 50% for *l*=0° and *b*=|50°|.

[65] Note that Figure 8 55 has been produced with data taken on 1st August 2004 on UT4 with MACAO. The magnitude of the star is 15.7 and the other images have been obtained by using neutral density filters, so the sky background got

Extension to m_R =18 is not out of reach if detector with high QE in the red can be developed as explained in section 8.2.1.4.5. In that case the SC becomes ~25% at the Galactic Pole and ~85% at intermediate galactic latitudes. In this regime, the sky background $m_{V=}$[19 - 20.7] starts to contribute with a corresponding sky background flux received by the WFS of [145 - 30] e-/sub-aperture/s compared to the NGS flux = 375 e$^-$/sub-aperture/s.

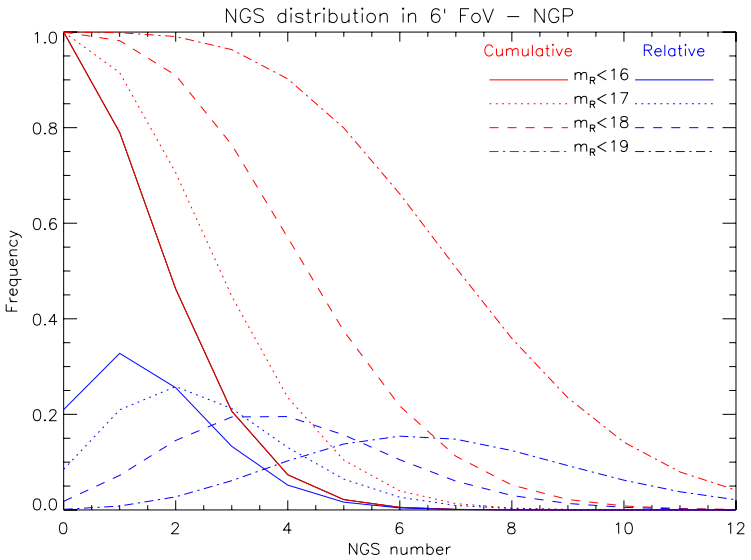

Figure 8-53: Frequency of circular 6 arcmin diameter fields as a function of the number of NGS included at the North Galactic Pole for different NGS limiting magnitudes

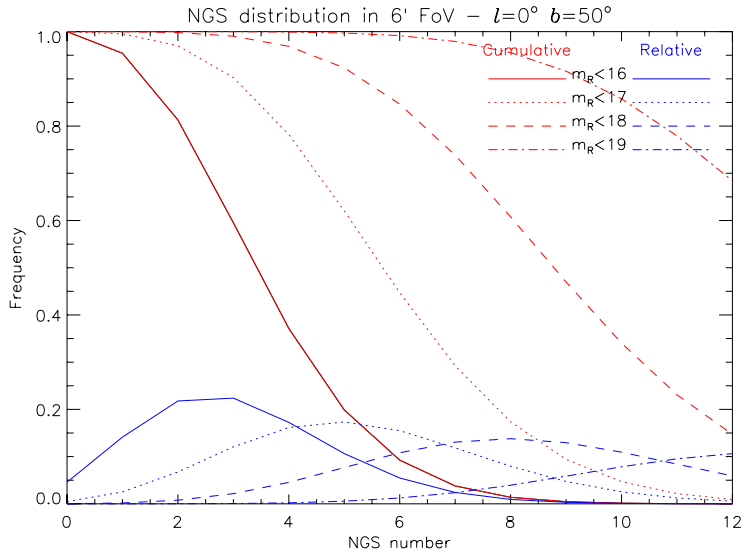

Figure 8-54: Frequency of circular 6 arcmin diameter fields as a function of the number of NGS included on them at at l=0° and b=|50°| for different NGS limiting magnitudes.

In the following we provide the performance of the GLAO using a visible SH WFS for both the "good" and "bad" seeing conditions" respectively r_0~20cm and r_0~10cm -0.53" and 1" seeing at 0.5 µm.

---

dimmed to. The label "dimmed" in the picture is there to emphasise this aspect. The images are exposures of 30 seconds, the seeing reported by DIMM was between 0.65" and 0.8" and tau0 was beween 1.9 and 3.3 ms.

Figure 8-56 provides the Ensquared Energy within a pixel of 50 mas at NIR wavelength. We see that for a NGS flux of 2e-/sub-aperture/s corresponding to m_R =17 the EE is about 12% in K band under good seeing conditions. This value drops to 2% for bad seeing conditions.

More detailed simulations can be found in RD25.

Higher Ensquared Energy values, or correction at shorter wavelengths, will require the implementation of multi- Laser Guide Stars as confirmed by the study made for the VLT GLAO system: GALACSI.

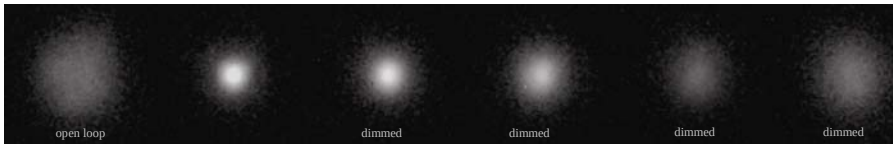

Magnitude:	**15.7**	**15.7**	**16.87**	**18.00**	**19.26**	**19.86**
CWFS raw flux:	**1.9e5 c/s**	**1.9e5 c/s**	**7e4 c/s**	**3e4 c/s**	**0.9e4 c/s**	**6e3 c/s**
FWHM:	**527 mas**	**89 mas**	**117 mas**	**143 mas**	**248 mas**	**401 mas**
Raw Strehl:	**2%**	**24%**	**15%**	**10%**	**5%**	**2.2%**

Figure 8-55: Performance of the VLT MACAO system on UT4

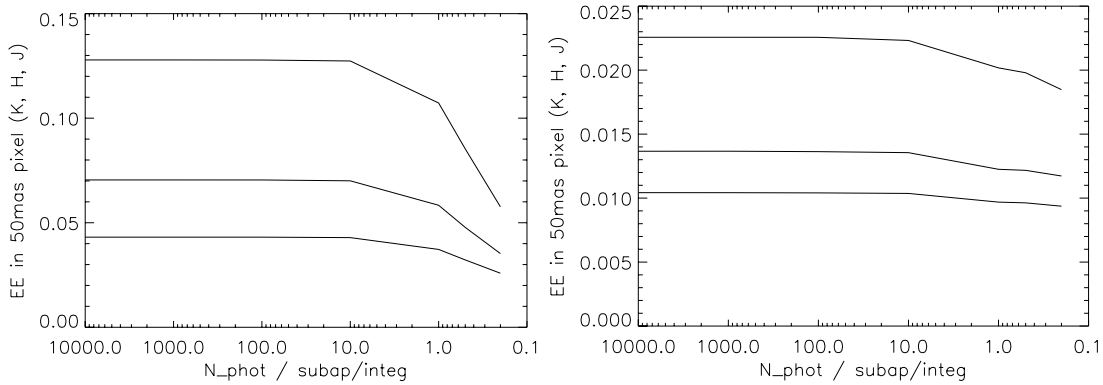

Figure 8-56: GLAO Ensquared Energy in 50mas for seeing of 0.53"(left) and 1" (right) at 0.5µm; 6 NGSs

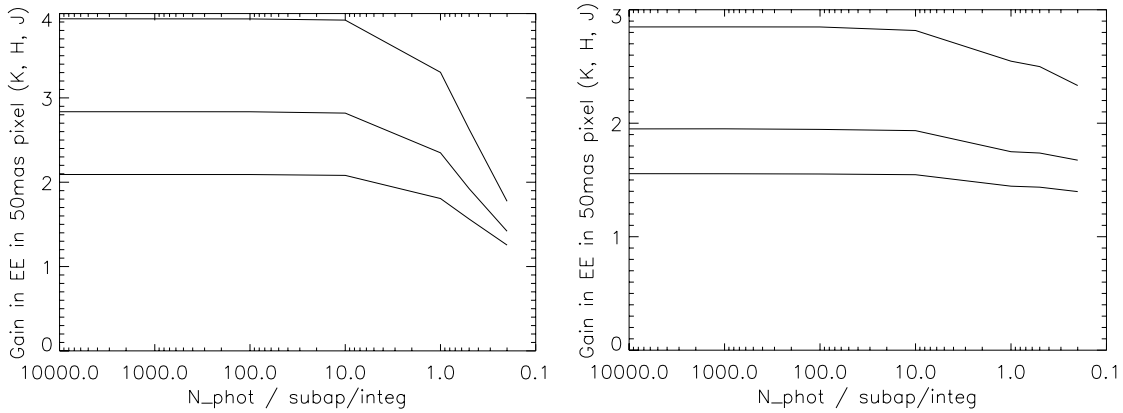

Figure 8-57: Gain of EE in 50mas brought by GLAO relative to seeing for seeing of 0.53"(left) and 1" (right) at 0.5µm; 6 NGSs

Figure 8-57 provides the gain of Ensquared Energy within a pixel of 50mas brought by the GLAO correction with respect to seeing. We see that this gain is between 3.5 and 2.5 in K-band for the good and bad seeing conditions for m_R =17.

Reducing the corrected FOV to 3' improves the EE from 12 to18%. However, if he technical FOV is also reduced to 3' this would affect the sky coverage.

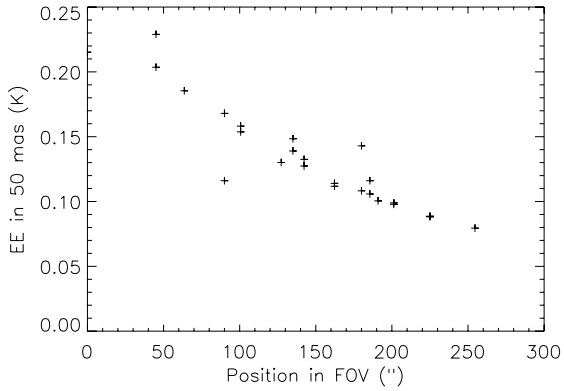

Figure 8-58: EE vs field of view position (K-band); 3NGS in 3' plus 3 NGSs [3-6']; faint star 1e-/sub-aperture/s, good seeing model

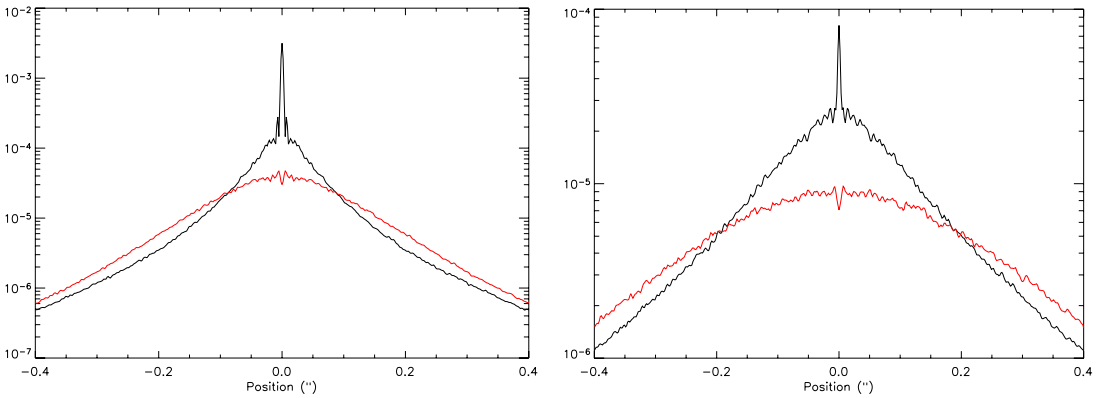

Figure 8-59: Corrected PSF with GLAO using 6 NGSs, 6', good seeing (left) and bad seeing (right), K band, on-axis, 10ph / subap / NGS top curve is GLAO, bottom curve is the uncorrected seeing.

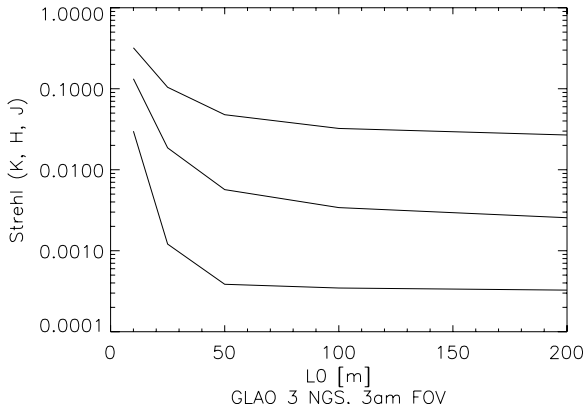

Figure 8-60: Effect of the outer scale of turbulence (L_0) on the Strehl obtained with GLAO with 3 NGSs within 3' FOV; good seeing; Top to bottom: K, H, J.

Another important performance parameter for GLAO is the corrected PSF uniformity over the FOV. Figure 8-58 provides the PSF uniformity assuming 3 NGSs within the central 3' FOV and 3 additional NGSs located in the annular FOV [3-6'].

Figure 8-59 provides the corrected PSF shapes with GLAO with 6 NGSs of magnitude of 15.1. Note the diffraction peak probably due to the effect of the turbulence outer scale L_0=25m also shown Figure 8-60.

8.2.2.4 Near-Term development plan

8.2.2.4.1 Modelling and Simulation

First order simulations have been performed to estimate the GLAO performance in near Infrared (NIR) with a 98x98 actuator systems. Sky coverage has been evaluated based on a maximum of 6 NGSs and wavefront sensors.

Statistics of turbulence profiles are now becoming available thanks to the special effort made to develop dedicated profiler tools like MASS (Multi-Aperture Scintillation Sensor) and the SLODAR (Slope Detection And Ranging). As measurements continue to be gathered, more information about the amount and the structure of the ground layer will be obtained. Based on these data, GLAO performance should be updated.

The number of NGSs to be used for wavefront sensing, the optimum technical FOV and the maximum magnitude difference between the NGSs should be tuned according to the science requirements: Ensquared Energy, corrected FoV, PSF uniformity, sky coverage.

Extensive parametric simulations remain to be done to tune the design parameters:

- Optimization of the Shack Hartmann wavefront sensor geometry fitting the M6AM geometry (Circular, hexagonal, squared)
- Optimization of the Shack Hartmann wavefront sensor pixel scale and FoV
- WFS linearity issues
- Effect of the turbulence produced by the telescope itself over the first 200-400m and variation of the turbulence along the telescope pupil
- Study of the variable M6AM conjugation altitude effect on the GLAO performance
- Full error budget of the GLAO system

8.2.2.4.2 AO concept and design

The detailed implementation of the GLAO wavefront sensors and their number into the OWL Adapter-rotator will be developed during phase B.

Although the present baseline is currently the Star Oriented concept with averaging of the wavefront measured from each wavefront sensor, concepts using the Layer Oriented approach with numerical or optical co-addition still needs to be studied.

The vignetting of the scientific FoV produced by the shadow of the wavefront sensors needs to be minimized. Potential use of a large dichroic may solve this issue but may require an evolution of the optical design towards longer backfocal distances. A reassessment of the optical design is planned at the beginning of the design phase.

Trade offs between the length of the wavefront sensor -instrument non-common optical path and the stability of the pupil matching should be studied. To correct for flexures, an internal metrology system may be required between the wavefront sensor and the instrument although this is less critical than in the case of SCAO.

In case the required density of actuators appears not to be achievable in the time and budget allocated, we have not identified at this stage any fall-back solution using a second stage post-focal deformable mirror mainly due to the large technical FOV to be propagated into the optical path up to the pupil plane where the second stage deformable mirror would have to be located.

We envisage developing the M6AM test facility such that the GLAO mode is fully tested before being installed at the telescope.

At ESO, several second-generation instruments are currently being designed for the VLT based on GLAO correction (GALACSI for MUSE, GRAAL for HAWK-I) combined with the development of the VLT Adaptive secondary and the new generation of the CCD WFSs. The purpose of GALACSI is to improve by a factor 2 the ensquared Energy within 0.2" in the visible over a FOV of 1', while GRAAL will increase the Ensquared Energy within a pixel of 0.1" in the IR over a FOV of 10' diagonal. Both GLAO systems make use of multiple LGSs providing higher sky coverage and the expected performance even under bad seeing conditions. Apart from their own scientific interest at the VLT, they are considered as an essential step toward the implementation of more performant GLAO systems at the OWL telescope.

Furthermore, preliminary studies on GLAO for ELTs are also in progress in the frame of OPTICON-JRA1 and the ELT design study in the AO WP. In this context, the MAD demonstrator can provide an early insight into important aspects of GLAO, such as wavefront reconstruction and control techniques.

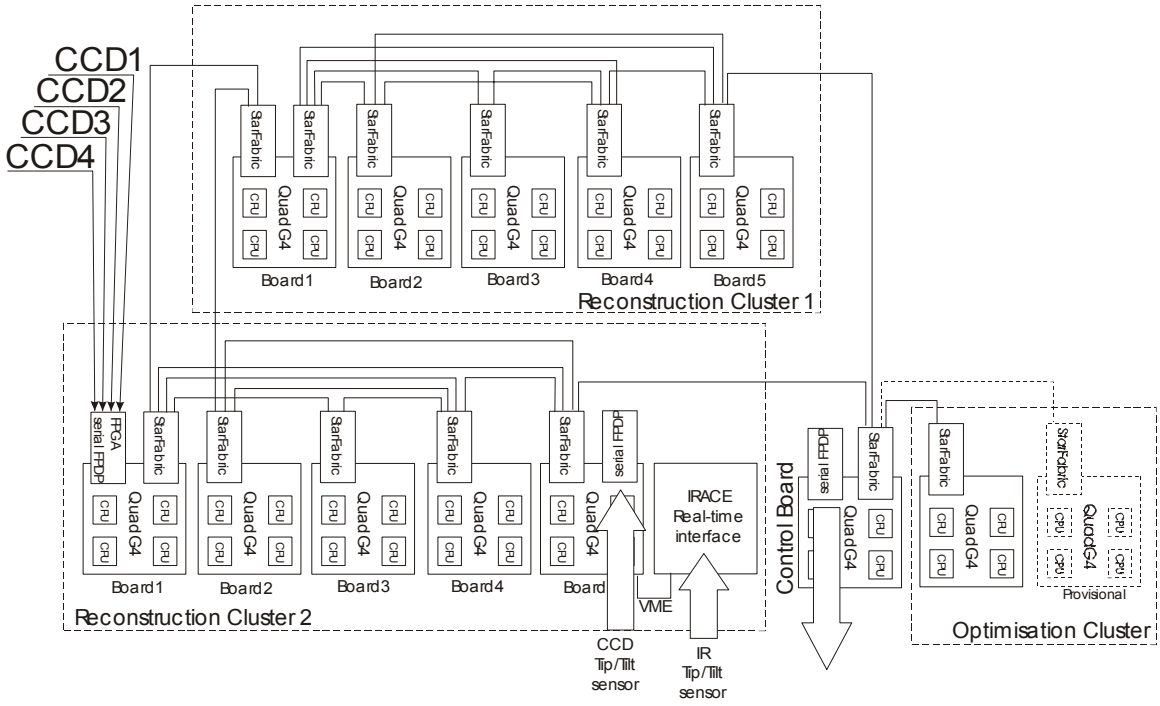

Figure 8-61: HAWK-I concept based in CPU-only SPARTA architecture. With the new FPGA architecture the number of computational units will be reduced.

The GLAO star-oriented configuration of MAD comprises three Shack-Hartmann WFSs and one bimorph DM conjugated to the telescope pupil. Also, the maximum scientific/technical FoV of MAD is 2 arcmin. With MAD we will be able to investigate different aspects of wavefront reconstruction for GLAO.

The calibration aspects regarding GLAO are also being studied on MAD. It essentially consists in minimizing the calibration error and the calibration time as described as described in the dedicated paragraph of SCAO and MCAO and in RD27..

8.2.2.4.3 AO key component status and development

The key components, corrector and wavefront sensors are essentially identical to the SCAO system. There is no additional component development required for the implementation of the GLAO system.

The RTC concept is based on the same modules used for the SCAO case, so no special development is needed apart from the development of a 6-channels input processor since the

current hardware developed under the OPTICON/JRA-1/SPARTA project supports only 4 input channels.

This concept is also used in MAD, with a prototype SPARTA architecture, and with higher performance in GALACSI and GRAAL.

8.2.3 Distributed Multi Object Adaptive Optics

A highlight science case is: First light- The First Galaxies and the Ionization State of the early Universe. It aims at peering into the Dark Ages of the Universe when the universe was re-ionized by the UV flux emitted by the first sources of light. Recent observations of the high redshift universe suggest that stars and galaxies started to form and to assemble early in the redshift range of 7-15. Understanding this key epoch is of paramount importance and requires the following exquisite instrument capabilities on OWL:

- Multi Integral Field Unit (IFU) observing mode
- Number of IFU targets: 30 or higher for a 6x6' FoV
- Image quality at 30% ensquared energy: 50 mas or better at selected area in the field (direction of the IFU targets)
- Spatial sampling: 10-30 mas
- Spectral resolution: 5000-8000
- Spectral coverage: Y (1.06 μm) to K (2.2 μm) bands
- IFU field of view 0.8''

The underlying Adaptive Optics concept – namely Multi-Object Adaptive Optics (MOAO) or Distributed Adaptive Optics - Figure 8-62- is therefore to correct atmospheric turbulence in selected directions of the sky where the IFU are pointing.

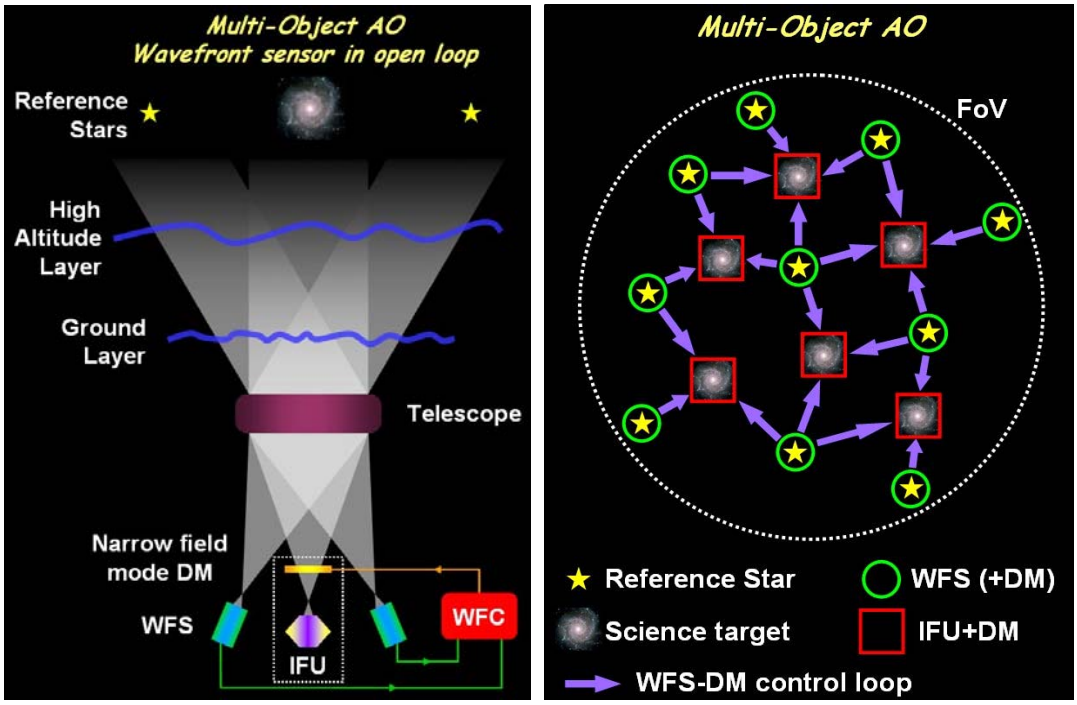

Figure 8-62: Concept of Multi-object Adaptive Optics or Distributed Adaptive Optics with wavefront sensors in open loop

This can be accomplished by paving the focal plane with WFSs units in the direction of the reference sources for a local determination of the turbulent wavefront and with Deformable

Mirrors (DMs) in each of the IFU channels. In this approach the Adaptive Optics system operate essentially in open loop as the wavefront sensors do not see the correction applied by the deformable mirror and therefore do not operate around the zero position. This concept requires wavefront sensors with a high dynamic and linearity and deformable mirror with high linearity and blind position accuracy. This extends the FALCON (Fiber-spectrograph with Adaptive optics on Large fields to Correct at Optical and Nar-infrared) concept described [102].

Alternative MOAO concepts are being considered to reduce the potential WFS dynamic and linearity issues by adding local deformable mirror to each wavefront sensor -Figure 8-63-. In this concept, the correction is optimized in each IFU and WFS directions. High linearity and blind position accuracy of the local deformable mirror are required. The drawback of this approach is the increase of complexity as more deformable mirrors need to be controlled.

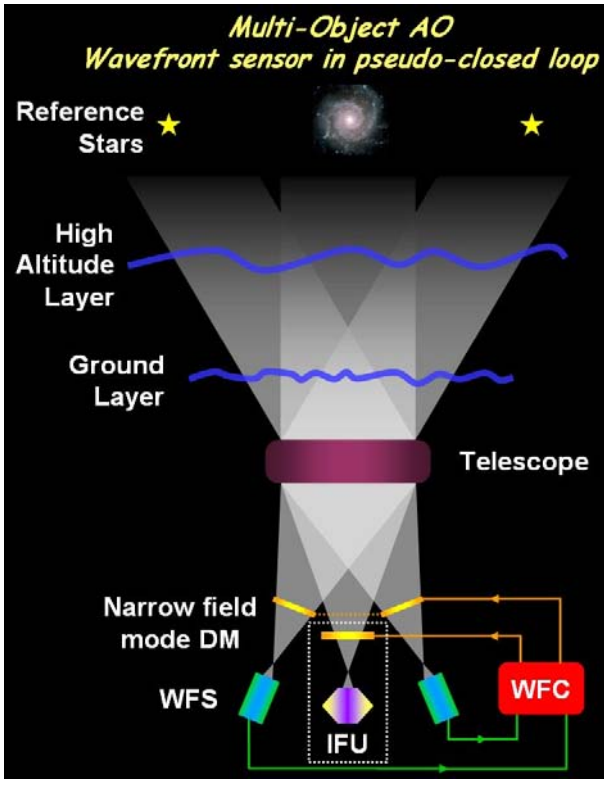

Figure 8-63: MOAO concept with the wavefront sensor in pseudo closed loop

In the following, we will assume that the MOAO system is combined with the GLAO system described in section 8.2.2. Several reasons motivate this approach:

- The availability of the M6AM unit
- The reduction of the local DM stroke requirements (expected to be critical)
- The complementarity of the two concepts

In this concept the wavefront of all available wavefront sensors in the FoV will be combined to control the M6AM unit in order to minimize the wavefront residual over the whole FoV while the local DM correction will be optimized in the direction of each IFU (and optionally each WFSs – Figure 8-64).

In the following section we will assume a GLAO + MOAO system with the WFSs in pseudo closed loop. This concept may evolve in phase B based on the studies and demonstration experiments planned. The possible AO implementation concept is derived from the MOMFIS (Multi-Object Multi Field Infrared Instrument) study described in 12.2.3.4 and a possible development plan towards the construction of such instrument.

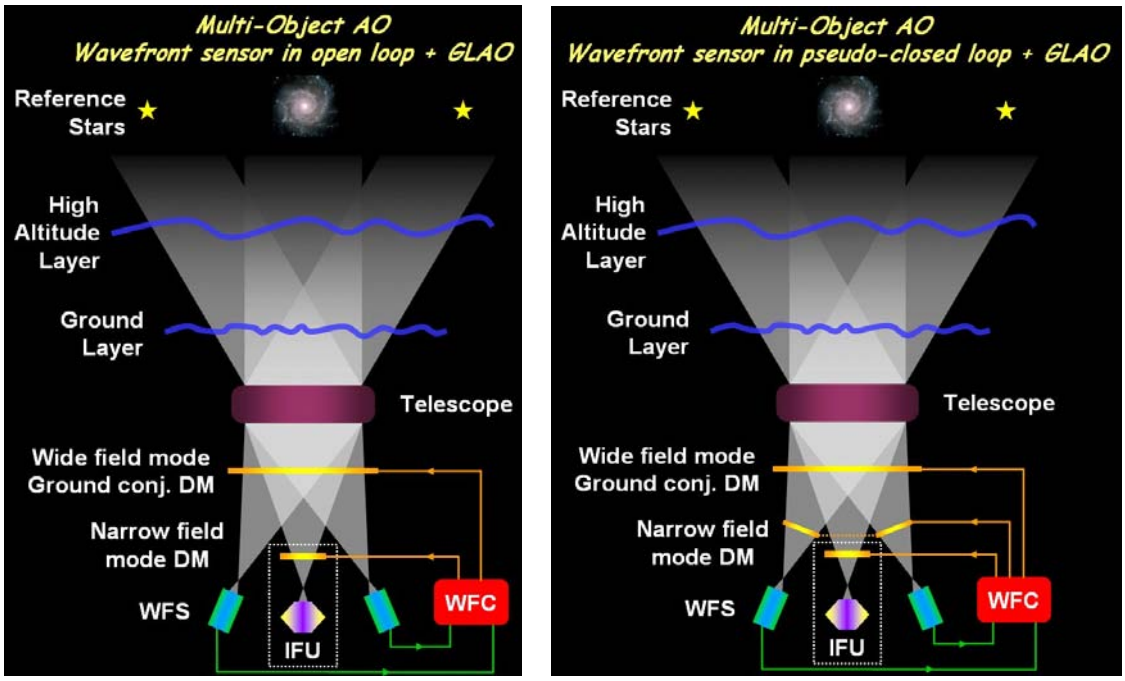

Figure 8-64: GLAO combined with MOAO concept with the wavefront sensor in open loop (right) and in pseudo closed loop (left)

MOAO should support telescope nodding at 0.1 Hz by fast opening/closing GLAO loop (0.1s).

MOAO should also be able to correct for differential atmospheric dispersion between the wavefront sensing NGS and the Science object during an observation by applying offsets to the wavefront sensor. The calculation of the offset shall be done by the software based on the science beam effective wavelength provided by the instrument, the spectral types of the NGSs provided by the observer, the science and guide star coordinates provided by the observer, the relevant atmospheric data (Temperature, Pressure, and Humidity) provided by the observatory –with the required accuracy. MOAO will not correct for the atmospheric dispersion within the scientific band pass of the instrument.

8.2.3.1 Implementation Concept

8.2.3.1.1 Overview

Figure 8-65 represents the high level functional diagram of the instrument. The Science channels are represented in blue and consist of:

- A target selection system: it direct a science beam from the telescope focal plane to the deformable mirror
- A deformable Mirror: it corrects the wavefront in the direction of the target
- An Integral Field Spectrograph (FoV 0.6-1”, sampling 20-30mas, spectral resolution 4000-8000).

The reference sources (assumed here to be NGSs but the concept can be applied to LGSs equally well assuming LGSs can be implemented) are represented in blue. The NGS beams are directed from the telescope focal plane up to the WFS with a selection system partly similar to the target selection system. These NGSs can be acquired over the full instrument FoV. In the implementation example 10 WFSs are foreseen, but this number can be freely adjusted.

Figure 8-66 provides the general implementation of the system. An important feature of MOMFIS is that it uses the same selection system (pickoff mirrors) to direct the light to the science and to WFSs channels, providing full configuration flexibility. NGS can be as close as 5” from the target FoV. Up to 10 or more reference sources can be selected.

8.2.3.1.2 Wavefront sensor

For linearity reasons important for the MOAO concept, the baseline for the WFS will be a Shack Hartmann with 100x100 sub-apertures and potentially with 6x6 pixels/sub-aperture. This is quite similar to the SCAO and GLAO WFSs. At this stage it is not clear whether the WFS buttons will also be equipped with a local deformable mirror reducing the linearity effect due to the pseudo-open loop or whether the number of pixels will be enough to ensure a good correction in this mode. Several control schemes will have to be studied during phase B.

To reduce the stroke requirements on the local deformable mirror, it is foreseen to use the wavefront measured by all wavefront sensors in the FOV to correct for the Ground layer using the M6AM unit. The wavefront to be corrected by the local deformable mirror in the direction of the targets or in the direction of the WFSs is essentially the remaining turbulent layers.

8.2.3.1.3 Micro deformable mirror

Preliminary studies performed in the frame of the VLT FALCON concept study have shown the importance of a linear response of the local deformable mirror. The micro-deformable mirrors based on the electrostatic concept seem well adapted for this application. Assuming a 250µm actuator pitch the size of the DM is 25mm. It remains to be determined whether the amount of residual turbulence to be corrected by the MDM is compatible with the stroke which can be delivered by this kind of technology.

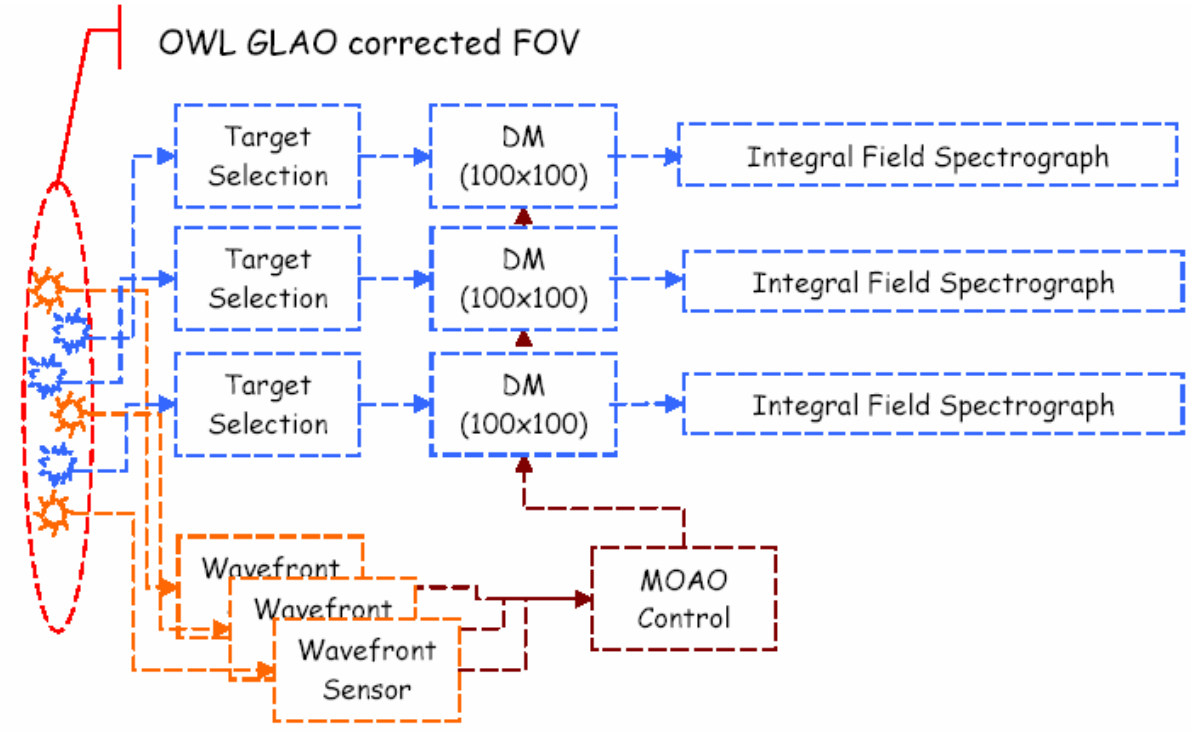

Figure 8-65: MOMFIS schematic functional diagram (Courtesy LAM, France)

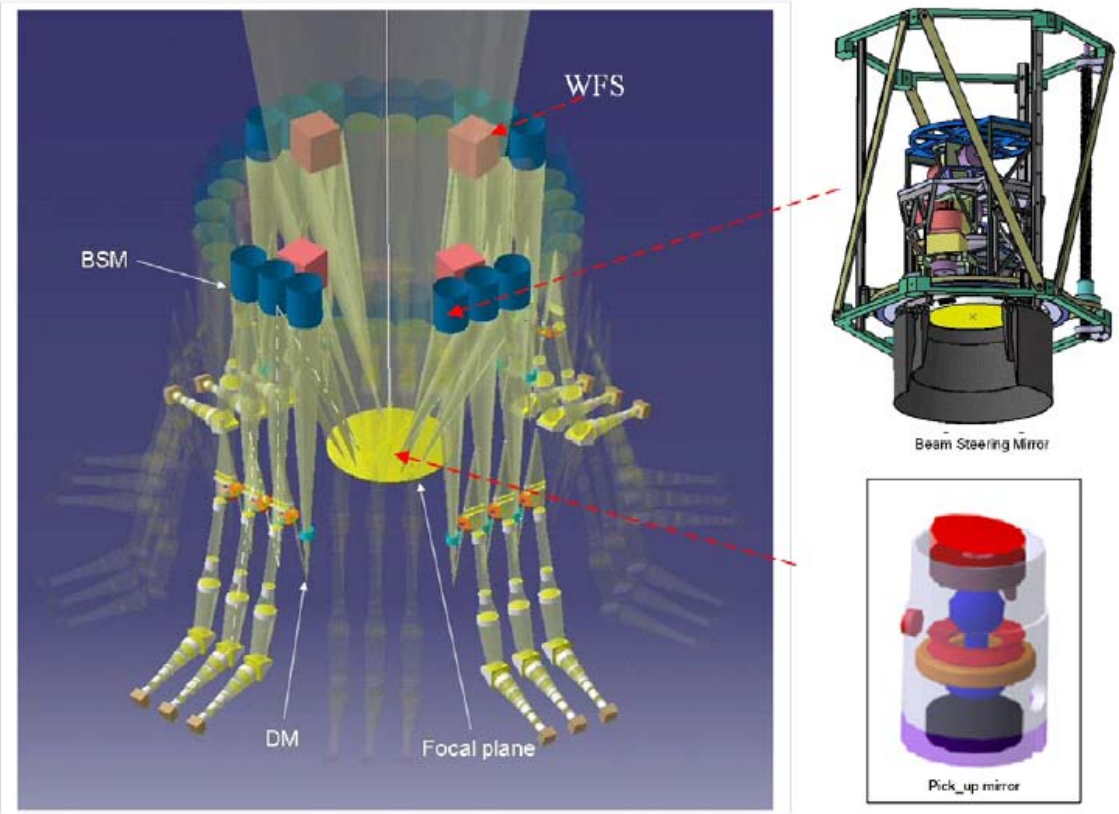

Figure 8-66: MOMFIS general view of the implementation: in the focal plane small pick-off mirrors are positioned with a robot, directing the target beams steering mirrors and the reference star beams to the WFS. The steering mirrors direct in turn the beam to the DM and IFU units (Courtesy LAM, France)

8.2.3.1.4 Control and Real Time computer

MOAO is a multi-sensors / multi-mirrors system. Sensors are actually complete AO systems and they incorporate a local mirror for local control (the local mirror is optional but it is the current baseline). Three sensor systems measurements can be combined to drive a mirror (the corrector, serving one IFU) placed to correct a different region of the sky, architecturally similar to the GLAO case, but without averaging the measures in order to optimize the correction in the direction indicated by the position of the correcting mirror. All the sensor measurements are also combined to control in common M6AM, used to correct for large common aberrations, including tip and tilt.

The sensor systems are distributed on the field over guide stars, while correctors (IFUs) are distributed on the field in correspondence to the scientific object(s) of interest. Guide stars are grouped in order to have 3 of them for each corrector. Groups are called “clusters” and there are as many clusters as correctors. A star can belong to multiple clusters.

Guide stars run a local control loop with the local DM.

Each cluster collects the measurement of each sensor of the cluster (and the DM position) to compute the correction on the cluster DM.

Figure 8-67 shows the control architecture of the MOAO system. The 10 sensor systems or buttons receive the light from different guide stars. The picture shows 3 of them. The control loop is a standard SCAO control for each sensor system (or button).

All the gradients of the 10 sensor systems are collected and averaged by another RTC that will drive M6AM with this input. This is fully equivalent to the GLAO control system.

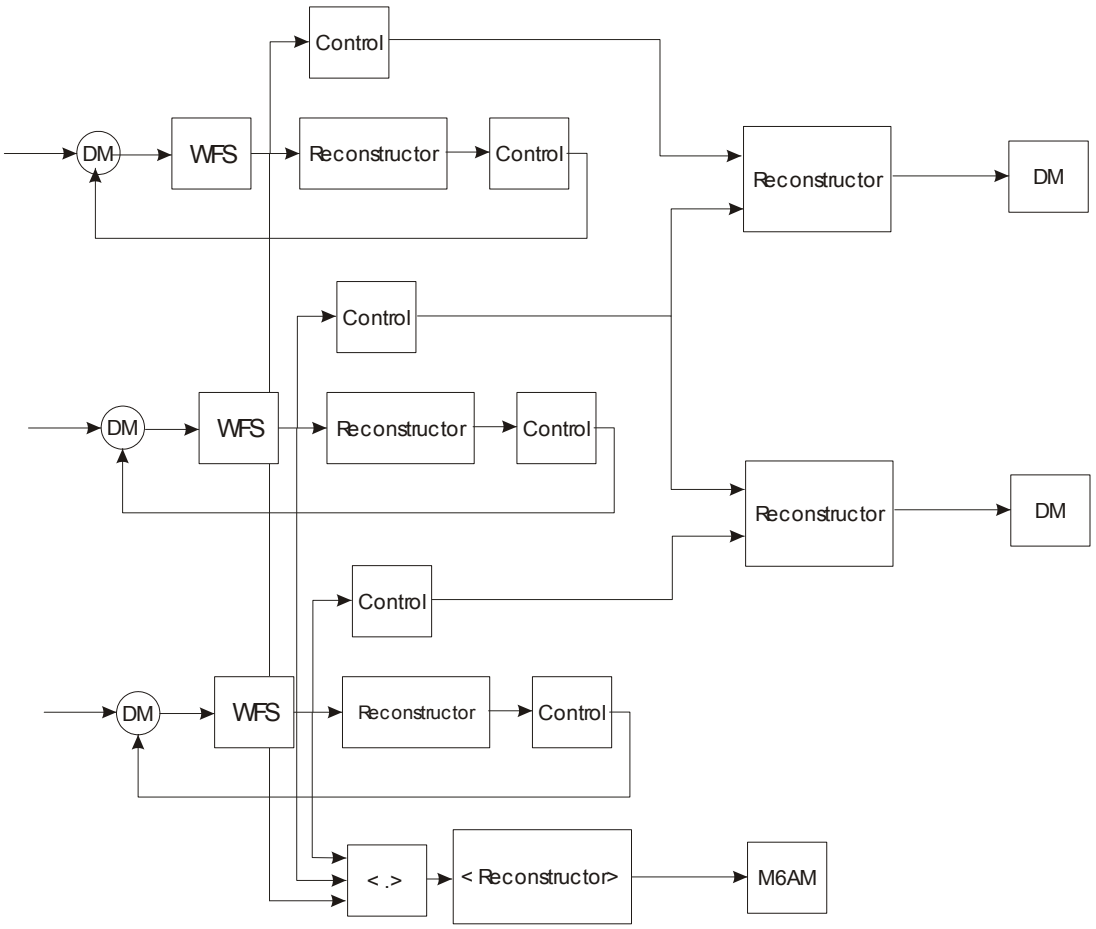

Figure 8-67: MOAO control loops

The goal of the MOAO system is to correct the field around 30 science spots. On the light path of each of them a deformable mirror corrects the light. To control the DM, each of the 30 science spots (or IFU) has its own RTC. This RTC is configured to receive the measurements of the atmosphere of the three closest buttons in order to reconstruct the turbulence in the direction it is actually looking. Of course, no button is looking exactly in the direction of any of the IFUs, so this reconstruction is done in open loop since the effect of the IFU DM is not observed by any sensor.

The IFU RTC needs to receive information about the atmosphere, not the residuals that the button sensor is looking at. This information is contained in the actual position of the mirror in each button. Unfortunately it would be inconvenient to wait for that information, since one full frame is required to produce it. In this case the IFU RTC would run with one additional frame delay, which is unacceptable. In the case of a simple integrator, the button control system will run with:

$$y[n]=y[n-1]-gAx[n] \qquad \textit{Eq. 8-2}$$

Where ‘y’ is the position of the mirror, ‘x’ is the gradient vector, ‘g’ the gain and ‘A’ the control matrix. If now we run the following system:

$$s[n]=s[n-1]-gx[n] \qquad \textit{Eq. 8-3}$$

$$y[n]=As[n] \qquad \textit{Eq. 8-4}$$

One can easily see that the output signal ‘y’ is identical to the previous case, but now we have a signal that is proportional to the DM position and that can be computed in a very short time. This

is the signal that will be sent to the IFU RTC without delay and that can be used to reconstruct the turbulence along the IFU direction.

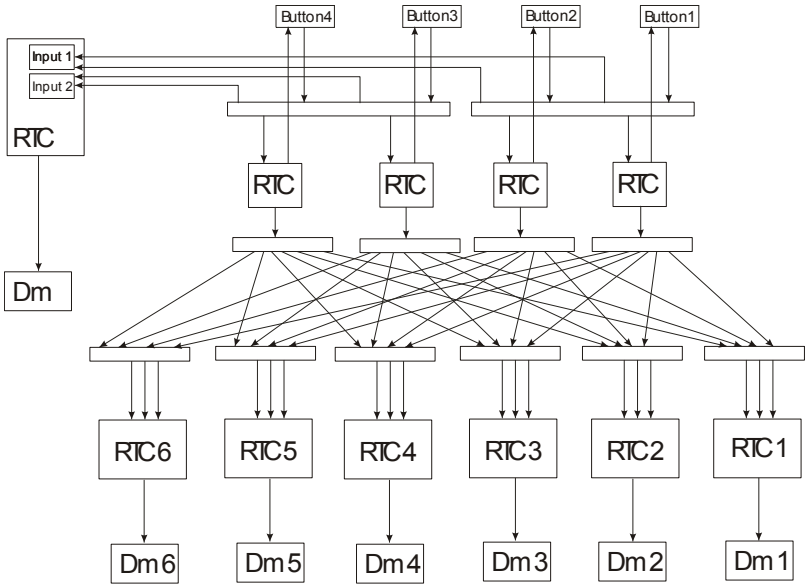

Figure 8-68: MOAO Real-Time Computer Concept. The diagram shows an example with only 4 wave-front sensors with local DM and 6 clusters each serving one IFU. The Dm on the right side is the M6AM.

Each wavefront sensor system is similar in concept to the SCAO system, so each of them will be a clone of such system. The correction of the global DM M6 is similar in concept to the GLAO system, with additional complexity due to the number of sensors. The real additional complexity is given by the cluster control since the measurements of the three sensors cannot be averaged together but a full reconstruction matrix has to be used.

The system is made by three classes of sub-systems, one which is identical to the SCAO case, one very similar to the GLAO case and a new concept to implement the cluster.

8.2.3.2 Predicted performance

The MOAO performance was estimated using real scientific targets, and the associated guide stars constellations (“fields”, see Table 8-14). The analytic simulation too, Cibola, was used for this performance estimation.

Field denomination	**Corresponding number in** Figure 8-68**,** Figure 8-70
UKIDSS-XMM-LSS (center)	Field 0
UDF (center)	Field 1
COSMOS (center)	Field 2
CFHTLS-d1 (center)	Field 3
AC114 (center)	Field 4
Abell 1689 (center)	Field 5

Table 8-14. Field references.

Using real astronomical fields allows us to show that even if sky coverage is limited, some interesting fields can still be observed. In Figure 8-69, we can see that Abell 1689 and AC114 can be observed with quite good performance (gain of a factor of ~20 in ensquared energy within a 50 mas pixel in H band, 1’’ seeing), whereas UKIDSS-XMM-LSS and UDF have rather small gains (factor ~2). We can also see there is a significant benefit in using 8 rather than 3

guide stars, and that it is better to take the brightest ones rather than those closer to the the observed fields. We have done the same analysis with 12 NGS instead of 8, and the gain was minimal, especially compared to the added system complexity. In Figure 8-69, the solid lines represent the 8 NGS case, the dashed lines the 3 NGS case. The top line is when the brightest 8 (or 3) stars are considered, the bottom line when the nearest (to the center) are used.

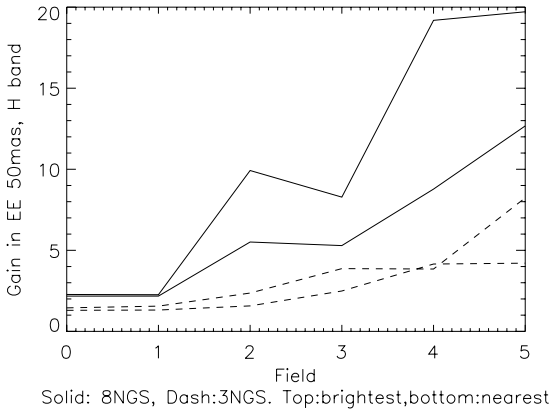

Figure 8-69: Gain in Ensquared Energy in a 50 mas pixel for each scientific target, H band, 1" seeing.

The distribution of the guide stars both spatially and in brightness can be seen in the following two plots (Figure 8-70). On these figures, the solid lines represent the 8 NGS case, the dashed lines the 3 NGS case. The top line is when the brightest 8 (or 3) stars are considered, the bottom line when the nearest (to the center) are used.

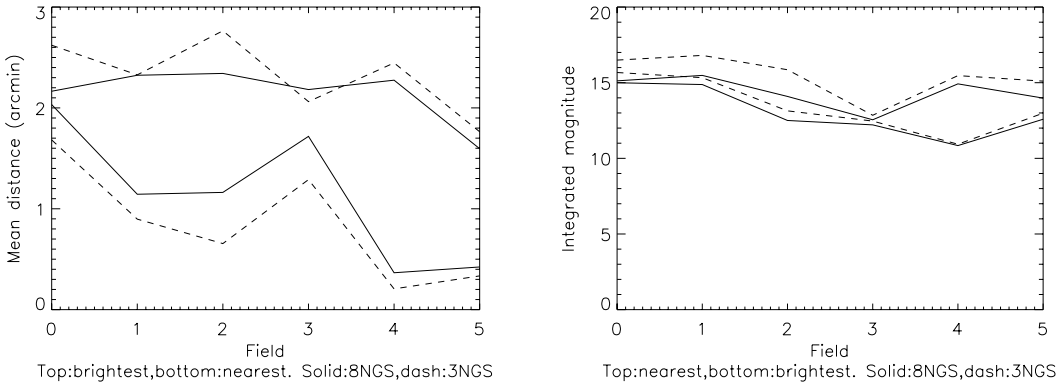

Figure 8-70. Left: mean distance to the center of the field (arcmin) for the considered constellations. Right: integrated magnitude of all the used NGSs

A more detailed analysis of the MOAO performance based on analytical simulations as well as the assumptions and AO parameters are provided in RD26.

8.2.3.3 Near-Term development plan

The following development plan aims at developing a MOAO instrument as a first generation OWL instrument. This assumes the availability of the GLAO correction capability at the telescope from the beginning.

It is worth noting that alternatives can be considered e.g. limiting the FoV of the instrument to the MCAO FoV and decresing the Multi-object capability. While such a solution would dramatically simplify the instrument, it is likely that it would also reduce its scientific value.

8.2.3.3.1 Modelling and Simulation

Simulations have been performed by ESO using CIBOLA software. Simulations efforts will be continued at ESO and at various institutes (LAM, GEPI, LESIA, ONERA) involved in MOMFIS & FALCON developments. A multi-simulations approach using different software environments is considered necessary to confront and compare the results. Simulations will be performed for a wide range of input parameters, such as seeing conditions, turbulent layer heights etc. Of crucial importance is the issue of Sky coverage which will be given special attention.

8.2.3.3.2 AO Concept and design

The following items are critical to an MOAO system and will need to be demonstrated / validated first with laboratory tests:

- Open loop wavefront measurements and operation, WFS linearity
- Control command algorithms
- DM performance: open loop, reliability, reproducibility, stability, linearity etc..
- Calibration issues

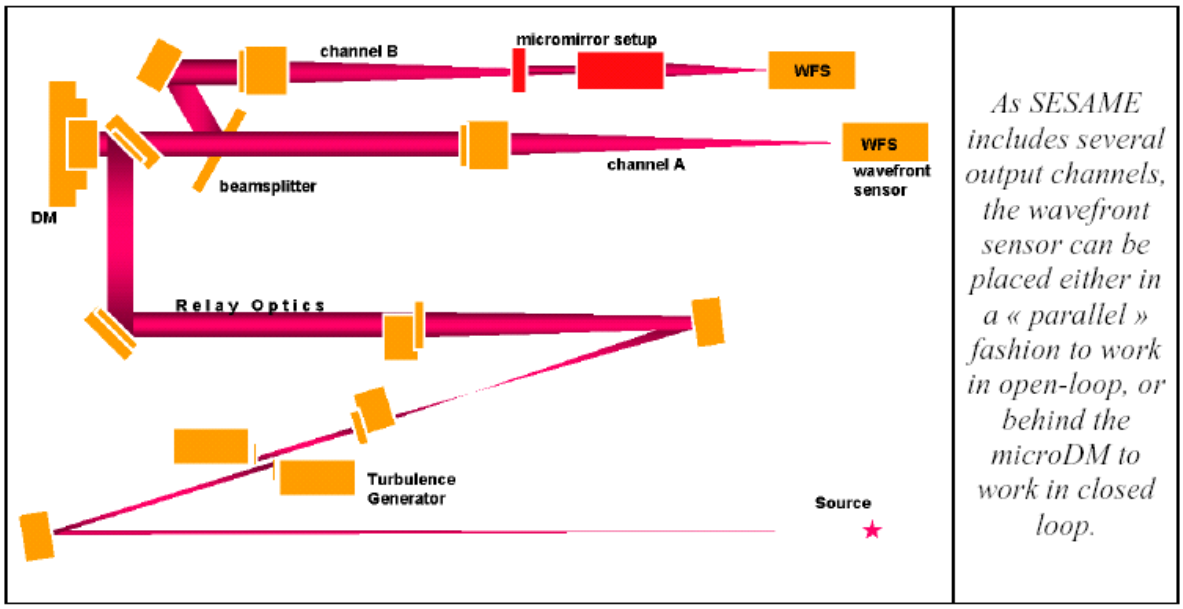

Figure 8-71: Optical setup of SESAME (Courtesy LESIA)

A test bench called SESAME is under construction at LESIA (France) and will be used for this purpose. It is shown in Figure 8-71. It allows carrying out tests either in closed loop or in open loop. It will be extensively used to characterize the MOAO approach both at component and at system level by the MOMFIS team:

- Mirror deformation, comparison to models, mirror calibration etc..
- Wavefront sensor test. The open loop WFS operation will be tested (in particular linearity and dynamic) by direct comparison of the reconstructed wavefront from two WFSs on two parallel channels. R&D is foreseen on reconstruction algorithms in the frame of OPTICON JRA1.
- Single direction, on-axis optimization. A wavefront sensor measures the turbulent wavefront on-axis and the MDM is controlled in open loop. The residual error is compared to the model. Calibration errors can be introduced and their impact measured.

- Single direction, off axis optimization. A tomographic reconstruction process is required and robustness of the tomographic reconstruction process with seeing and turbulence profile variation will be investigated.
- Simulation of the GLAO corrected turbulence by removing the ground layer phase screen
- Multi WFS operation. The core MOAO operation can be tested by placing several WFS in the FoV and controlling the DM(s).

After the results of the laboratory tests a demonstrator may be required to validate the MOAO concept on-sky- similarly to the MCAO demonstrator MAD.

8.2.3.3.3 AO key component status and development

MOMFIS will require the development of large stroke Micro-Deformable Mirror with 100x100 actuators with a high reliability, reproducibility and stability. The actuator pitch should be small -250µm- to be compatible with the volume requirement of the IFU and potentially WFS buttons.

The RTC concept is based on component and technologies already used in the previous systems with the exception of the switch that is used to dynamically route the buttons to the IFUs. Currently available products feature 8 ports with very low-latency figures. Products with 32 or more ports are also available but we have not tested them yet.

Some R&D is being pursued in the frame of the OPTICON JRA1 at LAOG (France) in this field: 2kx2k MDM with 6 µm goal 10 µm stroke and 1 µm goal 2 µm inter-actuator stroke. Although the inter-actuator may be on the short side, this is a first step toward large stroke MDM with a number of actuator close to what is required for the MOMFIS application.

8.3 Second generation Adaptive Optics

The second generation adaptive optics capability of OWL starts with the replacement of the passive, temporary M5 unit with an adaptive one. This should allow for a limited but not negligible increase of the corrected field of view, mirror M5 being conjugated to an altitude of ~7 km. The diameter of this mirror would be 3920 mm for 10 arc minutes unvignetted field of view but this diameter could be reduced to 3630 or 3420 mm if slight vignetting in the active, respectively adaptive control fields could be tolerated. The second generation Adaptive Optics includes:

- Multi Conjugate Adaptive Optics (MCAO)
- Extreme and high contrast Adaptive Optics for EPICS (Extra-Solar Planet Imaging Camera Spectrograph)

The MCAO makes use of the same wavefront sensors baseline described the for GLAO correction with optimization of the reconstructed wavefront on the portion of the field of view interested by the scientific instrumentation. The high altitude conjugated deformable mirror M5 has an actuator pitch of 25-40 mm depending on the error budget for the MCAO system. The single star footprint is 3.2 m and the meta-pupil (beam footprint) is 3.63m for 6'. For an actuator pitch of 25 mm the total number of actuator is 145×145 and 128×128 on a single footprint giving a pupil sampling of 0.78 m. The required stroke is lower than M6 due to the ground layer correction performed by M6. The Real-Time Computer technology for MCAO is essentially available today (albeit at a presumably high cost and with a non-optimal architecture).

EPICS will use M6 as a first corrector for large amplitude wave-front errors. A post focal XAO system with 1.710^5 degrees of freedom will provide the high Strehl and high contrast required for high dynamic range imaging. The current baseline for this system is to implement a two-stage correction, one based on a 500x500 micro-deformable mirror (20 cm actuator separation on pupil) to be controlled at about 1 KHz using a Shack-Harn sensor and a second stage with

150x150 actuators controlled at 3 KHz together with a Pyramid sensor. Significant technological devolpments are needed for the Real-Time-Computer.

8.3.1 Multi Conjugate Adaptive Optics

Multi-Conjugate Adaptive Optics (MCAO) aims to enlarge the FoV over which diffraction limit can be achieved. MCAO can be seen as a step forward on the GLAO concept where the correction is not applied only to the ground layer but also to other altitudes above the telescope aperture through additional deformable mirrors optically conjugated to them.

MCAO benefits from the simultaneous wavefront sensing of several NGS located in and/or around the FoV which is the target of the correction. The light of these NGS probes the atmospheric volume interested by the FoV and provides, up to a certain extent, the information on the vertical distribution of the atmospheric turbulence (see Figure 8-72).

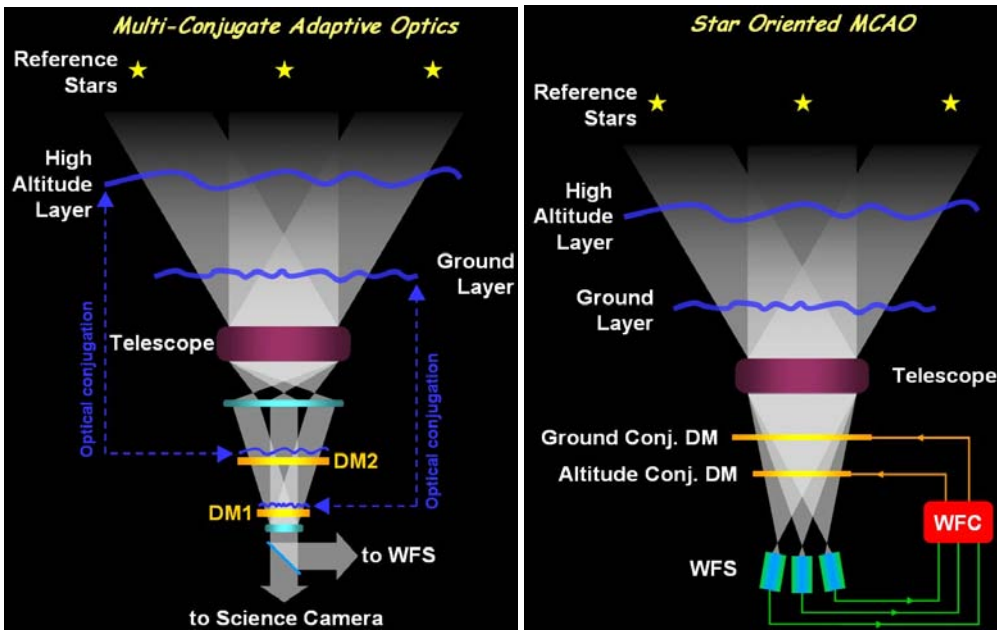

Figure 8-72: General MCAO concept (left). Star Oriented MCAO concept (right). Each NGS wavefront is measured with dedicated WFS and the signals are recombined to determine the correction to be applied to each DM conjugated at different altitudes.

MCAO suffers from limitations due to anisoplanatism, limited number of correction altitudes and availability of NGS (Sky Coverage). For these reasons the Strehl correction achieved with MCAO can be significantly lower than one obtained with SCAO and the correction uniformity across the field is not optimal.

The MCAO concept presented here for OWL is a Star Oriented facility and it is an extension of the GLAO facility: the WFS used are the same ones implemented for GLAO and the ground conjugated DM is M6. The high altitude conjugated DM is the adaptive version of M5 which is conjugated at ~7 Km above the telescope aperture. As the initial implementation of MCAO will probably be based on NGS the sky coverage is naturally limited, especially at the galactic poles, and the Strehl correction and uniformity are not as high as when Laser Guide Stars will be implemented.

- In the case of OWL one of the instruments which will benefit from MCAO correction is ONIRICA (Owl Near InfraRed Imaging Camera, see Figure 8-73). The central lens is for the narrow field imaging mode (diffraction limit) 1 arcmin FoV and the image is split into several channels to the IR detectors. The large array of microlenses is for the wide field imaging mode (non diffraction limited) which can benefit also from GLAO (see section 12.2.3.3 for more information about this instrument).

It is worth noting that if the instrument's requirements in terms of correction do not match the ones provided by the OWL MCAO facility, the instrument itself should be equipped with its own AO system which can in any case partially benefit from the OWL MCAO facility.

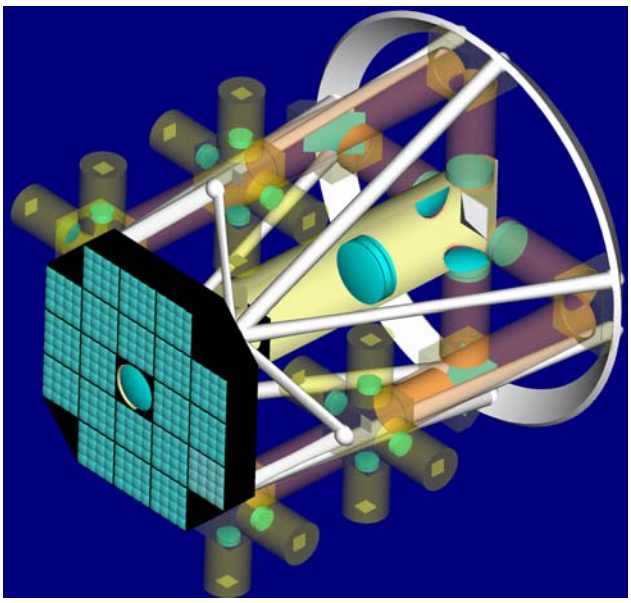

Figure 8-73: Opto-mechanical concept of ONIRICA (Courtesy INAF)

8.3.1.1 Performance requirements

The Multi-Conjugate performance requirements as applied to ONORICA are as follows (FoVs specified herein are in diameter):

- MCAO aims at providing diffraction limited images at NIR wavelengths (J-K bands) over a minimum 1' FOV using Natural Guide Stars (NGSs) for wavefront sensing.
- MCAO should provide the Strehl ratio performance according to Table 8-15 and Table 8-16 with a sky coverage of 5% at the North Galactic Pole and to sky coverage of 50% l=0° and b=50° (technical FOV of 6', NGS cluster of magnitude 16).
- The maximum un-vignetted technical FOV usable by the MCAO system is 6'.
- MCAO should support telescope nodding at 0.1 Hz by fast opening/closing GLAO loop (0.1s).
- MCAO should support small amplitude -1"- mosaicking in closed loop by offsetting the WFSs synchronously. The accuracy of the offset should be better than 1/2 of the spatial pixel size
- MCAO will not support chopping
- MCAO should provide in closed loop Field Stabilization to the telescope with the maximum amplitude characteristics provided in Table 8-1. For wavefront sensor dynamic reasons, the telescope guider will support MCAO for closing the AO plus Field stabilization loop before the control of the field stabilization corrector is taken over by the MCAO in closed loop.
- MCAO should permit to observe without AO (but with Field Stabilization) without any transmission loss with respect to the telescope. In that case, the field stabilization corrector is not controlled by the AO system.
- MCAO should make use of the two deformable mirrors (M5 and M6) conjugated at 0 and ~7 kms and implemented in the telescope optical train.
- MCAO should have the capability to correct for some of the telescope aberrations left by the active optics with an amplitude lower than 20% of the atmospheric wavefront at all

spatial and temporal frequencies. Errors beyond these values will be handled by the active optics.

- The transmission of MCAO should be maximized for the instrument observing wavelength T>95%;
- Vignetting of the scientific FOV by the MCAO wavefront sensors should be minimized (TBC)

- For the performance evaluation of MCAO seeing assumptions should be: 0.53 and 1" at 0.5 μm at zenith; with τ0=3 and 2ms. For the performance evaluation the outer scale of turbulence should be L0=25 m. For the determination of the AO design parameters the following atmospheric parameters should be assumed: turbulence outer scale L0=100m, seeing=1.5", τ0=2ms –Figure 8-4-
- MCAO shall be able to correct for differential atmospheric dispersion between the NGS and the Science object during an observation by applying offsets to the wavefront sensor. The calculation of the offset shall be done by the software based on the science beam effective wavelength provided by the instrument, the spectral type of the NGS provided by the observer, the science and guide star coordinates provided by the observer, the relevant atmospheric data (Temperature, Pressure, and Humidity) provided by the observatory – with the required accuracy. MCAO will not correct for the atmospheric dispersion within the scientific band pass of the instrument.

	Wave band	**K-band**		**H-band**		**J-band**	
	Guide stars magnitude	V=12	V=17	V=12	V=17	V=12	V=17
seeing, τ_0, L_0 @ 0.5μm	0.53", 3ms, 25m	32	24	13	8	3	1
	1", 2ms, 25m	7	4	1	0.3	0.04	0.008

Table 8-15: MCAO performance (Strehl Ratio, %) over 1' FOV vs. seeing and NGS magnitudes;

	Wave band	**K-band**		**H-band**		**J-band**	
	Guide stars magnitude	V=12	V=17	V=12	V=17	V=12	V=17
seeing, τ_0, L_0 @ 0.5μm	0.53", 3ms, 25m	2	0.1	0.8	0.1	0.2	0.03
	1", 2ms, 25m	0.3	0.07	0.06	0.03	0.006	0.001

Table 8-16: MCAO Strehl Ratio variation (in rms Sr) over the 1' FOV;

8.3.1.2 Implementation Concept

8.3.1.2.1 Corrective elements

The implementation of the MCAO system for OWL is conceived as an extension of the GLAO system with two deformable mirrors: M5 and M6. M6 is described in section 8.2.1.2.1.

M5 will be a 4-m class deformable mirror with an actuator pitch of 25-40 mm depending on the error budget for the MCAO system. It is conjugated to an altitude of ~7 Km, the single star footprint is 3.2 m and the meta-pupil is 3.63m for 6'. For an actuator pitch of 25 mm the total number of actuator is 145×145 (128×128 on a single footprint) giving a pupil sampling of 0.78 m. The required stroke is lower than M6 due to the ground layer correction by M6.

8.3.1.2.2 Wavefront sensors

As for the GLAO system six wavefront sensors patrolling the 6' FOV will be used for MCAO. The wavefront sensor design is similar to the one described in section 8.2.1.2.2.

As for the GLAO case, the vignetting due to the WFS buttons should be minimised within the central 2 arcmin FOV.

8.3.1.2.3 MCAO control

The MCAO loop control can be performed in different ways:

- Star Oriented Global Reconstruction;
- Optimization of Star Oriented Global Reconstruction for a given portion and direction in the FoV;

In all the cases the slopes retrieved by the WFSs are multiplied by the specific reconstructor to obtain the voltages to be applied to the two DMs. The vector of reference slopes for each WFS is obtained by a look-up table previously calibrated.

Star Oriented Global Reconstruction MCAO

In this approach the Interaction Matrix (IM) is obtained by stacking the WFS signals given by poking the single actuators (zonal control) or a set of actuators producing a selected base of modes (zonal control) of both DMs. Then the Reconstructor is obtained by inverting the IM in two possible ways:

- Least Square inversion via Single Value Decomposition (TSVD) with truncation of the zonal/modal eigenvalues with the lowest values;
- Pseudo open loop control [100] based on Minimum A-Posteriori variance reconstructor (MAP) which takes into account spatial a-priori knowledge on the turbulence and measurement noise. It gives a better performance in the whole FoV as it can properly handle the badly-seen modes that typically show up in MCAO systems.

Optimization of Star Oriented Global Reconstruction for a given portion and direction of the Field of View

This reconstruction approach boosts the performance in a given direction and smaller portion of the scientific FoV, as in the case of GLAO but giving a higher correction performance. The improvement in correction at this specified direction is achieved at the expense of the uniformity of the correction in the whole FoV.

The wavefront reconstructor is based on the minimum-variance (MV) reconstructor, R_{MV}, which can be expressed as the product of two matrices:

$$R_{MV} = P \times E \qquad \textit{Eq. 8-5}$$

The matrix E represents a full tomographic reconstruction of the turbulence volume (possible only when the vertical distribution of the atmospheric turbulence, obtained in real time from a vertical profilometer, is known), and the matrix P stands for an optimal projection from the reconstructed turbulent layers onto the two deformable mirrors taking into account the direction(s) where optimization is desired.

8.3.1.2.4 Real Time Computer

MCAO is a multi-sensor / multi-mirrors system. The proposed architecture is based on the Shack Hartmann Wavefront sensor.

The architecture of M6AM is the same as for the previous cases, as is that of the detector used. M5 will share the same technology for the actuators so given the additional size (3.5 m) the actuator grid will then be 145x145. In both cases the loop frequency considered will be 500Hz.

The architecture of the sensors is the same as for the GLAO system - Figure 8-74-. However measures cannot be averaged since all of them are required to reconstruct the turbulence at the desired altitudes. By reusing the same concepts described in the SCAO and GLAO cases, we

can allocate one computational unit for each quadrant of each detector, so we need 4*6=24 boards to implement the acquisition. Since sensor data are spread over 24 processing unit, it is convenient to keep this split and implement the reconstruction process in 24 different slices. Each slice will compute the matrix-vector product of 1/24th of the whole matrix by producing a partial command vector that needs to be summed to the other 23 to get to the final result that will then feed the PI controller.

The size of the system is rather big, but still achievable.

However the turbulence that has to be corrected by the upper DM M5 is expected to require much fewer actuators than the ones we actually have. This could lead to a reduction of these actuators on M5 or we can decrease the size of the control problem in the RTC by computing the reconstructor on a smaller basis and then interpolating the commands for the upper mirror in order to drive all the actuators.

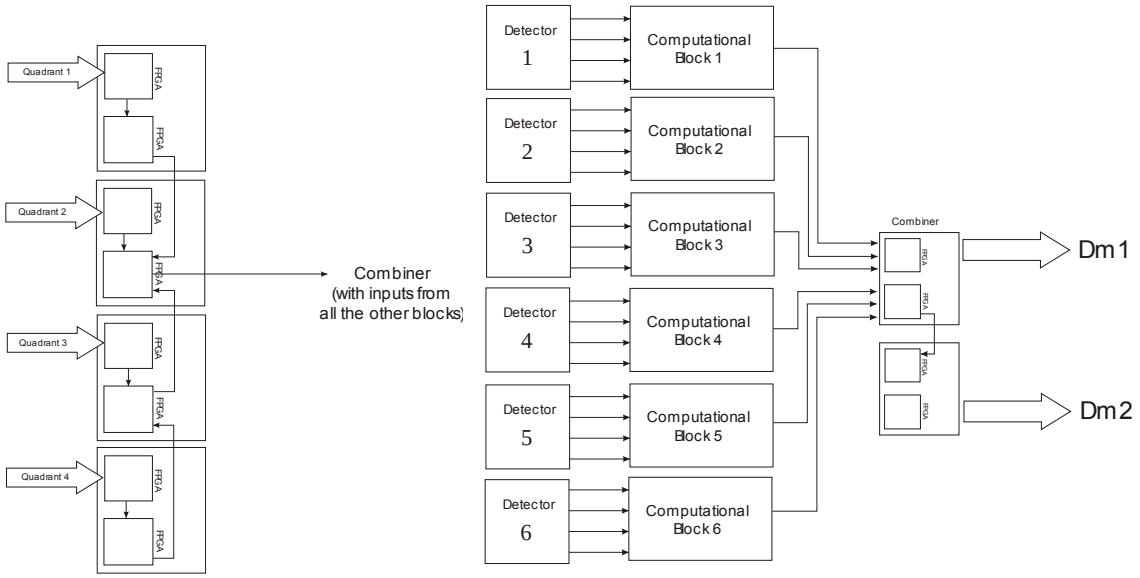

Figure 8-74: Architecture for a SH-based MCAO system with reduced number of reconstructed modes.

8.3.1.3 Predicted performance

A detailed analysis of the MCAO performance based on end-to end simulations as well as the assumptions and AO parameters are provided in RD25. Note that the MCAO performance provided here does not include yet all error sources -calibration errors, optical quality of the telescope, wavefront sensor and instrument optical paths, mis-registration error, atmospheric chromatism etc…- but only the pure AO performance part. In the MCAO mode, we believe that the accounting of the error budget on the final performance might have a significant impact for "high" Strehl and a small impact for the low Strehl.

The evaluation of the MCAO performance should cover two main aspects:

- The Sky Coverage for which the correction is available;
- The Strehl ratio performance in NIR

8.3.1.3.1 MCAO sky coverage

The proposed MCAO system is based on Natural Guide Stars. In the following, we will present the sky coverage achievable with the MCAO system proposed. More details about the SC are provided in RD27.

The Sky Coverage (SC) has been computed similarly to the GLAO case see 8.2.2.3.1.

The number of NGSs for wavefront sensing is limited to 6 which is a trade off between a minimum acceptable level of correction, Strehl uniformity and technological complexity of implementing multi WFS system in Star Oriented mode.

Figure 8-75 shows the frequency of 6 arcmin diameter fields as a function of the number of NGSs included in them. Several limiting magnitudes have been considered.

At the galactic poles (left) the sky coverage for fields with at least 3 stars of magnitude equal or brighter than 16 is ~20% and it drops dramatically when the minimum number of NGS moves to 6. In order to have acceptable sky coverage with at least 6 NGSs, it is mandatory to select stars down to 18, but at this flux levels a Star Oriented system may be severely photon starved unless high efficiency detectors become available.

At intermediate galactic latitudes (l=0° b=50°) the sky coverage for fields with at least 3 stars of magnitude equal or brighter than 16 rise up to 60% and also in the case the minimum number of NGSs is 6 the sky coverage increases up to 10%. Selecting 17 magnitude NGSs already provides sky coverage of ~50% at these galactic latitudes with the MCAO system working at flux regimes less critical than the one at the galactic poles.

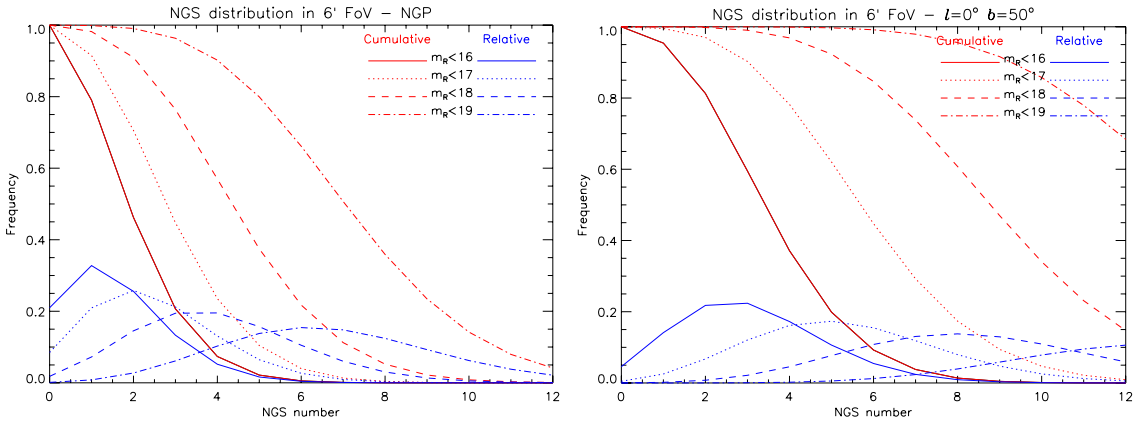

Figure 8-75: Frequency of circular 6 arcmin diameter fields as a function of the number of NGS included on them at the North Galactic Pole (left) and at an intermediate galactic latitude l=0° b=50° (right)

8.3.1.3.2 Simulation Results

In the following we analyze the Strehl correction performance in K Band for an asterism of different number NGS distributed in 6 arcmin FoV (see Figure 8-76). Figure 8-76 is based on an analytical model which is in reasonable agreement with our numerical model for bright stars but the analytical tool is more pessimistic for faint star (see Figure 8-77). Further investigations are being pursued to clarify this discrepancy.

In the plot of Figure 8-76, the analytical model (Cibola, written by B. Ellerbroek) was used to simulate the MCAO performance for 3, 6 and 8 NGSs, all of identical magnitudes. A good seeing model (0.5'') was adopted. The NGSs are placed in "reasonable" asterisms: in the 3 NGSs case, the three stars are in a triangle of 4' diameter. In the 6 NGS case, 3 stars are in a 3' (diameter) triangle) and 3 in a 6' triangle. In the 8 NGS case, 3 stars are in a 3' triangle, and 5 in a 6' (diameter) circle.The performance is shown on-axis (top curve) and 30'' off-axis (bottom curve). The solid line is for 5th magnitude NGSs, dash: 16th mag, dot-dash: 17th mag and dot-dot-dash for 18th magnitude (an A0 spectrum was assumed, which is about 1 magnitude less photons than a G0 star). We can see that for faint stars, even with 8 NGSs, Strehls below 10% (at K band) are obtained.Adding guide stars from 3 to 8 increases the performance by adding photons, but the performance remains fairly poor, in terms of Strehl ratio.

Figure 8-77shows the numerical simulation of a 3 NGS constellation, in 2' field, located at the edges of the field. 1 ph / sub-aperture / integration time (framerate is 500 Hz) corresponds roughly to 17th magnitude in the above plot. We can see that the bright end performance is in rough agreement, whereas for faint stars, the analytical code is more pessimistic.Top to bottom shows the performance in K, H and J bands. Same seeing as for the analytical model.

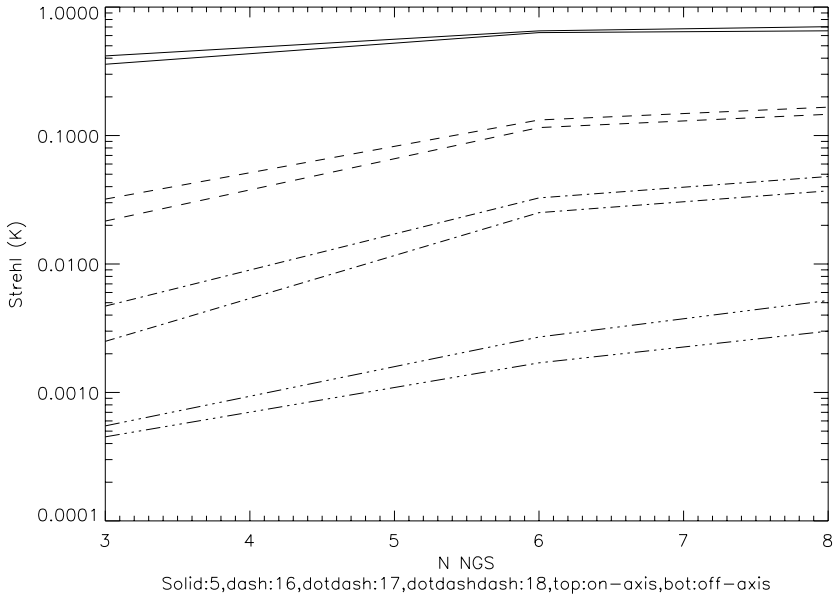

Figure 8-76: Strehl (K-band) as a function of the NGS number distributed on a 6 arcmin FoV optimized in the central 1 arcmin. Solid line: Mv=5, dashed line: Mv=16, dashed-dotted line: Mv=17, dashed-dotted-dotted line: Mv=18. For each magnitude: top line on-axis, bottom line: off-axis.

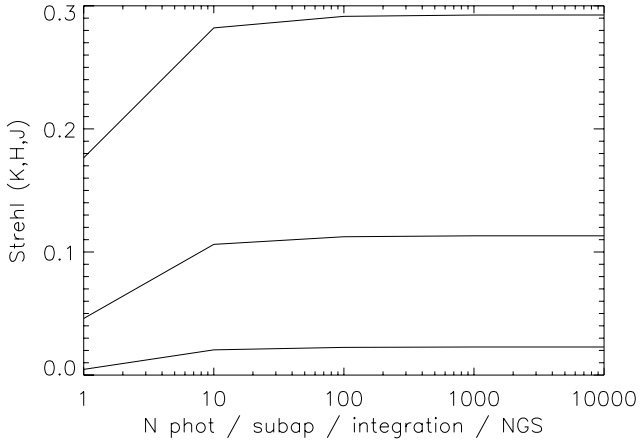

Figure 8-77: Strehl (on-axis) for the good seeing model, MCAO, 3 NGSs, 2' FOV, K, H, J (top to bottom), Mv=16 corresponds to 5 photons/subap/frame

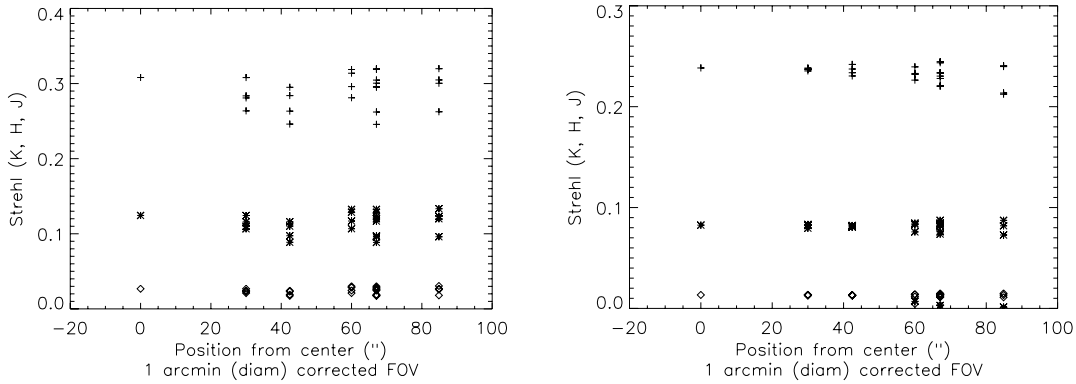

Figure 8-78: Numerical simulations of MCAO correction (Strehl ratio in K band, H and J bands (top to bottom)) on a 6 NGS asterism (Mv=5 (left plot) and Mv~16 (right plot)), the good seing model (~0.5'' was used). Correction is optimized for a 1' FoV (diameter).

The last plot shows the variability of the Strehl in the field of view (numerical model). The crosses show the Strehl at various locations. Some variation is seen, and the performance peaks towards the location of the guide stars. This is a well known effect, already observed in the MAD simulations. It may be possible to reduce it by adopting another control algorithm.

From Figure 8-76, we see also that the MCAO performance strongly depends on the angular separation of the NGS asterism. Ideally, one would select a compact NGS asterism to get better performance but of course this will limit immediately the sky coverage.

We see that the MCAO system needs to have a variable tomographic capability for both “small” and “large” FoVs to optimise the Sky coverage and the performance in the scientific FOV. Further numerical simulations remain to be done to confirm the NIR performance expected in MCAO.

From the above analysis, it is important to note that Strehl ratios in NIR using NGSs only for wavefront sensing will always be limited to a couple of tens of % in most cases because of the magnitude of the wavefront sensor NGSs. Extrapolation to higher Strehl ratios or to correction at shorter wavelengths will require the implementation of Multi- Laser Guide Stars. Moreover, the uniformity of the Strehl in the field of view is not maximal, because to gain sky coverage, large separation asterisms need to be used, creating “holes” in the Strehl ratio map where NGSs are not present

Combining the sky coverage plots and the results of the simulations for Strehl correction performance it is clear that in the NGS based MCAO the sky coverage is significantly low especially at high galactic latitudes. Moreover the correction achieved is already modest in K band and becomes very small at shorter wavelengths. The analysis presented here shows that at the Galactic poles the sky coverage is 25% with 5% Strehl and drop to 1% for a Strehl of 10%.

Laser Guide Stars can solve this problem because they can be available for any region of the sky and they can provide much higher fluxes increasing significantly also the MCAO correction performance extending it to shorter wavelengths. The number of Laser Guide star needed for OWL is still under investigation as well as the concept for they implementation (see sub-section on LGS in 3rd generation AO section).

On the other hand it is also possible to select specific targets which are surrounded by useful NGS to perform MCAO correction. The number of available fields with these characteristics will be low but for some astronomical applications where observing on a specific direction of the sky is not mandatory (i.e. Cosmology with deep fields) it may be sufficient.

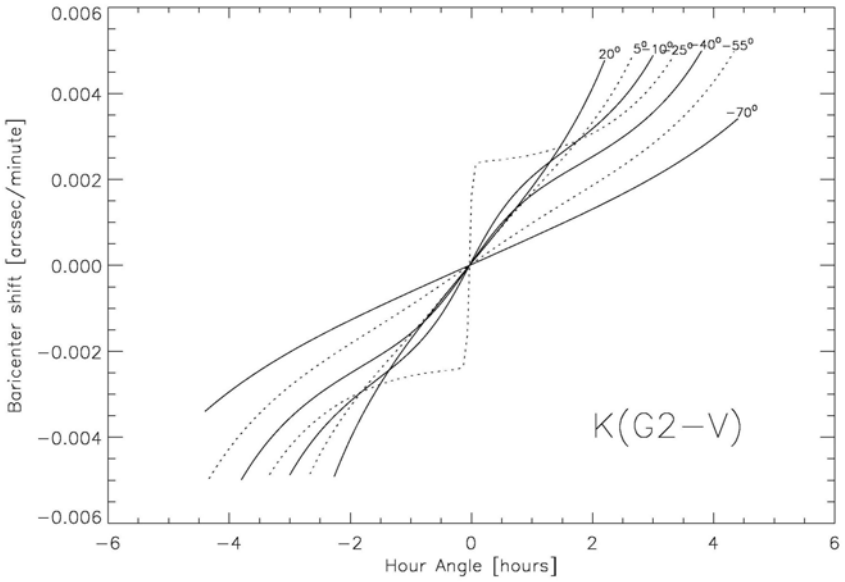

Figure 8-79: Barycentre speed of a G2-V star due to the differential atmospheric refraction between the WFS effective wavelength and the instrument observing in K band for different target declinations

Differential image motion - The differential image motion due to atmospheric dispersion between the WFS-NGS effective wavelengths and the science wavelength - Figure 8-79- should be taken into account. In the case of MCAO this effect is critical since the images are almost diffraction limited. The compensation can be implemented by applying offsets to the WFS which have to be updated continuously (~1 Hz).

There is a second order effect of the atmospheric dispersion within the FoV between stars of different spectral type observed through the band pass of the instrument filters.

Figure 8-80 shows the barycentre speed for a B5-V and a M5-V star with respect to a G0-V all observed in J band. The speed is computed at different declinations and hour angles for Paranal. In all cases the speed is always lower than 4×10^{-2} mas/minute, that is, 1/50 of the diffraction limit FWHM (Full width at half maximum) in J Band. This permits individual exposures of the order of 1 minute and even larger for H and K Band without smearing the diffraction limited PSF across the FoV –for different object spectral type. However, special care should be taken when co adding individual exposure for different Zenithal distances over long exposure times because of the "warping" of the FoV astrometry due to the different colours of the stars.

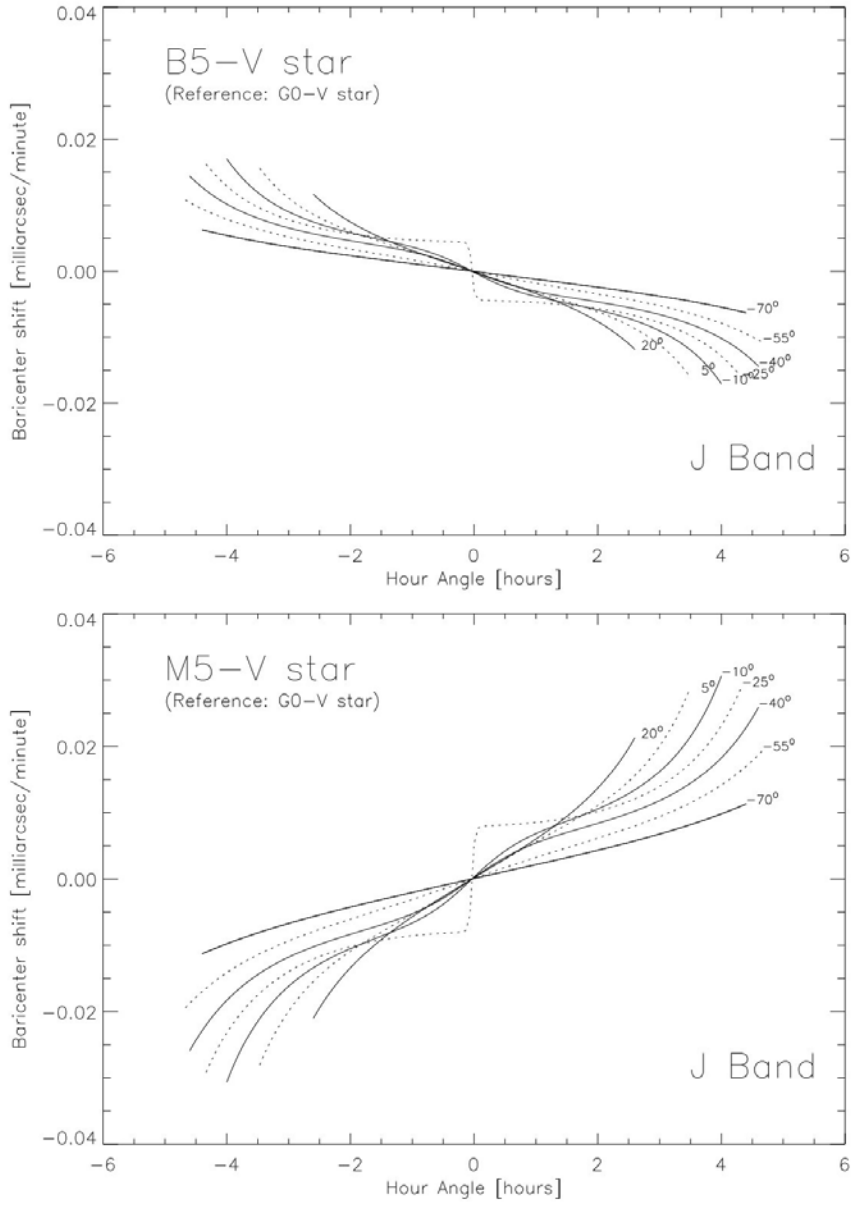

Figure 8-80: Barycentre speed of a B5-V star (top) and a M5-V (bottom) with respect to a G0-V star observed in J Band. The curves stop when the Zenithal distance is larger than 60°.

8.3.1.4 Mid-Term development plan

8.3.1.4.1 Modelling and Simulation

First order simulations have been performed to estimate the MCAO performances in NIR with a 98x98 M6 and a 145x145 M5 actuator system. Discrepancies between numerical and analytical simulations remain to be clarified and best Strehl ratio versus sky coverage needs to be tuned. Full numerical simulations of the MCAO system require a large amount of computing time on our cluster. Sky coverage has been evaluated based on a maximum of 6 NGSs and wavefront sensors but also this value will be subject to further investigation.

The number of DMs required both to increase the 2' FOV correction and the sky coverage needs to be investigated.

The corrected PSF uniformity needs to be assessed in detail as this parameter is scientifically important.

The actuator density for the M5 needs to be optimized in view of the error budget.

The effect of magnitude difference between the NGSs for wavefront sensing should be studied

Statistics of turbulence profiles are now becoming available thanks to the special effort made to develop dedicated profiler tools like MASS and the SLODAR. Measurements should be pursued to get more significant information about the amount and the structure of the layers and their variability. Based on these data, MCAO performance should be updated.

Extensive parametric simulations remain to be done to tune the design parameters in particular:

- Optimization of the SH WFS geometry fitting the M6AM geometry (Circular, hexagonal, squared)
- Optimization of the SH WFS pixel scale and FOV
- WFS linearity issues
- Effect of the turbulence produced by the telescope itself over the first 200-400m and variation of the turbulence along the telescope pupil
- Atmospheric refraction and differential atmospheric refraction needs to be studied
- Study of the variable M6AM conjugation altitude effect on the GLAO performance
- Full error budget of the MCAO system
- MCAO calibration issues beyond the experience acquired with MAD.

8.3.1.4.2 MCAO design

The detailed implementation of the MCAO wavefront sensors into the OWL Adapter-rotator will be developed during phase B.

As in the case of GLAO the present baseline is currently the Star Oriented concept with global reconstruction from each WFSs signal. Effort to define a Layer Oriented concept with numerical or optical co-addition will continue and the results compared with the SO approach.

The considerations made for GLAO (section 8.2.2.4.2) apply to MCAO as well. In addition:

Should a third deformable be required, the design of a post focal AO system with sufficient FOV –up to 6'- needs to be produced.

Activities on the M6AM unit are identical to the SCAO case.

The feasibility and conceptual design of the M5AM unit will be pursued in phase B.

As envisaged for the M6AM unit, a laboratory test facility of the M5 unit alone will be required. Ideally a thorough laboratory testing of M5 and M6 together in MCAO mode is highly desirable. The corresponding test facility needs to be studied for instance by replacing the spherical mirror proposed for the M6 unit by the M5 mirror and adding a corrector to correct for field aberrations.

This approach may not be compatible with the present schedule for OWL as the M6AM unit may be already in operation when the M5 will be tested. Options will be analyzed in Phase B.

In the domain of MCAO reconstruction and control, research should be pursued both in the frame of MAD and in collaboration with other world experts. In particular, the reconstruction and control methods optimizing the corrected field diameter require significant research and demonstration.

8.3.1.4.3 MCAO calibration issues

The calibration M5 and M6 with the 6 WFSs for different positions in the field is a complex subject which requires further work especially for the determination of the command matrices. This subject is partially being studied with MAD but the problem will be more complex with OWL because no internal source will be available to calibrate M5 and M6 for all field positions. In addition, internal telescope turbulence may limit the accuracy of the calibration. For these reasons, either synthetic values from field extrapolation of the interaction matrix or on-sky interaction matrix measurements should be looked at carefully already with MAD and its turbulence generator and on-sky and later with the VLT Adaptive secondary. The feasibility of a synthetically reconstructed AO system is under study. If it can be demonstrated that all hardware aspects can be simulated accurately enough to provide the required performance, this solution would obviously be the best. It is however possible that one need to combine simulated and measured interaction matrices. Several options to do so are being investigated.

Using a simulated IM to build the system control matrix is a possibility that is under investigation. The strategy is to stick as much as possible to the reality. Indeed, WFS and DM models must be accurate. Thus, when one can measure the influence functions of its DM, it is obviously more accurate to use this model instead of a simulated one. This is what has been chosen for MAD. As described in RD27 section 7, tests are being run on MAD with the turbulence generator MAPS in order to quantify the performance of a controller built by following such an approach. The measured DM influence functions and a diffractive model of the SH with a uniform subaperture plate scale are used to simulate the IM. The loop closes and provides a significant performance in terms of strehl ratio but worse than the one achieved with the measured IM. Indeed, the misregistration between DM actuators and SH subapertures still have to be measured and included in the simulations.

In RD27, the same approach is presented in the DSM case. The SH model is diffractive and the DM influence functions are the output of the FEM (because no influence function can be used when the mirror does not exist).

In the case of ALTAIR (the AO system currently in operations on GEMINI north), a synthetic IM has been used successfully since the start. The DM model consists in analytic influence functions that have been fitted on measured one. In this way, the computational time is reduced.

New calibration issues arise in the MCAO case. Indeed, the fact of dealing with several DMs and WFSs might increase the calibration time. If the calibration must be performed on sky, the night observing time will be reduced. Another potential problem may be the drift of the DMs (creep for example) while one of them is being calibrated. This will bias the interaction matrix and thus be detrimental to the system performance.

To overcome these issues, a possibility would be to consider all DMs as a single device and to define global modes (Hadamard or system) on this fictive meta DM. Then, both DMs will be actuated at the same time during the calibration. In this way, no DM will creep or drift during the calibration. In the case of the Hadamard modes, it is interesting to notice that the calibration time will be independent on the number of DMs for a given expected measurement signal to noise ratio.

Another idea would be to modulate both DM with different frequencies (multiplexing) and to disentangle their contribution in the Fourier space.

Global modes can also be defined in the WFS space considering all WFS as one device. Then, the calibration can be performed by applying a global bias to the WFS offsets. A modulation of the bias will certainly be necessary to overcome the turbulent residual on the WFS signal in MCAO. This scheme could be applied also to GLAO although in this case the closed loop residual would be higher.

The last issue to take into account in MCAO calibration is the mapping of the FoV. Indeed, the interaction matrix should rigorously be calibrated for each target asterism. The off axis aberration should be taken into account along each guide star direction. Since the altitude DM footprint position changes with the guide star angle, off axis calibration is fundamental in MCAO. The idea would be to define a grid sampling the FoV. An interaction matrix is measured for each position of this grid (in red on Figure 8-81). Then, when a real asterism of guide stars (in yellow on Figure 8-81) is observed, the interaction matrices for each WFS are built by interpolating the closest ones that were measured on the grid. In the framework of the PhD work of Johann Kolb (available end 2005), the required sampling of the FoV will be defined for MAD (with its bimorph DMs and SHWFS). The goal is to minimize the impact on the performance coming from the difference between the measured and the extrapolated interaction matrix. An acceptable threshold in terms of wave front error, strehl ratio and correction uniformity should be defined. The first results tend to show that a grid of about 50 recording points in the 2 arcmin FoV should be enough to extrapolate the IM to any GS position and bring a loss of SR smaller than 5% relative.

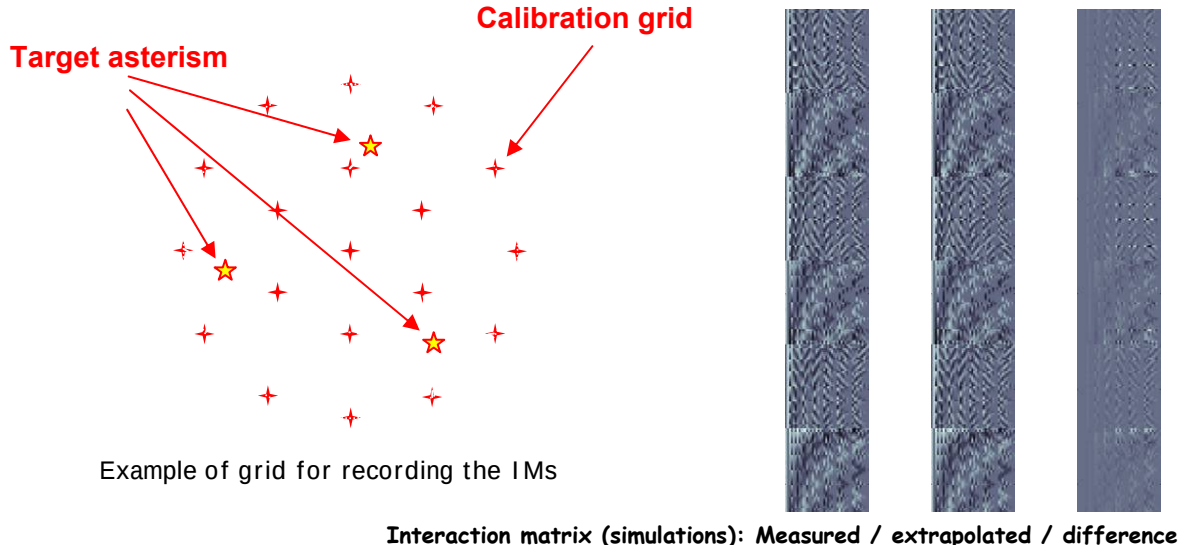

Figure 8-81: Mapping of the FoV for interaction matrix estimation in MCAO

8.3.1.4.4 AO key component status and development

Both the WFSs and the M6AM unit will be reused for MCAO.

The additional specific key component required for MCAO is the 4m-class deformable mirror with an actuator pitch of 25-40 mm. Detailed simulations may lead to larger actuator pitch. Apart from its diameter, the additional complexity of this deformable mirror is its concave shape. However, the actuator pitch and the high spatial frequency stroke – stiff modes requiring power to produce- are relaxed compared to the M6AM unit. These two effects will allow an increase of the thin glass shell thickness beyond 2mm, making the manufacturing easier. Main characteristics of the M6 and M5 deformable mirrors are provided in Table 8-8.

The RTC concept is based on technologies already considered previously. Worth of note is the presence of 10 port switches while we have tested so far only 8-ports, and the multi-layer RTC architecture: the latter case is significant and because board-to-board communication may play an important role. Therefore a prototype implementation (one small layer) is required.

MAD: An MCAO demonstrator

The European Southern Observatory has built and is testing a Multi-Conjugate Adaptive Optics Demonstrator (MAD) to perform wide field of view adaptive optics correction. The aim of MAD is

- To demonstrate on the sky the feasibility of the GLAO and MCAO techniques,

- To perform a first optimization of such techniques, and explore other innovative approaches through extensive in-lab testing
- To evaluate the critical aspects in building and running such instrument in the framework of OWL and of the 2nd generation VLT instrumentation.

MAD is seen as a crucial enabling milestone for OWL. It will be installed at a Nasmyth Visitor focus of the VLT to perform on-sky observations, planned in 2006. The MAD bench is shown in Figure 8-82.

MAD is a prototype GLAO and MCAO system performing wide Field of View (FoV) AO correction over 2 arcmin by using bright (m_v < 14) Natural Guide Stars (NGS) and it is built using existing technology and re-using as much as possible key components developed for existing ESO AO systems (Figure 8-82)..

MAD will be used to investigate two different approaches of GLAO and MCAO correction with two independent wavefront sensing techniques: the Star Oriented MCAO with a Shack-Hartmann Wavefront Sensors (SHWFS) sensing simultaneously 3 NGS with 3 sensors and the Layer Oriented MCAO with a Layer Oriented Wavefront Sensor (LOWFS), based on a Multi-Pyramid Wavefront Sensor sensing simultaneously 8 NGS. The Layer Oriented Wavefront Sensor is designed and built by an Italian consortium. The MAD Real-Time computer architecture is designed to support both reconstruction wavefront sensing approaches.

Adaptive correction with MAD relies on two deformable mirrors (DM, Figure 8-83). One is conjugated to the telescope pupil for ground layer turbulence correction, the other one to 8.5 Km above the telescope, thereby allowing for a larger corrected field than a single conjugate would permit. The MAD GLAO and MCAO correction are optimized for the K (2.2. μm) band for the median Paranal seeing conditions and the performance will be evaluated at this wavelength using a 1 arcmin IR camera (CAMCAO, supplied by a Portuguese consortium).

For the laboratory testing and tuning of the MAD system, a multi-layer turbulence generator MAPS (Multi Atmospheric Phase screens and Stars) is used to emulate atmospheric turbulence.

A detailed description of the system is provided in [8]

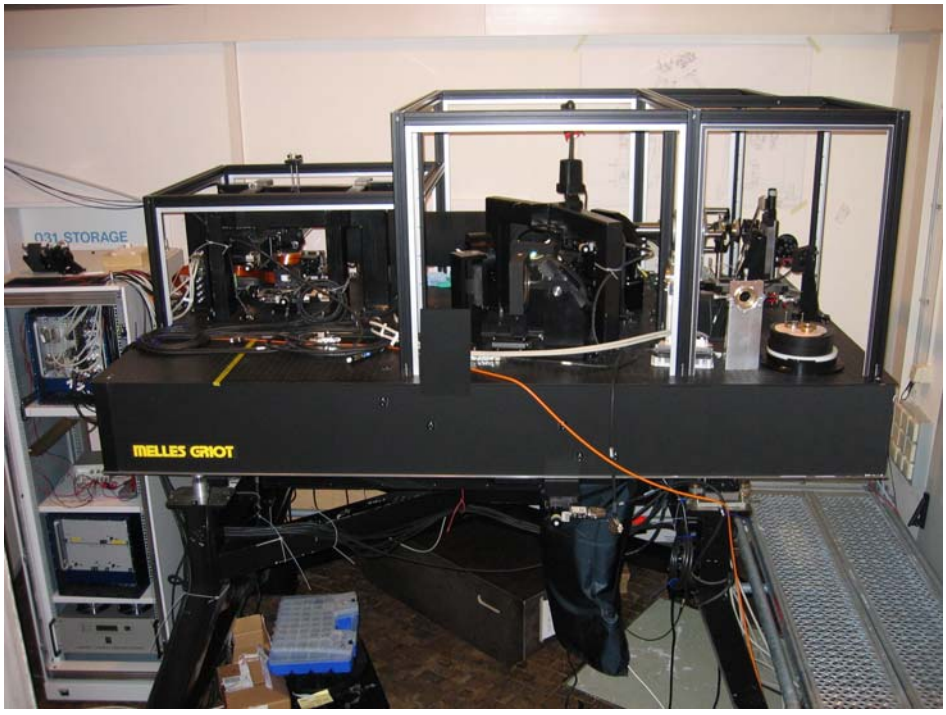

Figure 8-82: The MAD bench installed in the ESO optical laboratory during testing.

The multi-Wavefront Sensors unit (Figure 8-84) consists of 3 Shack-Hartmann sensors capable of scanning the whole 2 arcmin field of view. The lenslet array has 8 × 8 sub-apertures and a 2.4 arc seconds field of view.

The Layer-Oriented sensor (Figure 8-84) is based on a multi-pyramids Wavefront Sensor with eight pyramids allowing to observe simultaneously eight reference sources. Each pyramid is supported by a small cylinder with relay optics, the purpose of which is to enlarge the system focal ratio by a factor ~10 on the pyramids. The light modulated by the pyramid is split in two beams and the telescope pupil is re-imaged through two groups of lenses onto the detectors. The detectors are located at conjugates of the two deformable mirrors. The two sensor units (multi-sensors or layer-oriented) cannot be operated simultaneously.

The MAD detector system consists of 5 WFS cameras (3 for the SHWFS and 2 for the LOWFS) MAD has 5 CCD cameras (3 for the Shack-Hartmann sensors and 2 for the Layer-Oriented ones). The E2V CCD39 chips have FIERA controllers, which can drive the detectors simultaneously at identical (for the Shack-Hartmann CCDs) or different (for the Layer-Oriented CCDs) frame rates, up to 400 Hz.

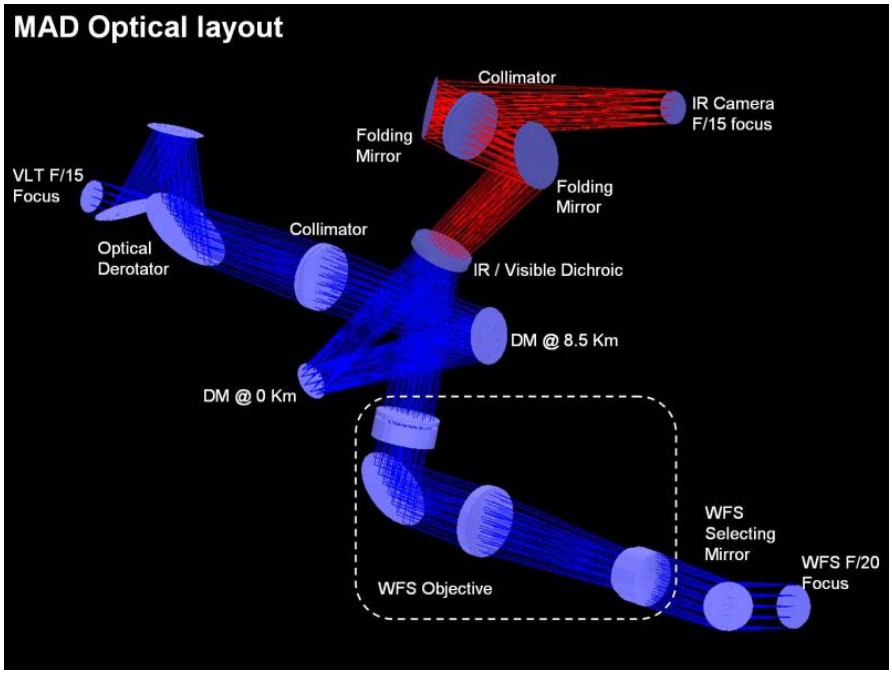

Figure 8-83: Optical layout of MAD.

The Deformable Mirrors (Figure 8-85) are copies of the ones developed for MACAO-VLTI and MACAO-SINFONI AO systems. The deformable mirrors are bimorph-type with a radial geometry of the actuators. The tip-tilt correction is provided by the MACAO-SINFONI Tip-Tilt supporting the MACAO-SINFONI DM.

The MAD Real-Time Control has been designed to support both the Star Oriented and the Layer Oriented wavefront sensing techniques and to implement both the Global and the Local Reconstruction.

The MAPS turbulence generator (Figure 8-85) emulates a time evolving three-dimensional atmosphere. The characteristics of the atmospheric turbulence will be similar to those of the Paranal observatory during median seeing conditions. The evolving atmosphere is reproduced by three rotating refractive plates (Phase Screens). The surface of the plate is chemically etched in order to generate spatially varying thickness.

Recently MAD passed two major milestones:

- 3rd March 2005: first light of Single Conjugated AO (SCAO) closed loop with one Shack-Hartmann sensor and the deformable mirror conjugated to ground;

- 3rd June 2005: first light of Ground Layer AO (GLAO) closed loop with three Shack-Hartmann sensors and the deformable mirror conjugated to ground.

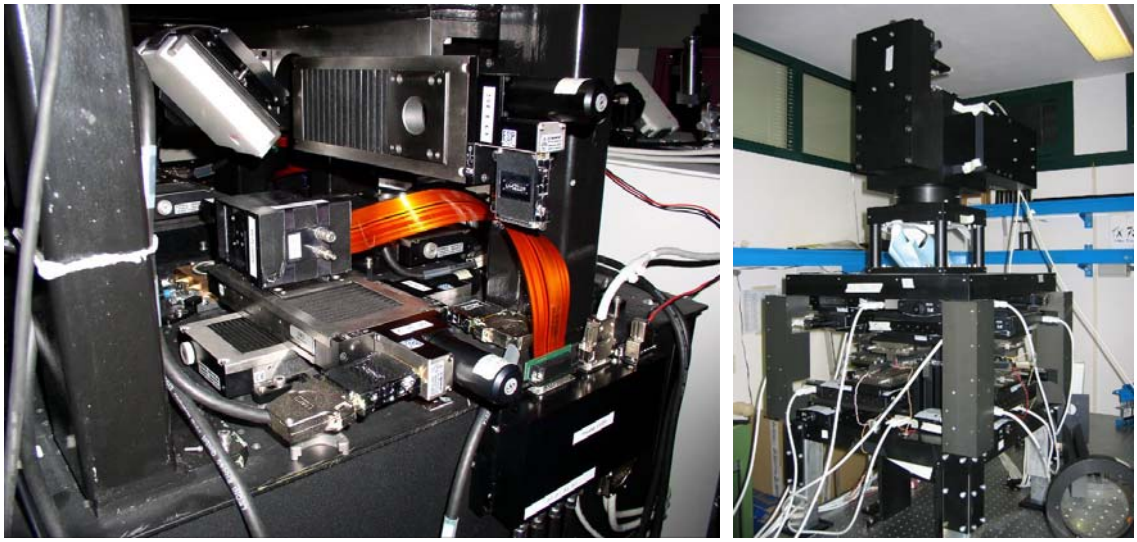

Figure 8-84: Left: the SH WFS area during integration. Right: the LOWFS during final testing.

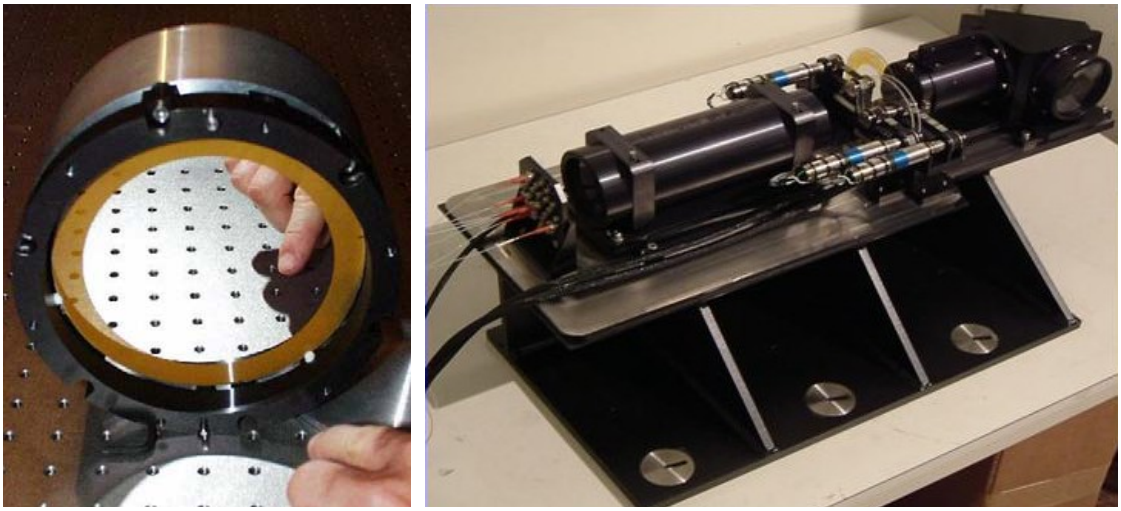

Figure 8-85: Left: MACAO bimorph DM used for conjugation at 8.5 Km. Right: the multi layer turbulence generator MAPS.

SCAO Closed Loop

The loop has been closed using one SH WFS and the ground conjugated DM. Only one rotating The loop has been closed using one Shack-Hartmann sensor and the deformable mirror conjugated to ground. Only one rotating phase screen with gentle atmosphere has been used in order to facilitate the first light operations. The seeing was 0.4" in V Band and the wind speed of 10 m/s. The loop was closed at a frequency of 115 Hz on m_v=6 star and a Strehl of 52% in K band has been obtained.

Figure 8-86 shows the open and closed loop images taken in K Band. The "cross- shaped" artefact in the closed loop image is due to a non perfect filtering of an unseen system mode.

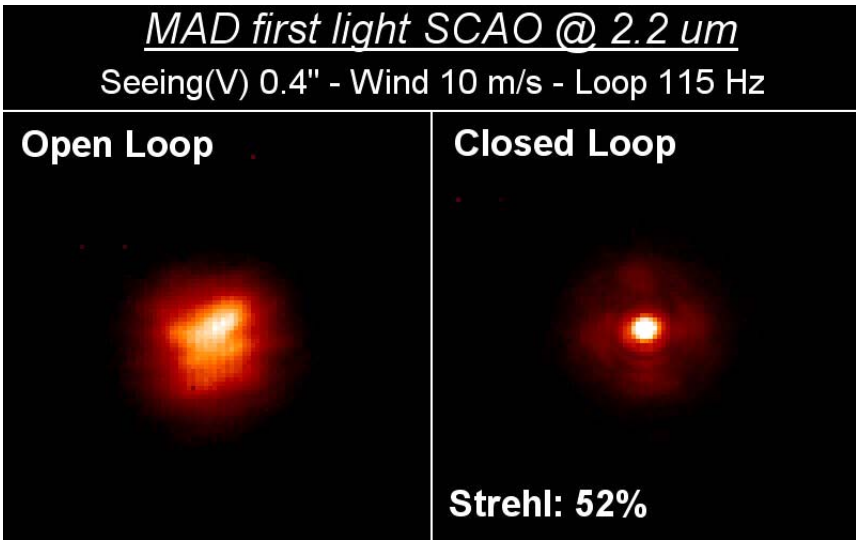

Figure 8-86: MAD first light SCAO closed loop

GLAO Closed Loop

The loop has been closed using three Shack-hartmann sensors located on a circle of 1.5 arc minutes diameter and at the vertex of an equilateral triangle. The correction was applied through the deformable mirror conjugated to ground. Only one rotating phase screen, located at 6 km altitude has been used to simulate a "gentle" anisoplanetism. The seeing was 0.45" in V Band and the wind speed 10 m/s. The loop was closed at a frequency of 115 Hz on m_v=6 star.

The FWHM in K band has been reduced by a factor ~2.5, thereby demonstrating experimentally that MAD is capable to perform GLAO correction (see Figure 8-87).

The gain in Encircled Energy is shown in Figure 8-88. Within the FWHM of the closed loop image, the gain of energy concentration is a factor ~2 in comparison with the uncorrected image.

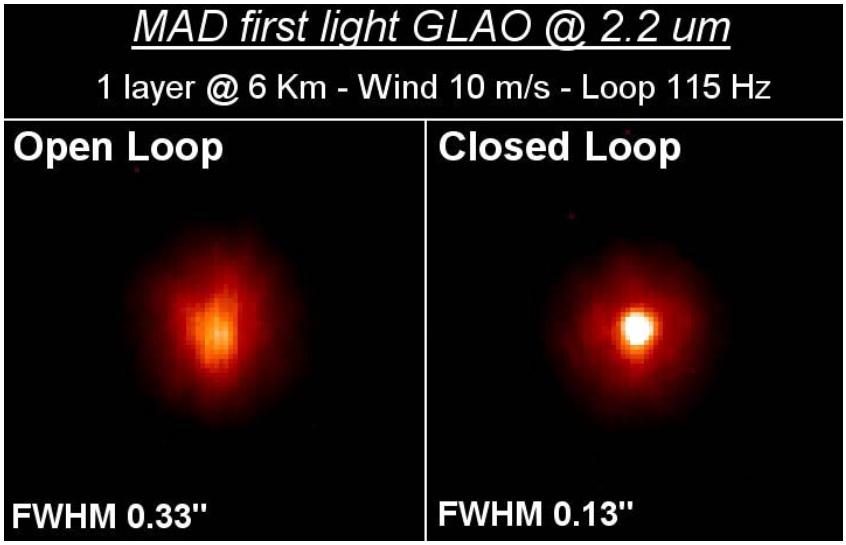

Figure 8-87: MAD first light GLAO closed loop. Only one phase screen at 6 Km altitude has been used and the guide stars were located on a circle of 1.5' diameter. The FWHM reduction factor is ~2.5.

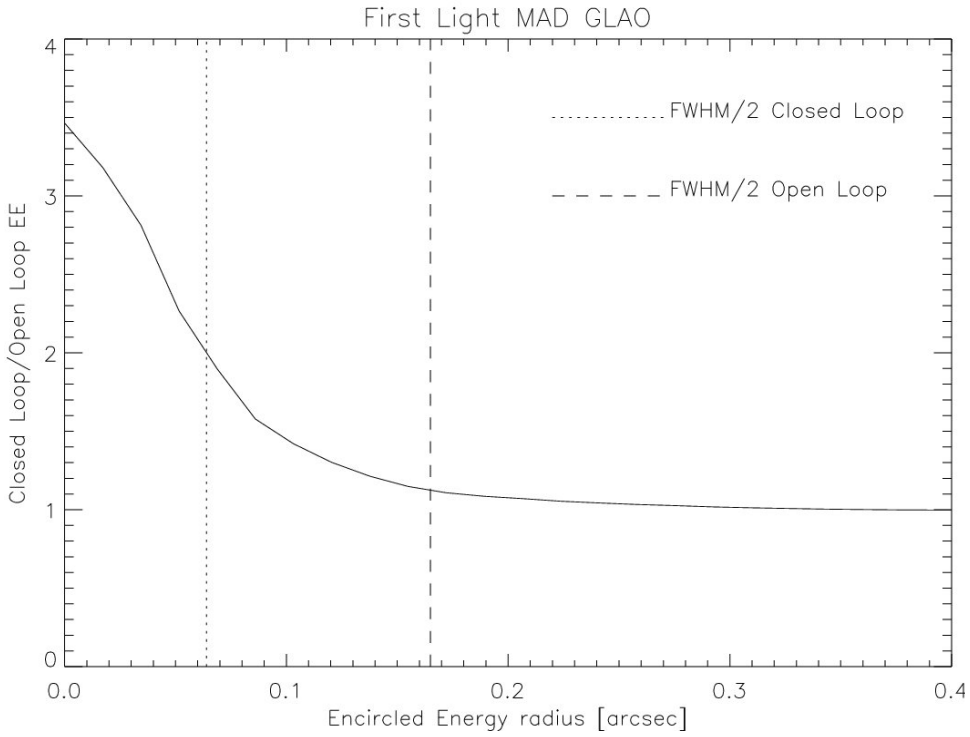

Figure 8-88: Encircled energy gain in the first light GLAO closed loop. At the FWHM radius of the corrected image the gain is ~2.

Optimal control algorithms for MCAO

The second generation AO will require more sophisticated control approaches, especially in the case of wide field AO as in MCAO.

In AO control, an AO system has to deal with a real time closed loop system with delays and linear models for the WFS measurements and for the DM correction. The optimal control problem actually breaks down into a stochastic estimation of the turbulent phase, followed by a deterministic control problem. The estimation problem is shown to be solved by Kalman filtering [101]. The specificities in MCAO are: a large number of degrees of freedom, the WFS measurements available only in particular directions corresponding to the Guide Stars in the star oriented point of view. Achieving a correction in a large Field Of View requires to interpolate the WFS measurements between the GSs. It implies a careful reconstruction process using prior information on the turbulent volume. This leads to a global optimization of the multi-variable servo-loop.

The Office National d'Etudes et de Recherches (ONERA, Paris, France) in the framework of OPTICON-JRA1 has developed an end-to-end MCAO simulation tool which includes the modellization of the spatial and dynamical behaviors of the different MCAO subsystems (spatial sampling, influence functions, temporal transfer functions) and the calibration errors and the capability to handle different control algorithms including Kalman filtering. The goal is to compare the different reconstruction-control algorithms in terms of correction performance and robustness with respect to different atmospheric conditions, guide star fluxes and calibration errors applied to MAD.

An experimental validation of the optimal control approach is also under progress at ONERA. This pioneering experimental work will validate the results obtained with the end-to-end simulation tool and help the specification and implementation of the future MAD optimal control. This validation is performed on the AO bench available at ONERA. The optimal control criterion consists in the optimization of the scientific off-axis performance using the on-axis WFS data. The first tests in static mode have been performed. The conventional on-axis correction has been compared to an off-axis Kalman-like regularized correction which uses the knowledge of the altitude and strength of the turbulent screen. A systematic gain brought by the off-axis optimization has been demonstrated ([126]).

The next step will be to define the optimal control algorithm (Kalman) to be implemented in the MAD star oriented configuration accordingly to the results obtained with the numerical simulations and the AO bench validations. ONERA and ESO in close collaboration will implement in the MAD system the optimal control algorithm and run MAD under the defined conditions.

8.3.2 Extreme Adaptive Optics and High Contrast Imaging: EPICS project

The Exo-Planet Imaging Camera Spectrograph for OWL (EPICS) feasibility study started significantly later than the other instrument conceptual studies, after the completion of the VLT Planet Finder phase A. The latter has demonstrated that it is necessary to combine XAO (eXtreme Adaptive Optics) with other methods (coronagraphy and differential detection methods) to reach the contrast permitting exoplanets detection. The interaction of error sources between the different sub-systems of EPICS calls for an absolute global system approach.

An overview of the whole EPICS instrument can be found in section 12.2.3.5 and the whole study in RD51. We present here an outline of the XAO system and of coronagraphy.

8.3.2.1 EPICS Top level performance requirements

A full system approach should be followed to meet the performance of EPICS. The top-level-requirements of the instrument are recalled in this paragraph.

- The instrument covers the wavelength range 0.6 – 1.7 micron
- The total field of view in all observing modes is at least 2″ in diameter at visible wavelengths and 4″ in diameter in the NIR.
- The inner working angle in all observing modes working at visible wavelengths is smaller than 30 mas (goal 15 mas).
- The spatial sampling will at least fulfill the Nyquist criterion at all working wavelengths. Over-sampling may be required to deal with interpolation issues in differential imaging.
- Earth-like planet up to 20 pc is detected in polarimetric and spectroscopic modes at SNR > 5 in one night of observation at a phase angle of 90°

Properties of Earth at 20 pc: Contrast 2e-10, m_V = 30.6, angular separation 50 mas.

- Jupiter up to 20 pc is detected in spectroscopic mode at SNR > 50 in less than 4 hours exposure time at a phase angle of 90°

Properties of Jupiter at 20 pc: Contrast 1e-9, m_V = 28.8, angular separation 250 mas.

- The AO control radius is larger than 0.4″ (goal 0.8”) at 800 nm

This control radius corresponds to about 1 AU at 2.5 pc, and ensures that – besides for the Alpha Centauri system – the prime targets are inside the control radius. Note that the control radius is given by the $\lambda/(2d)$, where λ is the observation wavelength and d is the actuator pitch of the deformable mirror. This Top Level Requirement corresponds to an actuator pitch of ~0.2 m (goal 0.1).

- AO limiting magnitude for achievement of Top Level Requirements: compatible with a sample larger than 100 stars for each spectral types G, K and M . This corresponds to the following limiting magnitudes for the three types of stars: Mv=7. for a G2 star at 25 pc, Mv=8.5 for M2 star at 20, Mv=9.5 for an M2 star at 15 pc.

8.3.2.2 EPICS Adaptive Optics concept

EPICS ultimate contrast requirement is 4-5 orders of magnitude higher than the VLT-Planet Finder science goal of about 10^{-5} – 10^{-6} contrast at 0.1 arcsec. When scaling from a 10-m to a

100-m class telescope, the contrast naturally improves by a factor of 100 for a given rms value of the wave-front error. This means that the XAO system for EPICS should provide a 2 or 3 orders of magnitude better starlight halo rejection than a simply scaled version of the VLT Planet Finder system. This matter of fact calls for system specifications that are tremendously more stringent.

- a significantly higher AO system frame rate (up to 3-4 KHz) to reach high rejection in the central part of the field-of-view (for separations less than 0.1 arcsec for the Earth-like planets detection goal).
- the systematic errors must be kept at a very low level on the low and mid spatial frequencies (f < 2.5 cycles/m in the entrance pupil frame). For VLT Planet finder, on these spatial frequency range, the static errors contributes by about 40-50 nm. A gain of at least an order of magnitude is needed (requirements: less than 5 nm rms).
- the wave-front sensing measurements error propagation on low and mid-spatial frequencies must be very low: the use of phase-type sensor instead of a slope sensor is needed at least for the correction of the halo at separations less than 0.1 arcsec.

The role of an XAO system for a planet finder is two-fold:

- Condition 1: to deliver a high Strehl Ratio (SR>90%) at the science wave-lengths in order to concentrate most of the candidate exoplanet's light in a diffraction core.
- Condition 2: to provide, in combination with a coronagraph, the level of rejection of scattered starlight, that permits planet detection and characterisation in a reasonable amount of time (intensity contrast better than 107 at 0.1 arcsec in J band.)
    - the part of the halo that averages out defines mainly the level of photon noise against which the planet needs to be detected. It directly impacts the total integration time needed.
    - the part of the halo that doesn't average out (mainly quasi-static speckles), is the most critical part and defines the ultimate level of contrast one can reach.

These guidelines are very important in the definition of the XAO post-focal system coupled to the coronagraph.

8.3.2.2.1 Common path system:

The common path AO system for EPICS is composed of M6 and a post-focal XAO system. The control of these two systems (M6 + XAO post-focal system) will be based on a Woofer - Tweeter scheme, where M6 is dedicated to the correction of the large PTV low spatial frequency aberrations whereas the post-focal system ensures the correction of the fast evolving aberrations and of the high spatial frequencies. To fulfil the requirements on the AO control radius, i.e. a 20 cm inter-actuator separation as projected on the 100-m pupil, the post focal corrector needs to be composed of at least 1.7×10^5 degrees of freedom. We use this number for the baseline system.

Wave-front sensing and computing time requirements trade-off:

The wave-front sensor in an XAO system is a very important component, and its noise propagation properties must be carefully taken into account. The ultimate science goal of EPICS calls for a very efficient scattered star light rejection very close to the center of the field-of-view. This translates, for an XAO system, to a very good sensitivity of the wave-front sensor to measure low and mid-spatial frequencies. This property is fulfilled by the so-called phase-type sensors. The noise propagation properties of the pyramid sensor are of phase-type nature: it has been shown that the gain in limiting magnitude can be quite important with respect to a Schack-Hartmann sensor for the correction of the scattered starlight halo at separations less than 0.1 arcsec [104].

Our first choice for the EPICS post-focal XAO system, was to couple a pyramid sensor with a single high density MEMS mirror with $1.7x10^5$ actuators and to control this system at 3 KHz. This is certainly a good choice in terms of noise propagation but revealed to be very risky in terms of required computing time and CCD read-out time requirements. Indeed, the signal provided by a pyramid sensor is a complex function of the entrance phase error, and is characterised by a very non-sparse interaction matrix (see RD51). As of today, the only way of deriving the correction commands from a pyramid sensor is to use a full rank matrix-vector multiplication. Some possibilities combining different approaches will be studied but are still in a very preliminary state.

Even taking into account a significant increase in computing power over the next 10-15 years, the control of a 1.7 10^5 degrees of freedom AO system at 3 KHz using a full rank matrix-vector multiplication seems extremely difficult, if not impossible, to achieve. For Shack-Hartmann-based systems the situation is different; at least two new methods for fast reconstruction exist : one using the sparseness of the zonal interaction matrices [106] and another one using Fourier methods permitting also a modal control [107], [108].

Two-stage post-focal XAO system.

The solution we propose is to split the wave-front sensing and the correction in two stages. This permits to alleviate a lot the requirements in terms of computing power as well as of WFSs CCDs read-out. Here is a brief description of this concept (see also Figure 8-89):

- the post focal corrector will be composed by two post-focal Deformable Mirrors:
  - post-focal DM_1 (with an equivalent d_1 = 0.2 m actuator pitch): $1.7x10^5$ actuators controlled at 1KHz or so, providing the required 0.4 arcsec control radius at 0.8µm. The cut-off spatial frequency of this system is $f_{c1} = 1/d_1 = 2.5$ cycles/m. This system alone already permits to get a high Strehl greater than 90% in J and H band (it fulfils condition 1), but is unable to provide an acceptable rejection in the central part of the field-of-view.
  - post-focal DM_2 (with an equivalent d_2 = 0.67 m actuator pitch): $1.5x10^4$ actuators controlled at 3 KHz. The cut-off spatial frequency of this system is $f_{c2} = (2d_2)^{-1} = 2.5$ cycles/m. This system will permit to increase by an order of magnitude the rejection of the scattered light for separations less than 0.1 arcsec (it fulfils condition 2).
- After reflection by the two DMs, the beam is split between two wave-front sensors with different pupil sampling. This solution, known as hierarchical wave-front sensing, has been proposed [109] as a way to increase the sensitivity of the Shack-Hartmann sensor. We use this concept with a different scope, i.e. to optimise the system in terms of correction bandwidths at the expense however of some moderate loss in terms of sensitivity. Moreover we propose to use two different types of wave-front sensors:
  - WFS_1 (Shack-Hartmann WFS): very High Order WFS (500x500 sub-apertures) to control the post-focal DM1 at a 1 KHz frame rate. A possible control algorithm for this stage is a Fourier reconstructor using optimized modal control in the Fourier domain [108] for spatial frequencies f such as fc2<f< fc1. The gain for spatial frequencies f < fc2 are essentially put to 0 (or to very low values) because the measurements of WFS1 for this range would be much more noisy than the one provided by WFS2.
  - WFS_2 (pyramid WFS): medium order WFS (150x150 sub-apertures) to control the post-focal DM2 at a 3 KHz frame rate. A full rank matrix-vector multiplication is used.

This way of control is also more flexible, depending on the goals of a given observation. For detection of both gas giants and rocky planets, the light splitting (50/50 for example) is ajusted to provide a level of the halo more or less balanced in the field-of view. For follow-up observations the light splitting and temporal control bandwidths can be ajusted in function of the location of the target. More light can be sent for example to WFS_1 to ensure a higher halo rejection in case of a follow-up observation of rocky planet near the center of the field of view.

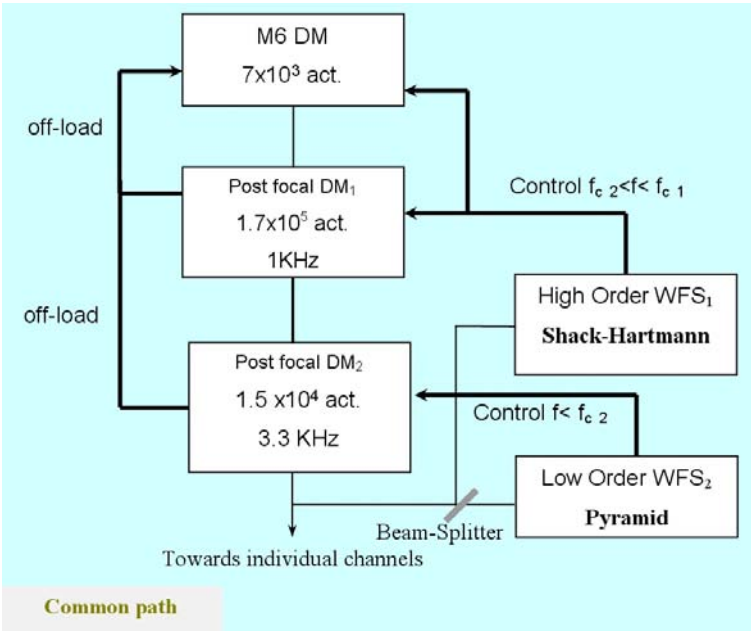

Figure 8-89: Common path XAO concept for EPICS.

8.3.2.2.2 Individual Channel paths

Each scientific channel will be equipped with an active mirror of about 10^4 actuators for the correction of the residual static error in the common path AO system before the coronagraph. A focal plane sensor (focal plane interferometer [111] and/or phase diversity) is used to measure and compensate the static errors using an artificial source for calibration and the starlight itself with a low temporal bandwidth (see Figure 8-90).

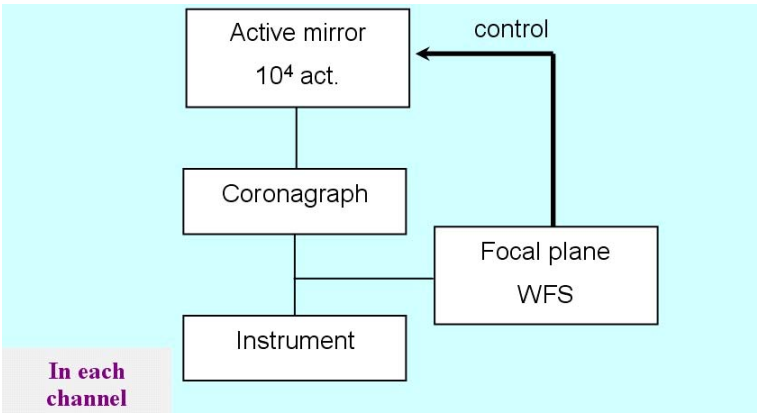

Figure 8-90: Individual scientific channel path.

8.3.2.3 Coronagraphy

The coronagraphs are very critical components of EPICS and their interaction with AO residuals needs to be carefully studied. Since the science instruments cover a very broad band of wavelengths, it has been chosen to equip each individual channel with its own coronagraph. This choice permits to optimise the coronagraph parameters with more flexibility. Whereas a sufficiently achromatic coronagraph dedicated for the visible range is probably the most challenging one, the ones for J and H band could eventually, if an acceptable concept is found, be combined in one single coronagraph. But no definite concept has now been chosen. Coronagraphy is a very fast evolving field with a lot of very new ideas that appeared recently (see RD22 for a review). For EPICS two concepts have been considered and some preliminary results have been obtained. The first concept, the double stage reticulated Lyot coronagraph is described in RD22 and permits to deal with diffraction residuals induced by gaps between the

segments. This concept is quite complex to simulate and has been studied only in the diffraction limited case for the moment. The second concept, a prolate apodized double stage Lyot coronagraph is less complex but doesn't reach a contrast as high as the reticulated double stage coronagraph.

An important issue about coronagraphy is the criterion to choose for its performance.

- The first obvious requirement is that the rejection of the coronagraph is such that the diffraction residuals are significantly lower than the AO residuals. This criterion ensures that the photon noise contribution to the halo induced by the coronagraph is negligible. If only this criterion were important, the requirements on the intrinsic performance of the coronagraph would be quite moderate.
- To be rigourous, one has to take into account the type of instrument behind the coronagraph. In case of differential imaging, one has to deal with the effect of the coronagraph on, for example, the differential chromatic aberrations in the case of wave-length splitting differential imager or an IFS. These have a direct impact on the ultimate contrast achievable and on the calibration procedures to be implemented.

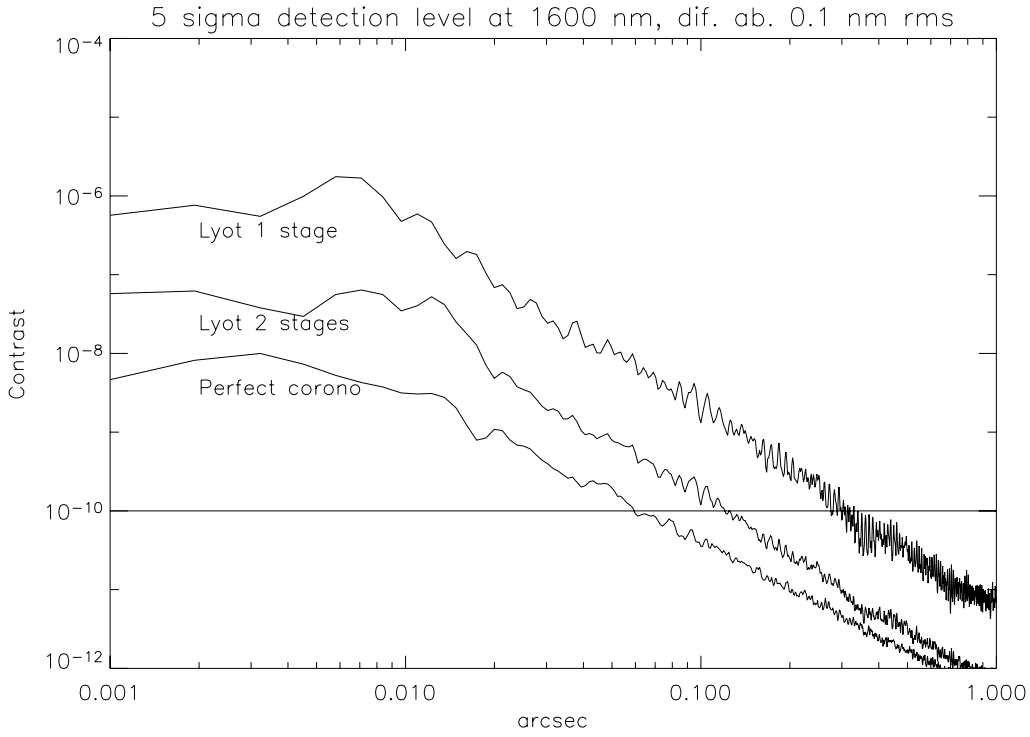

Figure 8-91: 5-sigma detection level after differential imaging for 0.1 nm rms differential chromatic error before the coronagraph (circular average). λ = 1600 nm.

In the example shown in Figure 8-91, we compared by numerical simulations a perfect coronagraph that is able to reject the whole diffraction residuals and the more realistic double stage Lyot coronagraph with prolate apodization (see RD22 for intrinsic preformance). The simulation considered monochromatic light and differential chromatic aberrations with 0.1 nm rms error occurring before the coronagraph.

One can see that with a perfect coronagraph the residuals are about 2×10^{-10} at 50 mas separation, compliant with the TLRs. The same differential error but as seen though the double stage Lyot coronagraph with prolate apodization translates in a 5 σ detection level of only 10^{-9}. Note that these curves have been obtained by circular averaging. A more complete study should take into account blind zones in the field of view like the diffraction by the spider. Figure 8-92 shows that the residuals for the perfect coronagraph are due to wave-front errors only, whereas the one for double stage prolate apodized Lyot coronagraph, the diffraction residuals are prominent and directly correspond to the so-called pinned speckles.

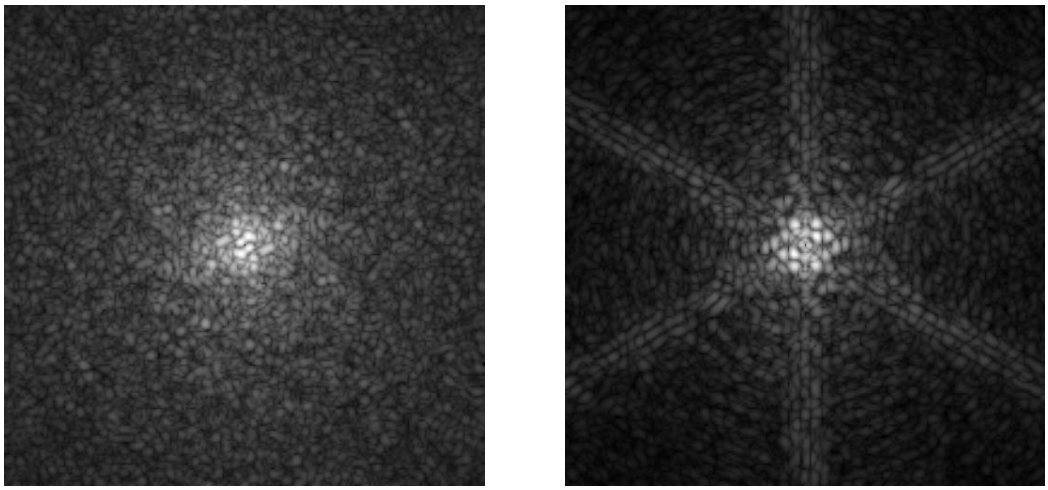

Figure 8-92: Residuals after dual imaging with a perfect coronagraph (left), and a double stage Lyot coronagraph with prolate apodization (right.)

This simulation shows that the intrinsic performance of the coronagraph has an important impact of the differential aberrations that can be tolerated in the system. The same simulation is foreseen for the double stage reticulated Lyot coronagraph but is more complex to compute since one needs to well sample the gaps between the segments.

8.3.2.4 Correction of co-phasing errors

Co-phasing residuals on an ELT is often presented as an important show-stopper for planet finding. Lardiere et al. [110] estimate that the co-phasing rms residuals should be at the level of 1 nm so that its contribution to the halo remains negligible with respect to the AO residuals. Their main argument is that piston errors cannot be corrected with usual continuous deformable mirrors, so that dedicated fast piston correctors should be implemented. We demonstrate that a continuous mirror can actually correct for piston errors, or more specifically it can correct for the Fourier components of the wave-front that affect the field-of-view of interest. For this we considered a typical co-phasing errors figure from M1 and M2 with 20 nm rms total error and fitted, using a Fourier method, a phase function whose spectral content is limited to spatial frequencies less than fc_2 the cut-off frequency corresponding to the second stage DM_2 inter-actuator separation (67 cm). The initial wave-front map and the DM_2 fitted correction wavefront are represented in Figure 8-93 and the residual wave-front (difference of the two) is represented in Figure 8-94.

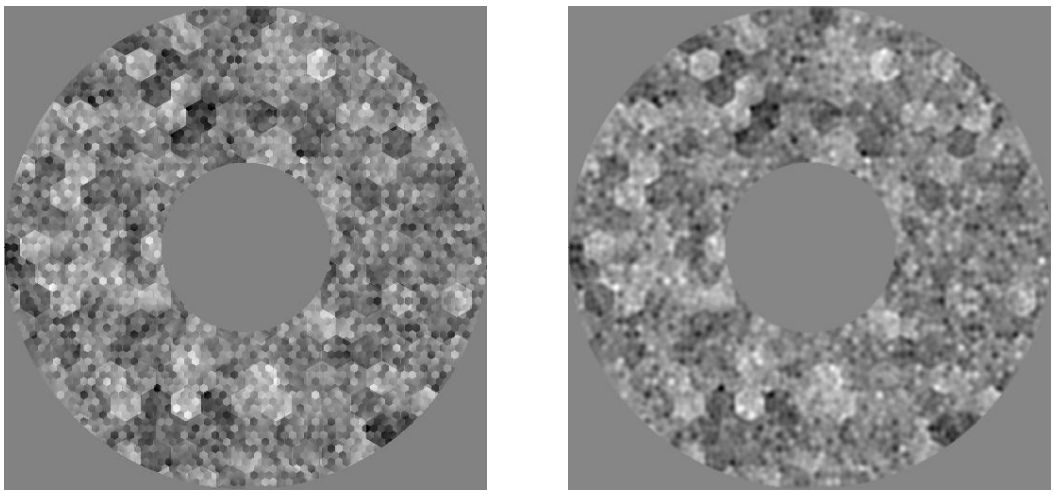

Figure 8-93: AO correction of co-phasing residuals. Left: initial co-phasing errors. Right: best fit with DM2 (0.67 actuator separation).

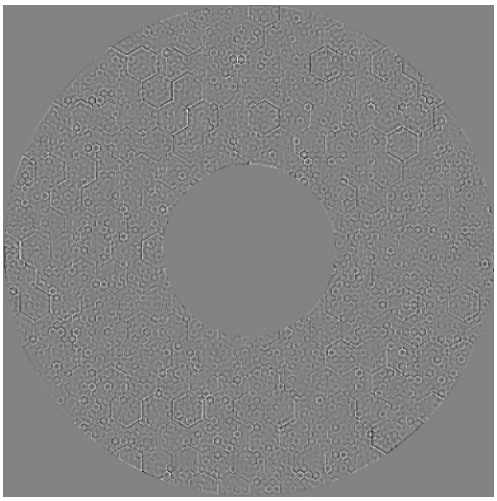

Figure 8-94: Residual left by best fit of DM_2.

The best fit obtained with DM_2 leaves a residual of 6 nm rms. A cut in the three wave-front maps is represented in Figure 8-95. One can verify that indeed, DM2 is unable to correct for the 'jumps' of the wave-front at the segment edges, and those appear still in the residuals. These jumps can even be as high as several tens of nanometers. However, what counts for imaging is the spatial content of the phase. Since we are interested to obtain a very high contrast in the centre of the field of view, the most important is to correct the low spatial Fourier components. It is exactly the case of the residual phase of Figure 8-94.

To convince ourself that such a residual error figure can be acceptable, we simulated the coronagraphic images corresponding to the wave-fronts with co-phasing residuals and co-phasing residuals plus correction by best fit of DM_2. The results are shown in Figure 8-95. One can see that indeed if the co-phasing residuals only are present, the halo is very bright and the raw contrast is larger than 10^{-6} at 50 mas. After correction by DM_2 the residual is only about 10^{-9} in the centre of the field of view, so negligible with respect to AO residuals.

It is important also to notice that the pyramid sensor is sensitive to piston errors [104] contrary to the Shack-Hartmann, so that it will be able to measure them. This is another reason of why a phase-type sensor should be used.

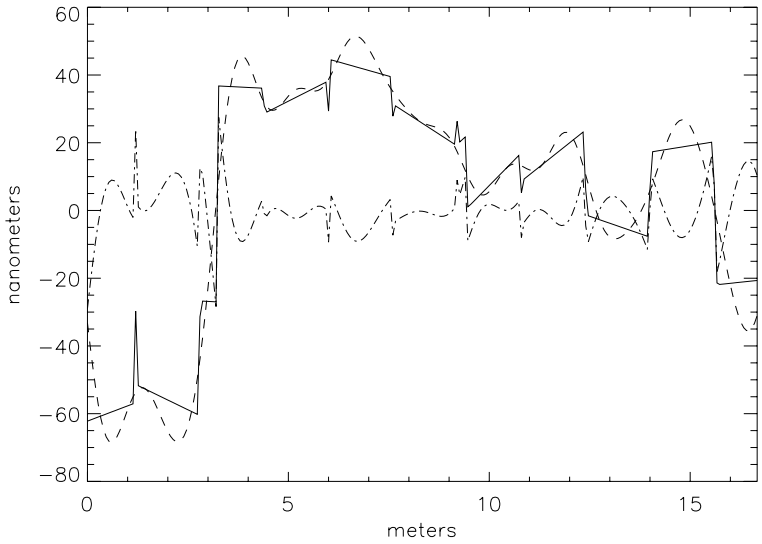

Figure 8-95: Cut in wave-front maps of Figure 8-102 and In Figure 8-94. Solid line: initial co-phasing errors (piston and tip-tilt, 20 nm rms). Dashed line: DM_2 fit. Dotted-dashed-line: residual error figure after correction by DM_2 (6 nm rms error residual of high spatial frequencies).

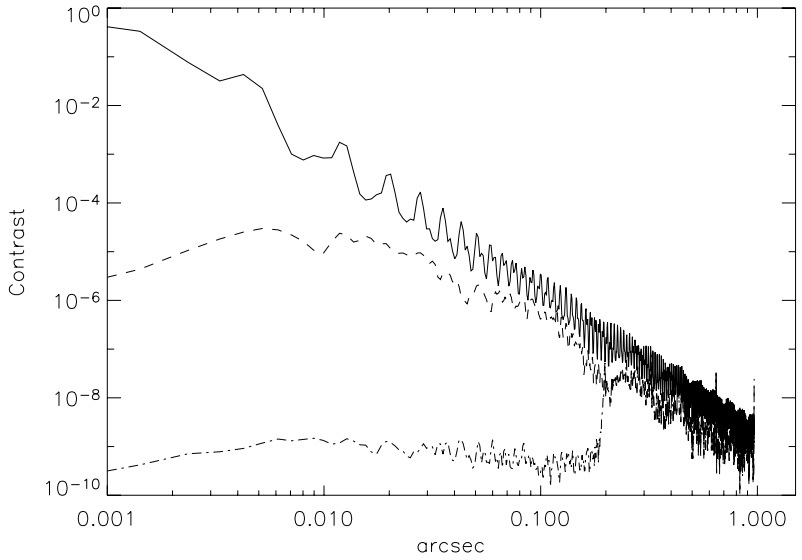

Figure 8-96: Effect of co-phasing on coronagraphic image at 1600 nm (Circular average of 2D image). Solid line: PSF without coronagraph. Dashed line: Coronagraphic image with initial co-phasing residuals of 20 nm rms. Dotted-dashed line: Coronagraphic image of residuals after AO correction (6 nm rms).

8.3.2.5 EPICS performance

The scientific spectral regions of EPICS are located in the R, J, and H bands and cover thus a wide range of wave-lengths. The choice has been made to use the I band [800-1000] for wave-front sensing since this region had a lesser scientific interest. Moreover, since the I band is located between the visible and Near IR scientific wave-lengths, the effects due to air chromaticity (anisoplanetism due to differential refraction, chromatic seeing) become acceptable. The high Strehl obtained in I band (nearly 80 %), is also an advantage for the pyramid sensor to work in a more linear though diffractive regime with best sensitivity. Typical Strehl Ratio values for medium seeing are given in Figure 8-97. In the near IR, the Strehl is larger than 90% and still attains 70 % in R band. The detailed error budget of EPICS AO system is described in RD51.

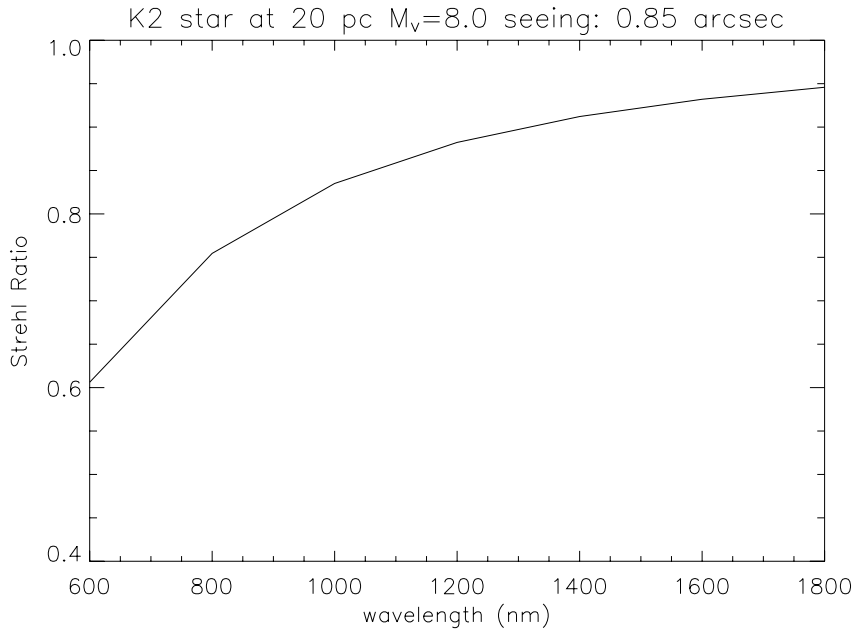

Figure 8-97: Strehl ratio versus wave-length.

More important than the Strehl ratio, the PSD of the phase error has a direct impact on the residual halo after coronagraphy thus on the final contrast. For this reason, the use of a phase-type sensor for correcting the central region of the PSF makes sense as it can be seen on Figure 8-98. The correction is however limited to about 30 mas, separation at which the air chromaticity becomes the main limitation.

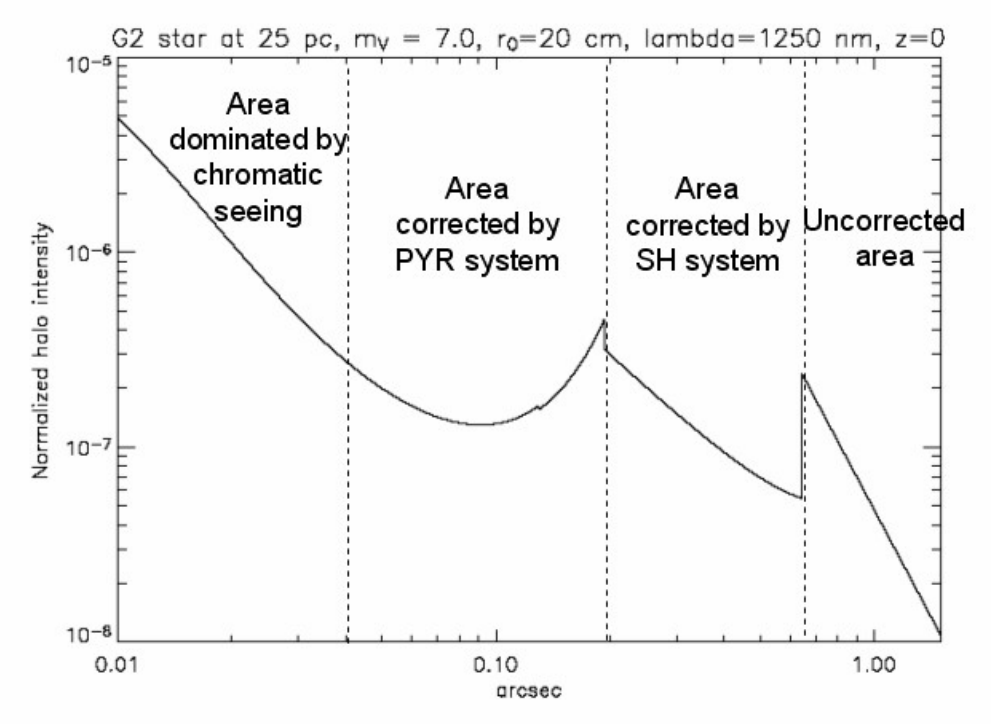

Figure 8-98: Theoretical point spread function after a perfect coronagraph.

An analytical model taking into account the main error sources has been developed to produce the kind of curves of Figure 8-98. The performance in terms of Signal-to-Noise ratio for the detection of exo-planets can be directly derived from these curves (see RD51).

8.3.2.6 Technological requirements for EPICS

EPICS requires significant technological developments of hardware:

- CCDs: 1KxK (goal 3Kx3K) detectors with fast read-out (3 KHz) and low noise (read-out noise less than one electron) are required. Developments of L3CCD are already part of the OPTICON Joint Reasearch Activity 1.
- Micro Deformable Mirrors): EPICS requires a micro deformable mirror with about 2.105 actuators. Actually only 1K micro DM2 with about 1 micron mechanical stroke are available (Boston Micro-Machine). A 2K micro DM with larger stroke will be developed in the frame of OPTICON.
- Real-Time-Computers
- Coronagraphic masks: high precision coronagraphic masks (in phase and in amplitude) are needed.
- Optical polishing and coating quality: a number of optical surfaces in the EPICS design need to be of extremely good quality (less than 1 nm rms error). The effect of coating on super-polished surface is an important aspect of this topic.

8.3.2.7 Future development plan

The EPICS feasibility study has shown the necessity of important Research and Developments in the field of high contrast imaging. This includes AO developments itself, new methods for wave-front sensing and instrument concepts and realisation of very high quality optics. High contrast imaging is an emerging and a very active research field: new limitations, new ideas and new instrumental concepts fundamentally different from the proposed approach here may appear in the coming years in the frame of high contrast instruments developed today –VLT or GEMINI PF- and demonstrators like ESO's High Order Test bench, HOT.

Laboratory experiments:

In particular we intend to study the following items theoretically and with laboratory experiments also beyond HOT in the frame of the FP6 ELT design study:

- optimation of pyramid wave-front sensor, by theoretical work with end-to-end simulations and with experiments
- Woofer-Tweeter control scheme theory and experiments
- Realisation and testing of "super-polished optics" and effect of coating on error figure.
- investigation of new concepts like the focal plane interferometer: this idea could permit ultimately to be unsensitive to static and differential aberrations, since the coherence of the speckles itself can be used to disentangle them from a planet image.
- Developments in coronagraphy
-

VLT Planet Finder studies:

The experience and results of the Planet finder development phase will be extremely valuable. Important feed-back is expected from extreme Adaptive optics developments as well as developments more related to the instruments: polarimetry, diffraction effects in an IFS, etc.

Real-Time Computers

Many developments are required to reach the goals of this ambitious system. To make it achievable we need to improve 4 technologies that are the foundations of the main design of all the other systems. Table 8-17 illustrates these four technologies and the improvement that is required in order to implement XAO in two specific cases 500x500 and 1kx1k sub-apertures.

Technology	500x500	1k x 1k
Input/output communications. Today it is based on a 2.5 Gb/s serial communication. The 10Gb/s is becoming available and it has been used as the baseline for the other designs. Here we need 50 Gb/s for the first case, 100Gb/s for the second	5	10
Faster processing elements, faster CPU-to-CPU busses, faster memory.	10	30
Integer arithmetic. FPGAs perform faster if integer arithmetic is used. By observing that input data (pixels) are integers and output data (control voltages) are as well, one could think of arranging the computation in integer arithmetics. Study is required here. However, performance gain is already known.	2	3
The sparseness of the interaction matrix of an XAO system is very high. However a control matrix (the inverse) is not. Smart algorithms will be able to take advantage of the sparseness of the IM and require less processing power.	5	10

Table 8-17. Four technologies to achieve the XAO requirements

Since this system is not supposed to be built before 2015, we can benefit from the technological advances that will happen in the next 10 year, and the corresponding efforts that can be spent

in studying better algorithms. Famous Moore's law predict an increase of computing power in 10 year by a factor 100, so the highest value we used, 30, is not so aggressive.

With the assumptions listed above, the 500x500 system would be made of 3 crates with 20 boards each, each carrying 2 high performance next-generation FPGA chips. Each crate will actually host 3 identical sub-systems, for a total of 9 identical sub-systems each processing one slice of the detector data. Final control values will be merged and exchanged with 6 back-end stages that will control the deformable mirror through multiple parallel lines.

The 1000x1000 system will have a similar complexity, but it requires more aggressive technological improvements and a higher parallelism.

In conclusion, the XAO system at 500x500 (more for the 1000x1000 case) is not achievable with today's available techonolgy. However, we identified 4 critical technologies to improve and the required factor of improvement is within reach for 2015.

Hardware Development

To get to the final performance of the last AO system, XAO, we need to strengthen the relationship with the industrial partner(s) even more than in the previous cases in order to aggregate in a super-performing board the latest technology in FPGAs, CPUs, busses and memory. This, of course, can only be done if the first level of co-operation had been successful. Unfortunately there not many similar applications around and industry could consider our as a small niche, so convincing them to develop the products we need might be difficult

Algorithms

The XAO system is too big to be implemented using plain matrix-vector multiply thus smart algorithms must be used. Fortunately there are several options.

Generic Algorithm Improvements

- The control matrix can be reduced in precision and compressed. Pixels are normally 16 bit values and mirror controls are 14 or 16-bit values. A loss-less compression, if possible, will allow us to reduce the storage size of the matrix, thus its loading time and the overall performance of the RTC.
- Fixed-point arithments. By observing that input data (pixels) are integers and output data (control voltages) are as well, one could think of arranging the computation in integer arithmetics.
- Multi-rate control: the RTC could send more than one command within a single frame time. Multiple commands can be generated by a sequence of approximated commands where the last is the final correct value. This technique is useful if the dynamic of the mirror is not particularly fast. In this way the mirror can be pushed toward the final value, even if approximated, very soon, and while it is reaching the position another refined value will be sent for the final adjustment.

Architecture Specific

- Local reconstruction algorithms can be used to maximise the parallelism of the reconstructor and the controller.
- Fourier domain techniques can be used to reduce the complexity of the reconstructor from n2 to nlog(n). However it has been developed so far only for Shack-Hartmann systems

System Specific

- SCAO and XAO systems are characterised by a large sparsity factor, i.e.: the interaction matrix is mainly made of zeros since the size of the influence functions is small. This characteristic can be exploited to design special algorithms that do not explicitly invert the interaction matrix.

8.4 Third generation Adaptive Optics

8.4.1 Introduction

The 3rd generation of Adaptive Optics relies essentially on the availability of the Laser Guide Stars for OWL. In the description of the 1st and 2nd generation AO systems, we have provided the performance of these systems and the corresponding limitations due to the number and magnitude of NGSs used for wavefront sensing. It should be noted that "3rdgeneration" is actually a misnomer: every effort will be made to have LGSs available as early as possible.

In the following:

- We will summarize the performance of the 1st and 2nd generation AO systems and identify where the LGS based AO systems should improve the situation
- We will provide preliminary performance expected for the GLAO and MCAO cases using LGSs in the ideal case
- We will summarize the main problems encountered with LGS systems on ELT in general and on OWL in particular and provide potential avenues to overcome these problems
- Finally we will introduce other LGS concepts which are being investigated in the frame of the European ELT design study.

8.4.2 Toward the 3rd generation AO systems with LGSs

Resorting to only natural guide stars for wavefront sensing allows one to have a simple AO system, since there is no need to produce a high quality reference in the atmosphere. However, this approach imposes some limitations for each AO system we have analyzed in this document.

Due to the limited time to prepare this document, the preliminary performance provided in this section does not include all specific ELT LGS issues listed later in 8.4.3.

8.4.2.1 From Single Conjugate to Laser Tomography AO

In the case of SCAO, the sky coverage is limited by the availability of bright (magnitudes 16-17) guide stars within the isoplanatic patch (~30''-1') from the object. The sky coverage is barely a few percent. This is well-known problem of this kind of AO system.

To improve this, one needs to resort to multiple laser guide stars. Indeed, using a single LGS is not sufficient, because of the cone effect (or focus anisoplanatism). The LGS being located at 90km and not infinity, the rays of light coming from the LGS do not follow the same path as those from the NGS. Therefore, an error is made when measuring the wavefront from an LGS to correct an object at infinity.

To overcome this issue, several LGSs have to be used, to probe the whole volume of turbulence above the telescope. This so-called LTAO (Laser Tomography AO) allows to use a single DM (M6 in our case) and to optimise the correction on-axis over a small FoV.

In the case of OWL, the LGSs should be located far enough off-axis to sense the whole volume of turbulence (geometrically the optimum distance is ~100" off-axis). If we want to limit the number of LGSs to 4-5, the optimum LGS off-axis angle should be compromised with the meta-pupil overlap at let say 8 km. For a given performance the corresponding optimum values remain to be determined by simulations. The expected performance of an LTAO system is expected to be slightly better than the MCAO with multi-LGS as the LTAO correction is optimised on-axis but lower than the SCAO system using bright NGSs because of the meta-pupil overlap and remaining cone effect. Detailed simulations are planned during phase B.

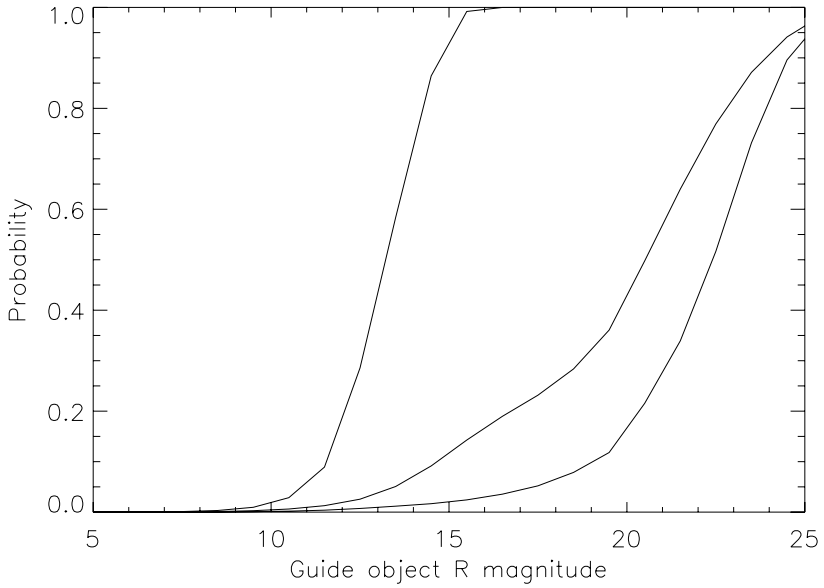

Figure 8-99: Probability to find a NGS/Galaxy versus magnitude over 2' FoV. Top to bottom: Galactic plane, 180-20°, Galactic Pole

It is known that LGS does not sense the atmospheric tilt. When using several LGSs, individual LGS tilts degenerate into unseen low order modes. To sense these modes a low order NGS WFS -3x3 Shack Hartmann for instance- either in the visible or in the IR is required. The limiting magnitude of this wavefront sensor scales with the telescope collecting area leading to an expected limiting magnitude of Mv=22-23 for a visible wavefront sensor.

In addition, the outer scale of turbulence reduces dramatically the phase variance of the unseen low order modes –see for instance Figure 8-26-. Based on this fact, we believe that an NGS located within a FoV of 2' around the object may be used to sense these modes with a marginal reduction of the on-axis performance due to the anisoplanatism. Alternatively three tip-tilt NGSs may limit the anisoplanatism effect. Figure 8-99 shows the probability to find such NGS or Galaxy within 2' FoV. We see that 60% Sky coverage can be achieved at the Galactic Pole with such concept.

The concept of LTAO (Laser Tomography AO) is planned to be demonstrated for the VLT second generation instrument, GALACSI, in narrow field mode. Multiple lasers are used in conjunction with a single deformable mirror to correct a small field of view. The multiple lasers are required to compensate for the cone effect. The advantage is that high sky coverage can be achieved through the use of LGSs and a high resolution (diffraction limited) can be achieved over a field limited by anisoplanatism.

8.4.2.2 Laser assisted Ground Layer Adaptive Optics

For GLAO, the lack of NGS also reduces the sky coverage, and can introduce non-uniformities of the PSF over the corrected FoV, because the brighter star will have better correction than the fainter ones.

One particularity of the GLAO is that only the low atmospheric layers are corrected. Those are well sensed by the sodium LGS. It is therefore conceivable that good performance can be achieved for GLAO with sodium LGSs, like it is the case for Rayleigh LGSs on 8m telescopes.

In has been recently suggested ([129]) to use a single LGS on an ELT, to provide ground layer correction at a low cost, with a large sky coverage. This is based on the approach proposed by SOAR telescope, to use an LGS to correct the ground layer, and "use" the cone effect to filter out the high altitude turbulence.

On a 4m class telescope, like SOAR, a Rayleigh LGS (at ~4km) is used.

We analyzed the performance (gain in EE in a 50 mas pixel) of such a system for OWL, as a function of the height of the LGS. The results can be seen in Figure 8-100.

In the K band, factors between 3 and 4 of gain can be obtained, over a field of view of ~2' (diameter), in good seeing. Even in J-band, a gain close to a factor of 2 can still be obtained. In this simulation, we have assumed that the spot elongation effect is perfectly corrected, and that a bright tip-tilt star is located on-axis.

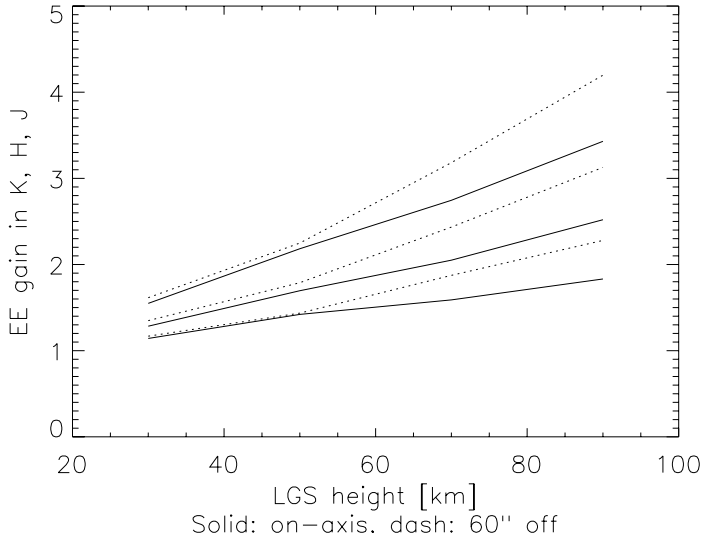

Figure 8-100: Performance (gain in EE compared to seeing) of a single on-axis LGS. Solid: on-axis, dash: off-axis. Top to bottom: K, H and J bands. The good seeing model was used (0.5'').

Since this idea was presented quite recently, we have not had time to thoroughly analyze the concept. It is not for the moment clear why the off-axis performance becomes better than the on-axis one when high altitudes LGSs are used. Intuitively, the opposite should happen. It might be due to the small number of iterations (500) for which the simulation was run.

The sky coverage for such a system should be close to 100%, since only the tilt needs to be corrected, and the diffraction limit is not the goal.

Further analysis is required, but this method shows some promise.

8.4.2.3 Laser Assisted Multi-Conjugate Adaptive Optics

The field of view of MCAO is significantly smaller than that of the GLAO. Therefore, the probability to find NGSs is even smaller. This introduces two effects:

- Low performance, because statistically, the NGS are far from the desired field
- High PSF variability, because the NGSs do not sample finely enough the atmosphere.

Using several LGSs helps solving the problem, by providing bright and nearby references to the WFSs.

Using multiple laser guide stars allows to obtain a large sky coverage in an MCAO system. We have modeled a system based on the M6 and M5 of OWL, correcting a field of view of 2' (diameter). The LGSs were placed in a configuration where 4 are at the corners of the field coordinates (± 1', ±1') and a central star. Sodium LGSs were assumed, providing enough flux so the WFS is not photon starved. The performance (Strehl in the K band) is analyzed in the 1' (radius) field of view. Good seeing conditions (0.5'') were used for these simulations - Figure 8-101-.

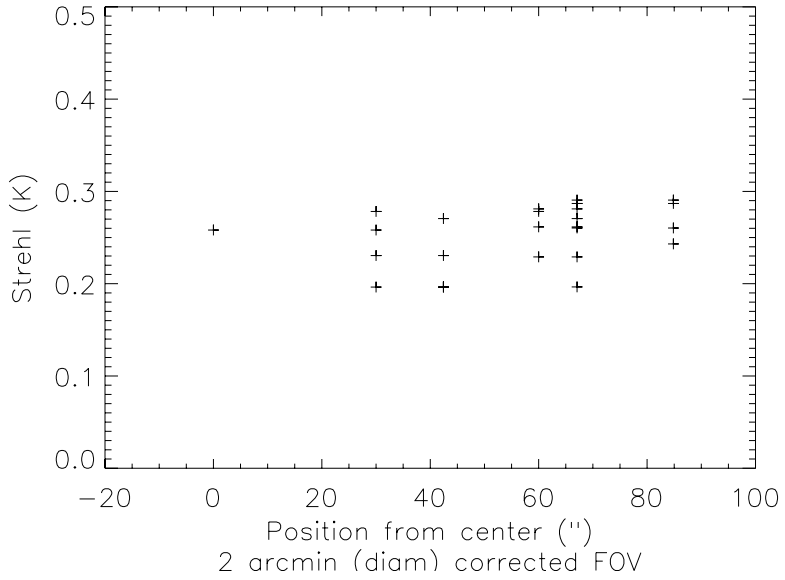

Figure 8-101: LGS MCAO performance (K-band). Tip - Tilt stars at LGS positions.

We can see that a Strehl ratio (K-band) between 20 and 30 % can be obtained over 2' (diameter) the field, in good seeing conditions.

It was assumed that each LGS provides a tip-tilt measurement. Of course, this is unrealistic, and the tilt problem of the LGSs must be solved with:

- Either a single NGS from which some low order modes are measured (presumably, a 3x3 SH sensor is sufficient). Due to the size of the telescope, this method should be quite sensitive.
- Multiple (at least 3) NGSs are used, from which only the tip and tilt are measured.

We have not yet investigated how to increase the performance of the system. In phase B, we will tackle this issue, and proceed to study the effect of increasing the number of sub-apertures, adding an extra DM, changing the number of LGSs.

However, we can see already here that 5 LGSs provide already acceptable performance.

8.4.2.4 Laser Assisted Multi-Object Adaptive Optics

The same sky coverage problems apply also to MOAO, and more particularly to the cosmological deep fields, which are the prime targets for MOAO. Although some fields are accessible with good performance (see Section 8.2.3.2), other fields are empty of bright stars, which have to be searched far away.

The use of Multi-LGSs for MOAO looks at this stage quite challenging as the number of LGSs may be increased to 10 or so. Further analysis and simulations remain to be performed to conclude on the performance and optimum number of LGSs.

8.4.3 ELTs and LGSs issues

The use of single or multiple Laser Guide Stars for ELTs has a series of difficulties described in this section. These issues depend on the telescope diameter and F/ratio. Table 8-18 provides a quantative evaluation of know LGS issues on ELTs versus telescope diameter.

These values have been computed according to the following formulae:

- Laser spot elongation for the subaperture at the edge of the telescope pupil :

$$\theta = \frac{\Delta H D}{2H_{Na}^{\ 2}} \qquad \textit{Eq. 8-6,}$$

where H_{Na} is the height of the sodium layer (90km), D the telescope diameter (100m) and ΔH the thickness of the sodium layer (10km).

- The seeing limited depth of field:

$$f = \frac{2H_{Na}^{\ 2} s}{D} \qquad \textit{Eq. 8-7,}$$

where, s seeing size disk and f is the depth of the field (taken from [113]). The stroke required in the WFS with dynamically steered sub-apertures is 23 μm (1m sub-apertures, 15 km refocusing):

$$x = \frac{d(D-d)r}{8H_{Na}^{\ 2} - 2r^2} \qquad \textit{Eq. 8-8,}$$

where x is the full mechanical stroke, d sub-aperture size, r is the range gate. If only 5km are used the stroke is 7.5 μm and if only 1 km is taken, then it reduces to 1.5 μm. The frequency requirement is above 1 kHz ([113])

Spot Elongation: The spot elongation is due to the thickness of the atmospheric sodium layer. The profile of sodium distribution varies in time, but a mean thickness of about 10 km is usually observed, with sometimes “spikes” of sodium density at given heights.

Observing the backscattered light from the extended sodium layer with an ELT is problematic, because from the side of the telescope (50 m in the case of OWL, if the LGS is launched from behind the central obstruction of the telescope), one doesn’t see a spot, but a stripe.

Spot aberrations: The spot aberrations are due to the design of any particular telescope, which are optimized to yield maximum optical performance for objects at infinity. Observing a LGSs at 90 km produces a severely aberrated image, on which wavefront sensing might be difficult. In addition, these aberrations change as a function of the distance to the sodium layer, which can vary from 90 km (observations at zenith) to ~180 km (observations at 60 degrees).

Number of LGSs: It has been argued that it may be necessary to add LGSs when the telescope diameter increases, as the cone effect gets bigger. On the other hand, simulations up to diameters of 30m have not shown large decreases of performance compared to 8 m telescope simulations ([127]). Therefore, the number of LGSs necessary on ELTs is still an open question, at least from the AO tomography point of view.

Fraticide Effect: The fratricide effect is due to the Rayleigh scattering cone of a LGS introducing noise into the measurements of a wavefront sensor from another LGS when using a continuous LGS. This effect also exists on 8 m telescopes and is being studied right now. On ELTs, it might be necessary to use more lasers to compensate for this effect or use pulsed laser which are more difficult to produce.

Laser defocus: When a sodium Laser Guide star is used the mean altitude of the sodium layer may vary with time. In addition, depending on the telescope zenith angle position the sodium layer is seen at 90 (zenith) or 160 km (at 50 degrees zenith angle) from the telescope. The wavefront sensor(s) sensing the laser scattered light should be defocused to follow the sodium layer. This defocus of the wavefront sensor becomes very important on ELT as it grows with the telescope diameter and is quadradic with the F-ratio. We believe that an optical design of a zoom up-front each wavefront sensor can be produced to compensate for that effect. However, one issue is the shadowing of the LGS wavefront sensor (s) in the scientific FoV due to the fact that the science focal plane is several meters before the average LGS focal plane – science beam foot-print-. The shadowing is independent of the F-ratio but linear with the telescope diameter. The easiest and may be the only way to overcome this problem is probably to

separate the LGSs and the science optical beams upfront the focal plane with a large sodium dichroic.

Depth of field: Finally, there is a depth of field issue due to the thickness of the sodium layer and the finite depth of focus of the telescope. The telescope might not deliver an image of the sodium layer where the whole layer is in focus. This will introduce a blur of the images of the LGS spot.

Finally, the depth of field issue is also due to the finite thickness of the sodium layer. When imaged through a telescope, the depth of focus might not be large enough compared to the thickness, which will introduce a blur of the images of the LGS spot.

Problem	OWL (100m, F/6)	60m F/15 F/6	30m F/15	8m F/15	Remarks
Spot elongation	13''	7.6''	3.8''	1''	Computed using Eq. 8-6
Spot aberrations	1.5''	0.33''	TBD	Diffraction limited	
LGS Number	7-12 ?	7-10 ?	5-9	5	For ~2' FOV
Fratricide effect	TBD	TBD	TBD	TBD	TBD
Laser defocus (90-160 km)	5.7-2.7 m	12.7-6 m 1.7-0.91 m	TBD	0.164m	
Depth of field of spot	390m	654m	1310m	4910m	Eq. 8-7

Table 8-18: Quantitative evaluation of the known LGS issues versus telescope diameter

8.4.4 Potential solutions to LGS issues

These, and other, possible solutions to LGS issues will be explored in the design phase.

8.4.4.1 Spot Elongation

One solution is the use of dynamic refocusing. In this scheme, a modulated membrane is used to follow the laser pulse as it propagates through the sodium layer. The beam is refocused (by changing the shape of the membrane) as the beam propagates, and therefore the circular shape of the spot is re-established. An experimental demonstration of this concept has already been made (see [112]). More recently, a variation on this scheme has been proposed, where the vibrating membrane and the microlens-array of a Shack-Hartmann WFS is replaced by a micro-mirror. The micro mirror is of piston-tilt type, and moving the mirror creates the sub-aperture and also follows the upgoing laser beam ([113]).

A completely different approach, which partly solves the problem of spot elongation is the design of a custom CCD for the WFS, which has elongated pixels and a radial geometry ([115]). This allows reducing the noise (since the CCD has the shape of the streak). Moreover, one could in principle follow the upward laser propagation by shifting the charges at the proper speed along the direction of the spot elongation, and hence reduce the effect.

8.4.4.2 Spot aberrations

To reduce the effect of the spot aberrations, one could design an optical corrector which acts like a deformable mirror in an AO system. The correction must be variable as a function of the sodium height. The stroke requirements for such a corrector must be investigated for the OWL case.

The concept of virtual wavefront sensor ([125]) permits to reduce, for some ELTs, the aberrations by putting the WFS before most of the optics. Options to implement this will be explored during the optical design iteration at the beginning of Phase B.

A “solution” is to investigate if one can tolerate these errors, i.e. to investigate if high order wavefront sensing is still possible from the aberrated beam and to correct the low order aberrations from a slow framerate natural guide star. In the case of OWL, the aberrations are concentrated in the lowest order modes, and vary at a moderate rate as the height to the sodium layer changes, so this could be a viable solution (see RD1).

8.4.4.3 Fratricide effect

To reduce the fratricide effect, one can increase the number of laser launch telescopes, and chose their location so as to minimize the impact on the WFSs

Pulsed lasers could be used, and different LGSs would be fired at different times. The WFS would then be synchronized so that it only sees the sodium return light and not the Rayleigh plume of any other WFS. In principle, this should work, provided a laser with the appropriate pulse format can be made.

8.4.5 New Laser Guide Star concepts

The subject of new Laser Guide Stars concepts is addressed in the ELT design study -WP 9400 “Novel Adaptive Optics concepts”-. In principle LGSs allow the achievement of full sky coverage, even at visible wavelengths, provided the laser power is sufficiently high to ensure a suitable spatial and temporal sampling of the turbulent layers. On the other hand it is well known that the use of LGSs presents several problems. Some of these are “intrinsic”, like the absolute tilt indetermination. Others, related to the finite distance of the artificial reference source are described in the previous section.

In this section we will introduce alternative wavefront sensing techniques, in order to overcome these problems. Four concepts are studied and are briefly described in the following. The study involves also an experimental validation. The participants of the task are: Durham University, ESO, Galway University, INAF, Lund University, MPIA Heidelberg, Tecnion.

8.4.5.1 Pseudo Infinite Guide Stars

The two main components of a “Pseudo Infinite Guide Stars (PIGS) wavefront sensor” are a mask with radial slits, placed in the focal plane of the telescope, and a reflective rod, placed on the image of the LGS (Figure 8-102). The focal plane mask selects specific angular directions, looking at the LGS rays as if they were coming from infinity (hence the name of the concept) and is sensitive to the radial wavefront aberrations. The reflective rod is optically conjugated to different portions of the LGS along its extension, thus allowing the use of the LGS light without temporal gating techniques; this device is sensitive to the azimuthal wavefront aberrations. The features of the two wavefront sensing devices make this concept well suited to an elongated artificial source at finite distance from the telescope, although the problem of the telescope aberrations has still to be investigated. PIGS is a pupil plane wavefront sensor and may be implemented in layer-oriented mode, using multiple LGSs.

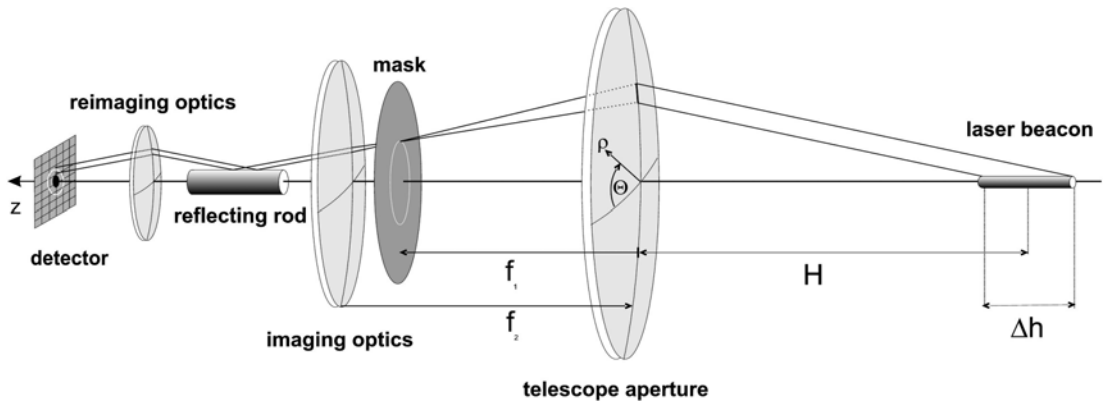

Figure 8-102: Pseudo Infinite Guide Star conceptual layout.

The concept, in particular the azimuthal part, has already been tested with positive results in the laboratory and on sky. Further experimental work is foreseen to test in deeper detail the radial wavefront sensing part and the multiple LGS mode.

8.4.5.2 Sky Projected Laser Array Shack-Hartmann

A Sky Projected Laser Array Shack-Hartmann (SPLASH) wavefront sensor is based on an array of focused laser beams, covering the whole telescope pupil and projected onto the Sodium layer (although the concept could also work with a Rayleigh laser); each beam is launched from an aperture of size comparable to r_0 and therefore the focal anisoplanatism is much reduced (Figure 8-103). This array of focused spots is imaged by the whole telescope and from the measurement of the instantaneous location of each spot it is possible to retrieve the local wavefront tilt, minus the global tilt over the full aperture. The applications of the concept to visible wavelengths seems to be limited by diffraction effects, although some solutions do exist, for instance the time-interleaving of the measurements, and others are under investigation.

The SPLASH concept is a way to measure the turbulence in the upward path. An interesting modifications, called Projected Pupil Plane Pattern, consists in projecting a collimated laser beam through the full telescope aperture and measuring the intensity fluctuations due to the wavefront curvature by taking snapshots at difference distances. In this approach the focal anisoplanatism is reduced thanks to the beam collimation.

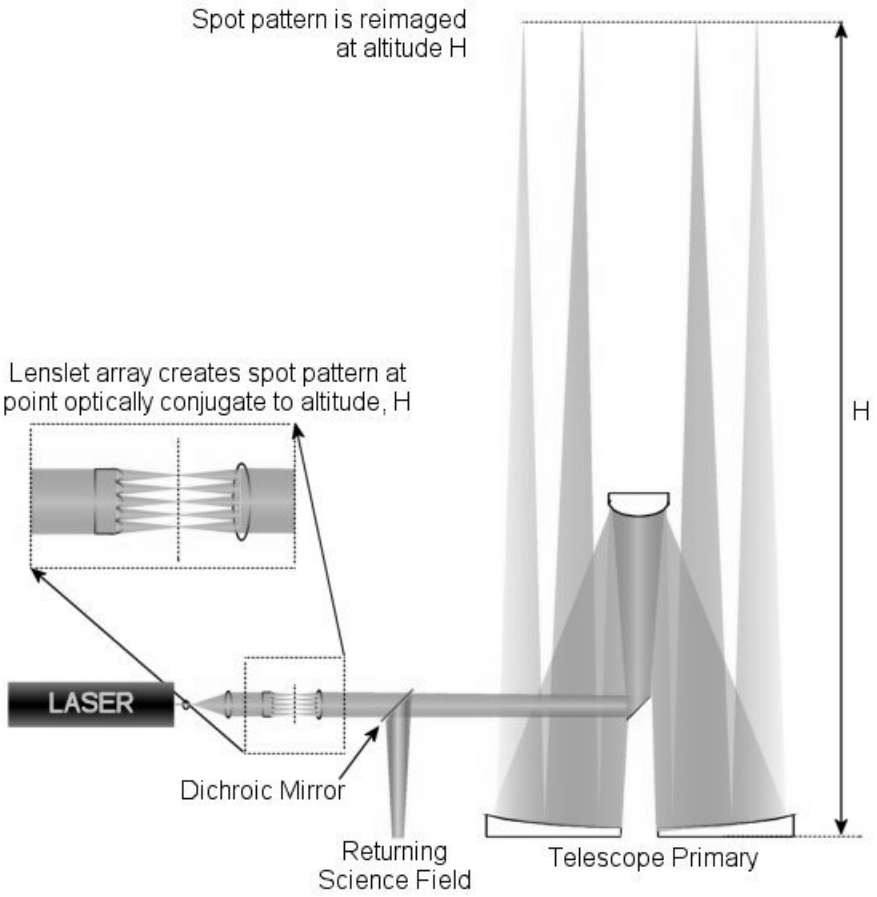

Figure 8-103: Sky-Projected Laser Array Shack-Hartmann conceptual layout.

8.4.5.3 Virtual Wavefront Sensor

The Virtual Wavefront Sensor concept (Figure 8-104) has been conceived in order to solve the LGS re-imaging problems typical of an ELT. It has been initially developed for EURO50 where

the only suitable LGS image is close to the Gregorian focus where the LGS WFS is also placed, responding to the atmosphere and to the shape of the adaptive secondary mirror. The wavefront measurement performed by this sensor (complemented by a NGS sensor to measure the low-order aberrations) does not allow to correct properly the image in the science focus, obtained by re-imaging the Gregorian focus. For this reason, a Test Source WFS is placed in the final image plane, looking at an artificial source placed in the Gregorian focus; this Test Source WFS controls a second deformable mirror placed in the optical train between the Gregorian and the final focus. The signals from the two WFSs (complemented by the NGS WFS mentioned above) are combined into what is properly called “Virtual WFS”, which works to null the virtual residual signal and thus controls both the adaptive secondary mirror and the deformable mirror placed in the post-Gregorian focus optical train.

A laboratory prototype has been set up to validate the concept.

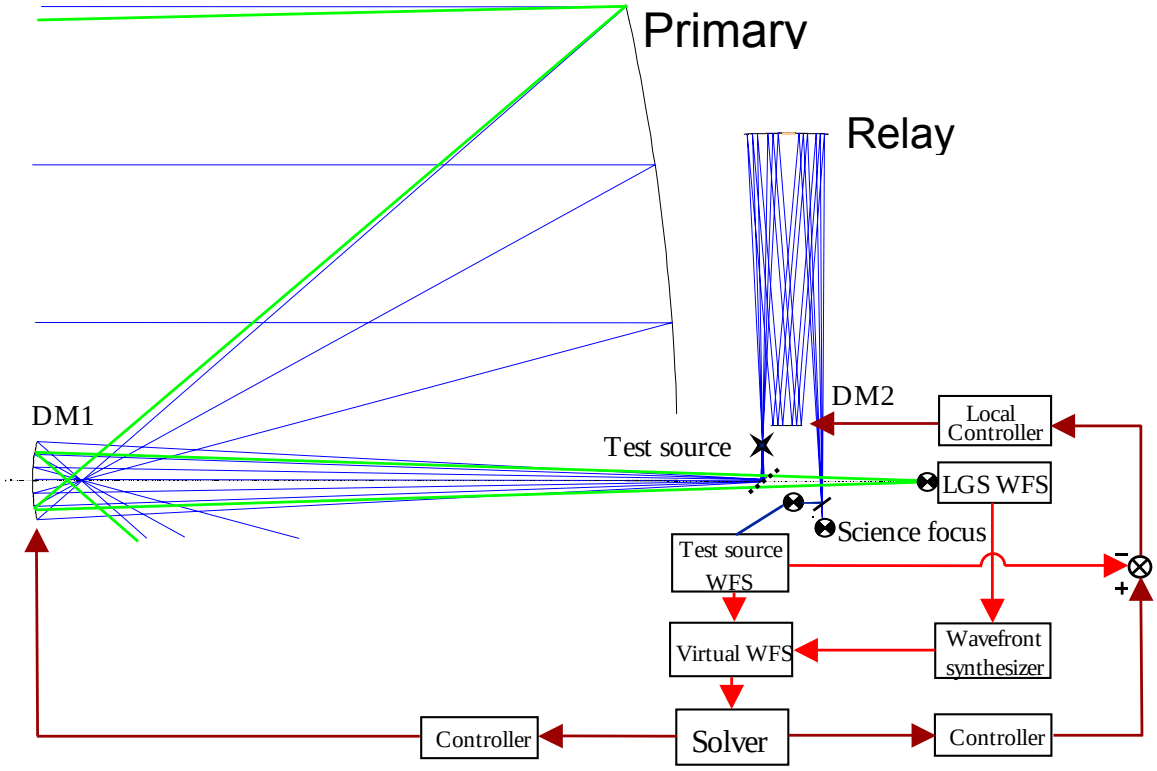

Figure 8-104: Virtual wavefront sensor conceptual layout.

8.4.5.4 Variable Wavefront Sensors

A Variable WFS may be realized by means of acousto-optics cells, devices which can modulate the intensity of a light beam by two orthogonal acoustic standing waves, creating a pattern similar to the one generated by a lenslet array; the lenslet pitch may be changed by simply changing the frequency of the acoustic wave -Figure 8-105-. Such a device may be placed in a pupil plane, realizing a variable Shack-Hartmann WFS. Several acousto-optics devices may be conjugated to the most relevant turbulent layers, realizing a multiple layer WFS (Figure 8-105). As opposed to a conventional Shack-Hartmann WFS, the idea proposed here is to image by each lenslet the whole field of view of interest; the image produced by the lenslet is shifted by the local wavefront tilt (over the lenslet aperture) and all the sources within the field (natural or artificial) contribute to the measurement of the local tilt. The most suited computational method for this kind of data is based on Fourier Transform, which is also less sensitive to spot elongation problems than simple centroid computation. The fact that each lenslet produces an

image of the whole field translates into the requirement of large detector formats and this, in turn, translates into large amount of data to process in real time. However windowing strategies may be implemented, reading only the relevant pixels, which are a small fraction of the total.

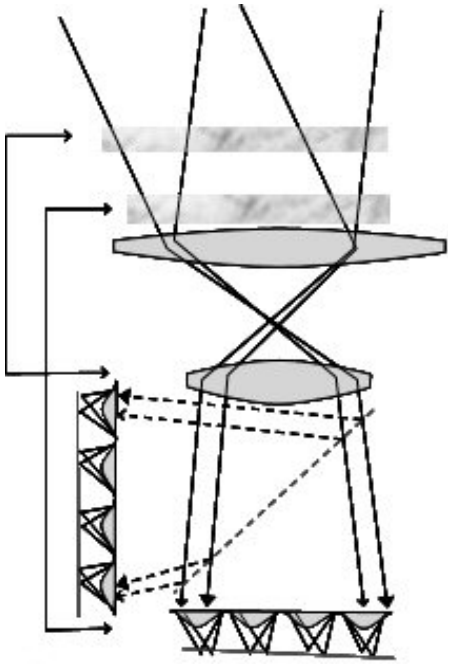

Figure 8-105: Variable wavefront sensor conceptual layout.

8.4.5.5 Laser Guided AO with on-sky phase shifting Interferometry

This method uses the coherent superposition of tilted laser wavefronts over the whole aperture of the telescope as indicated in Figure 8-106. Applying methods of laser phase shifting interferometry (LPSI) one can retrieve a local phase difference that can be used in the adaptive optics system like the gradients retrieved from a usual Hartmann sensor. The details of the proposed scheme are outlined in [103]. Here we summarize the principle and application to an extremely large telescope.

With a laser pulse split in two flat coherent laser wavefronts leaving the telescope- one tilted slightly with respect to the other- an interference pattern is created at any distance. When reaching a certain height in the atmosphere, both waves will have collected local phase changes. Due to the tilt in the wavefront, the path through the atmosphere to the point (x,y,H) of each wave is slightly different. This makes a phase difference occur which modulates the intensity of the interferogram that is written in the sky. With a wavefront camera that is gated at twice the time of flight to the point (x,y,H) the scattered light from this pattern can be imaged with the use of the full telescope aperture.

Using now several laser shots on timescales which are short compared to the coherence time of the atmosphere and applying known phaseshifts between the launched wavefronts, allows to retrieve the atmospheric induced distortions. It should be noted that the large wavefront distortions present in the atmosphere result only in gradients to be probed and choosing the distance *a* smaller than the coherence length r_0 of the atmosphere will avoid phase overlap.

With two beams overlaid, a tilt can be applied in one coordinate direction, though a phase difference -gradient- can be measured along this direction. To retrieve gradients in two coordinates several methods are possible, like overlapping more than two beams or polarization overlapping perpendicular measurements and disentangle the polarization planes at the detector as well.

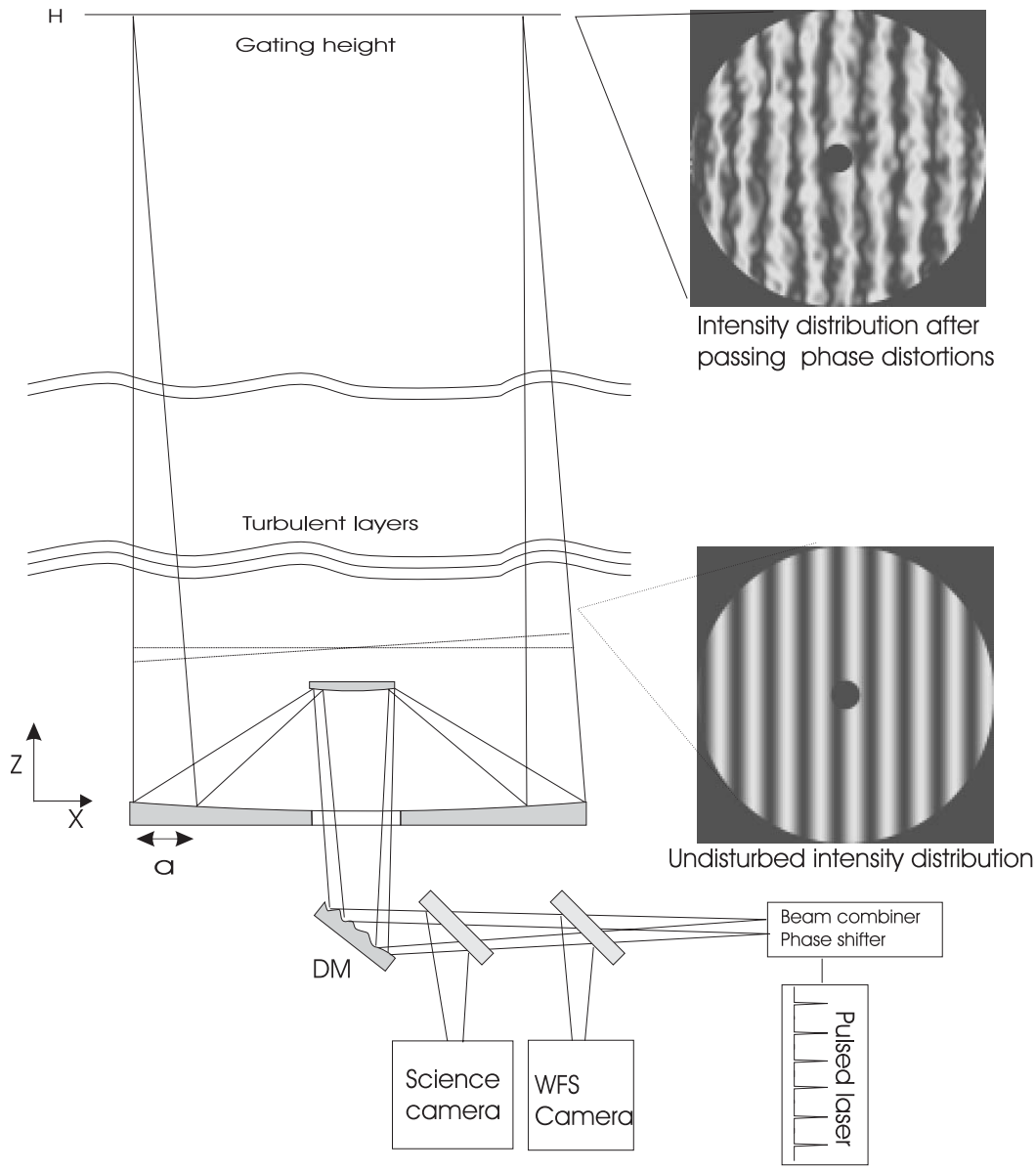

Figure 8-106: Basic principle of measuring atmospheric turbulence with phase shifting interferometry.

The resolution of the sensing can be chosen freely with the amount of tilt added to the beams to adapt to different conditions. Detecting the light scattered from low altitude will result in a ground layer correction. Extending the system to multiple detections at different heights or two beam systems with more deformable mirrors a complete sampling of the turbulent layers in the atmosphere is possible. Therefore high Strehl ratios are reachable and multiconjugate adaptive optics correction with an extended field of view is possible.

The extension of the proposed method to a multiconjugate correction is straightforward and illustrated in Figure 8-107. A first laser beam (consisting of the overlaid coherent wavefronts) is directed over the first deformable mirror to the telescope, expanded and launched over the full aperture as described before. This beam is detected at lower altitude and steers the first deformable mirror in a closed loop scheme. A second laser beam is then injected before that, hits the second DM and then joins the beam path of the first one at a beam splitter. To enable the splitting and separate properly both beams the two lasers could operate at different colors. The second laser is detected then at higher altitude, and DM number two is controlled, independent from loop number one, out of this signal. The type of backscatter which is used can be selected for the individual application. For the lower altitude scattering process Rayleigh scattering is probably a good choice. The upper altitude scatter could be Rayleigh-type as well, or resonance scattering in the earth sodium layer.

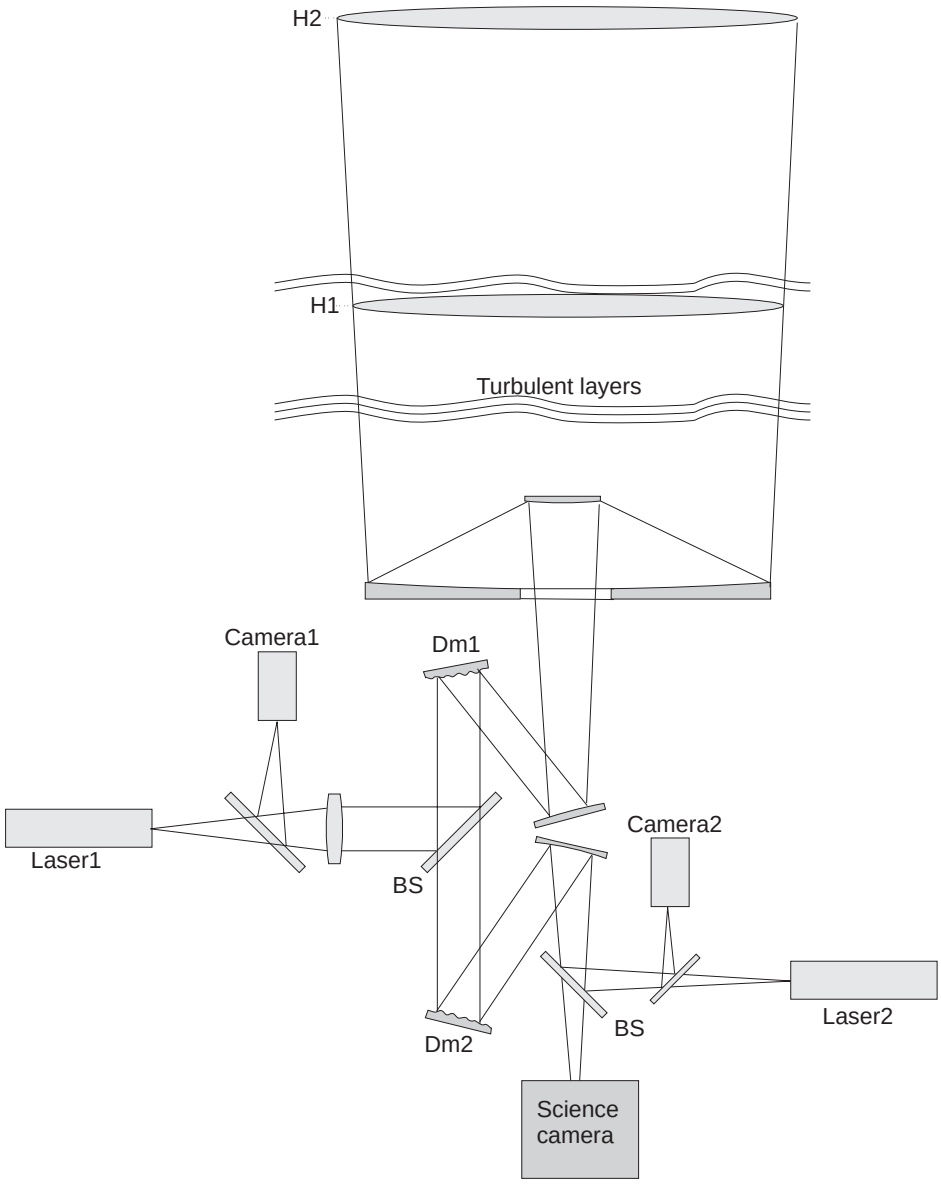

Figure 8-107 Schematic arrangement of a multiconjugate correction with lasers and LPSI.

The requirements for the laser have to be chosen accordingly. In general a pulsed system with 1-5kHz repetition rate and sufficient power to be detected at high signal-to-noise will be necessary. The power demands for the laser will decrease if a dynamical refocusing device is used, as proposed by [128]. Compared to usual guide star systems beam quality issues for the proposed scheme are totally relaxed, due to the full aperture launching of the laser. For Rayleigh scattering green lasers are available today that would fulfill all requirements.

The basic feasibility of the proposed method can be tested in laboratory experiments and on-sky with present day telescopes. The laser launching and detection system would not greatly change with telescope size.

Particular issues like field-of-view in the multiconjugate case, imaging capability of the main telescope for finite objects, stray light suppression onto the science camera or dynamical refocusing devices will be included in a feasibility study.

8.4.6 Strategies of the LGS program for OWL

8.4.6.1 Background

LGS-AO is in a maturing phase, with few systems starting to produce science and optimizing the operations or the subsystems.

ESO itself is placing the first LGS Facility on the UT4 telescope. Much experience has been already gained with the testing and integration in Garching, and will be increased further during integration and operation with AO in Paranal.

An increasing number of AO systems rely already or will rely on laser guide stars as reference sources for AO systems. LGS-AO is used for the visible range correction, at Palomar Observatory and in a number of air-force telescopes in New Mexico and Hawaii.

From the experience matured internationally so far, the following technological developments appear essential and are currently driving the ESO R&D strategy in this field:

- simplify, make possibly cheaper and ruggedize the laser sources at 589nm, to get 10W CW on air (15W CW in the lab), with a keys-on system.
- Propagate the laser beam up to the laser beam Launch Telescopes using single mode fibres, thus preserving the diffraction limited beam, avoiding mechanical vibrations to be transmitted to the beam, and avoiding stray lights in the telescope dome.
- Develop 3 kHz pulsed formats with macropulses of 2-3 microsec for the 589nm lasers
- Explore innovative propagation-sensing schemes, to avoid the focus anisoplanatism and the optical problems related to the imaging of the LGS with OWL.

8.4.6.2 Status and planned tasks

Fibre lasers (Figure 8-108) seem definitely the way to go for the second generation laser sources. Fibre lasers with powers of tens of watts are commercially available, but not at 589nm. We have followed the fibre Raman laser solution in-house at ESO, and collaborated with Lawrence Livermore Nat'l Labs for a sum-frequency fibre laser approach. The in-house activities have brought us to find together with industry a path to produce a fibre Raman laser at 1178nm, which is frequency doubled at 589nm using Periodically Poled non-linear crystals. We have chosen the name AFIRE (Advanced FIbre Raman Emitter).

Figure 8-108: Fiber laser

We are in the breadboarding phase, with ~2W CW at 589nm to be produced this summer, 5 W to be produced by December 2005, and a contract for a finally engineered fibre laser unit to be likely placed by March 2006. This laser will have the size of a 19 inch VME rack, servo-controlled in frequency, and deliver the beam via a single mode fibre right at the launch telescope focal plane.

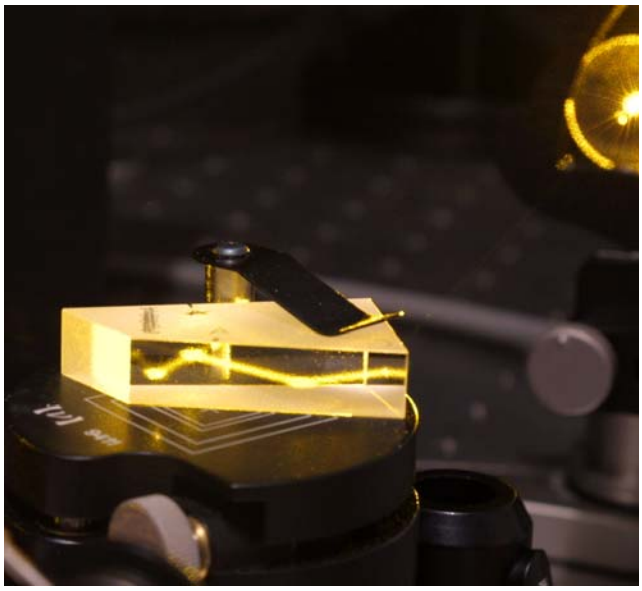

Figure 8-109: CW Raman laser

Since the laser delivers the beam via a single mode fibre, the problem of the laser beam relay disappears. In case of a solid state laser source, the beam has to be relayed. The fibre solution for future systems is Hollow Core Photonics Crystal Fibre Technology (HC-PCF). After the development of solid core PCF, we have started the development of HC-PCF. The throughput achieved with HC-PCF fibres is 1.2 dB/km, for the visible range it is possible to achieve 20 dB/km but the production technology has to be improved. We are placing at the time of this writing the contract with industry for this development, and have in place manpower and lab facilities for the two-year development.

The design of a pulsed format version of the ESO AFIRE laser will be developed via a contract with industry. A first assessment of the feasibility to obtain such a format from AFIRE is very promising.

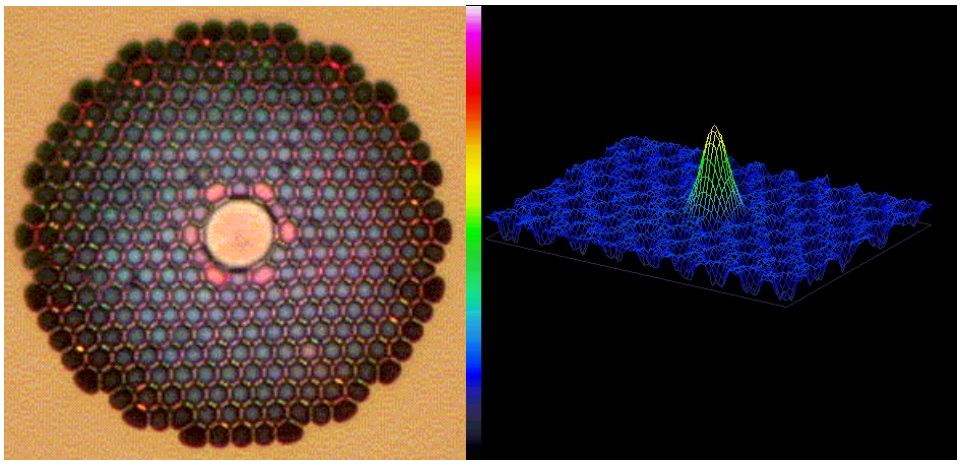

Figure 8-110: Hollow Core Photonic Crystal fibre.